



universität
wien

MASTERARBEIT

Titel der Masterarbeit

“Kinetic and thermodynamic analysis of the bl5 intron
bound to its protein cofactors”

verfasst von

Lukas Mühlhölzl

angestrebter akademischer Grad

Master of Science (MSc)

Wien, 2015

Studienkennzahl lt. Studienblatt: A 066 834

Studienrichtung lt. Studienblatt: Masterstudium Molekulare Biologie

Betreut von: Mag. Dr. Christina Waldsich, Privatdoz.

Table of contents

Abbreviations.....	7
Introduction	10
1. The importance of being RNA.....	10
2. Structure of RNA	10
2.1 Influence of mono- and divalent ions on RNA folding	12
2.2 General RNA folding paradigms	13
2.3 RNA folding problem	14
3. Group I introns.....	16
3.1 The splicing pathway of group I introns	17
3.2 The structural organization of group I introns	19
3.3 Folding of group I introns	23
4. RNA binding proteins and their role in RNA folding	24
4.1 RNA cofactors and chaperones facilitate RNA structure formation	25
4.2 DEAD-box proteins assist RNA in folding.....	27
5. Two proteins are necessary to promote bI5 splicing in yeast mitochondria	28
5.1 The yeast mitochondrial group I intron bI5.....	28
5.2 Splicing cofactor Cbp2	30
5.3 The structure and function of the DEAD-box helicase Mss116p	32
6. Mss116p and Cbp2 cooperate to facilitate bI5 folding in vivo	34
Scientific aims of the project	36
Materials and Methods	37
1. Plasmids	37
2. Strains.....	38
3. Transformation in Escherichia coli DH5α	38
4. Midi prep	39
5. Restriction digest	39
6. Phenol-chloroform purification	40
7. In vitro transcription	41
7.1 In vitro transcription - method 1	41
7.2 In vitro transcription - method 2	41
7.3 Transcript purification	42
7.4 RNA body labelling – method 1	42
7.5 RNA body labelling – method 2	42
7.6 RNA end labelling	43
8. Protein expression and purification.....	45

8.1 Expression.....	45
8.2 Purification	45
8.3 Removal of the 6xHis-tag	46
9. ATPase assay.....	49
10. Splicing assay	50
10.1 Adding Cbp2 to the unfolded bI5	50
10.2 Adding Cbp2 and Mss116p or KCl to the unfolded bI5	51
10.3 Adding Cbp2 and varying Mss116p concentrations to the unfolded bI5.....	52
10.4 Adding various Mss116p concentrations to the bI5/Cbp2 complex	53
10.5 Adding Cbp2 to the bI5/Mss116p complex.....	54
11. PAGE	56
11.1 SDS PAGE	56
11.2 Continuous denaturing PAGE	57
12. Filter binding assay.....	58
12.1 Adding increasing concentrations of Cbp2 or Mss116p to the unfolded bI5	58
12.2 Adding increasing concentrations of Mss116p to the Cbp2/bI5 complex and vice versa	59
12.3 Adding various concentrations of Cbp2 to bI5 folded at different concentrations of KCl or Mss116p storage buffer and vice versa	60
12.4 Assembly of the Bio-Dot apparatus.....	60
Results	63
1. ATPase assays	63
1.1 Activity of various Mss116p batches.....	63
2. Influence of Cbp2 and Mss116p on splicing efficiency of bI5.....	65
2.1 Cbp2 stimulates efficient splicing of the bI5 ribozyme <i>in vitro</i>	67
2.2 Salt influence on bI5 splicing efficiency.....	68
2.3 Mss116p enhances the Cbp2-assisted bI5 splicing activity	70
2.4 bI5 does not have hierarchical order for Cbp2 and Mss116p	74
3. Determining the dissociation constant of Cbp2 and Mss116p to bI5	82
3.1 Cbp2 binds with high affinity to bI5	82
3.2 Mss116p has a K_d to bI5 in the nM range.....	84
3.3 Cbp2 and Mss16p do bind specifically to bI5	85
3.4 Influence of Cpb2 on Mss116p-bI5 affinity	86
3.5 Influence of Mss116p on Cbp2-bI5 complex affinity.....	88
3.6 The influence of salt concentrations on the dissociation constant of Cbp2	89
Discussion	94

References	98
Appendix.....	107
Abstract	107
Zusammenfassung.....	108
Curriculum vitae	110

Abbreviations

A	adenine
A	alanine
ADP	adenosine diphosphate
amp	ampicillin
APS	ammonium persulfate
ATP	adenosine triphosphate
bp	base pair
BSA	bovine serum albumin
C	cytosine
Cbp2	cytochrome b pre-mRNA processing protein 2 of <i>S. cerevisiae</i>
CI	chloroform-isoamyl alcohol (24:1)
cob	cytochrome b gene
CTP	cytidine triphosphate
Cyt-18 and 19	tyrosyl-tRNA synthetase
DEAD	D - aspartic acid, E – glutamic acid, A – alanine
DMS	dimethyle sulfate
DNA	desoxyribonucleic acid
dsRNA	double-stranded ribonucleic acid
DTT	dithiothreitol
EDTA	ethylenediaminetetraacetic acid
EtOH	ethanol
exoG	exogenous guanosine
g	gravitational force
G	guanine
GDP	guanosine diphosphate
GMP	guanosine monophosphate
GTP	guanosine triphosphate
GTS	glycerol tris sodium chloride buffer
HEPES	4-(2-hydroxyethyl)-1-piperazineethanesulfonic acid
His-tag	histidine tag

IGS	internal guide sequence
IPTG	isopropyl- β -D-thiogalactopyranosid
J	junction
K	lysine
KCl	potassium chloride
K_d	dissociation constant
kDa	kilo Dalton
k_{obs}	observed rate constant
KOH	potassium hydroxide
L	loop region
LB	lysogeny broth medium
ME	mops EDTA buffer
min	minute
mRNA	messenger ribonucleic acid
Mg	magnesium
MgCl ₂	magnesium chloride
Mss116p	mitochondrial splicing system <i>S. cerevisiae</i> 116
mt	mitochondrial
NaCl	sodium chloride
NaOAc	sodium acetate
ncRNA	non-coding ribonucleic acid
Ni-NTA	nickel-nitrilotriacetic acid
nt	nucleotide
o/n	overnight
ORF	open reading frame
P	paired region
p.a.	puriss absolute
PAGE	polyacrylamide gel electrophoresis
PNK	polynucleotide kinase
pre-mRNA	precursor messenger ribonucleic acid
PSB	protein storage buffer

Q	glutamine
R	arginine
RecA	repair and maintenance protein for DNA in <i>E. coli</i>
RNA	ribonucleic acid
RNP	ribonucleoprotein
rpm	revolutions per minute
rRNA	ribosomal ribonucleic acid
S	serine
SDS	sodium dodecyl sulfate
SF	super family
SHAPE	selective 2'-hydroxyl acylation analysed by primer extension
siRNA	small interfering ribonucleic acid
ssRNA	single-stranded ribonucleic acid
StpA	DNA-binding protein in <i>E.coli</i>
T	threonine
TBE	tris borate EDTA buffer
<i>td</i>	thymidylate synthase gene
TE	tris EDTA buffer
TEMED	tetramethylethylenediamine
Tris	trisamine
tRNA	transfer ribonucleic acid
U	uracile
UMP	uridine monophosphate
UTP	uridine triphosphate
wt	wildtype
Y	tyrosine
Δ	deletion

Introduction

1. The importance of being RNA

In the 1950s, Stanley Miller proofed with his Miller-Urey-experiment that under early earth conditions organic compounds can arise from inorganic elements (Miller 1953). In 1968, this groundbreaking finding lead Francis Crick and Leslie Orgel to the hypothesis of the “RNA world”, which states that RNA, and not DNA, is the most-basic organic compound and progenitor to all living organisms (Orgel 1968; Crick 1968). Until the early 1980s scientists assumed that RNA is nothing more than a passive template for protein synthesis.

In 1982 the future Nobel Prize winner Thomas Cech was the first to discover the catalytic function of RNA (Cech 2012). During the last decades more and more RNA functions were found and categorized. Today RNA is distinguished in two major groups, coding and non-coding RNAs. Coding RNAs, mRNA, carry all genetic information that is needed for translation of proteins (Schroeder et al. 2004). In contrast, non-coding RNAs (ncRNA) are characterized by not being translated by ribosomes. ncRNAs do offer a wide field of application. While for example tRNAs fulfil a transport function, ribosomal RNAs (rRNA) are part of the protein synthesizing machinery. Short interfering RNAs (siRNA) are used for inhibiting certain gene expression (Eddy & Hughes 2001). Dozens of RNA functions have been revealed since Stanley Miller’s experiment and many more are waiting to be discovered.

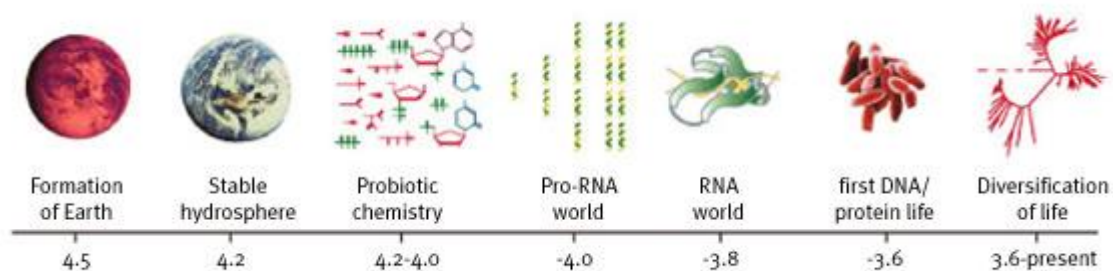


Figure 1: History of life

Timeline of important events starting with the formation of earth about 4.5 billion years ago until present (Joyce 2002).

2. Structure of RNA

The last decade was a period of prosperity in RNA research. Dozens of RNA properties and functions were revealed, but still, many questions remain unanswered. Today we know, the discovery and research of every single RNA function is a requirement for the entire understanding of a living

organism. To fulfil its function, RNA has to be folded properly. Prior to focus on RNA folding, it is necessary to determine RNA structural elements and their interactions (Schroeder et al. 2004).

Two moieties, ribose and nucleobases, build up into nucleosides, resulting in four different building blocks (figure 2). The structure of the nucleobases cytosine and uracil derive from pyrimidine, whereas adenine and guanine derive from purine. Nucleosides are connected by a phosphate group, which is attached to both, the 5' O of one ribose and the 3' O of the following ribose. Together, nucleobase, ribose and phosphate group form a nucleotide unit. Serially attached nucleotide units form the polymeric molecule, RNA. However, the antediluvian paradigm that RNA is a straight strand, with no secondary or tertiary structure is no longer accurate. Not only is RNA capable of forming single-stranded elements, it also can form double strand helices, with antiparallel chains and Watson-Crick base pairing, similar to DNA. While in the secondary structure cytosine is base pairing with guanosine, adenosine is base pairing with uracil. Individual helices are connected by single-stranded junctions. Tertiary interactions then form between different helices, single-stranded segments or a helix with a junction or loop, thereby leading to a specific 3D architecture of the RNA.

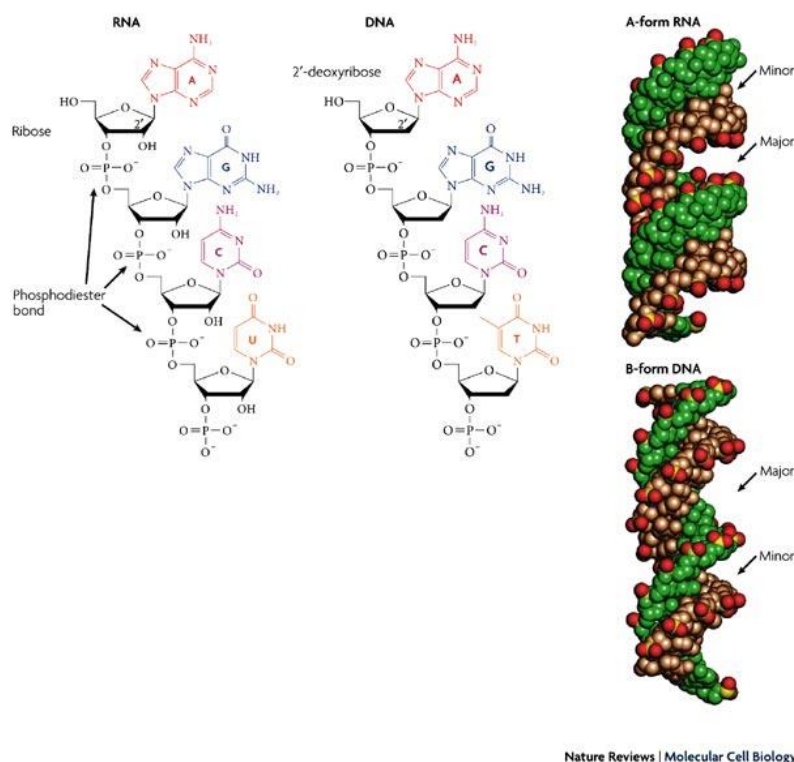


Figure 2: RNA compared to DNA structure

Example primary sequence of RNA and DNA; different helices of A-form RNA and B-form DNA. This figure has been adapted from Rana, 2007.

Major structural differences between RNA and DNA are found in the sugar molecule. DNA is lacking a hydroxyl group at the 2' C of ribose (figure 2). This additional hydroxyl group makes RNA much more reactive but also less stable. Also, this reactive group results in a higher tendency forming A-form

helices, rather than B-form helices that are preferred by DNA. RNA A-form helices have a distinctive narrow and a deep major groove (Rana 2007).

Additionally, there are several structural elements that are characteristic for RNA (figure 3). Single-stranded regions that do not engage in tertiary interactions, tend to adopt helical conformation due to base stacking interactions. Duplexes are double stranded RNA regions forming in A-form helices. Hairpin loops and its stems are often involved in protein binding. These are formed by two

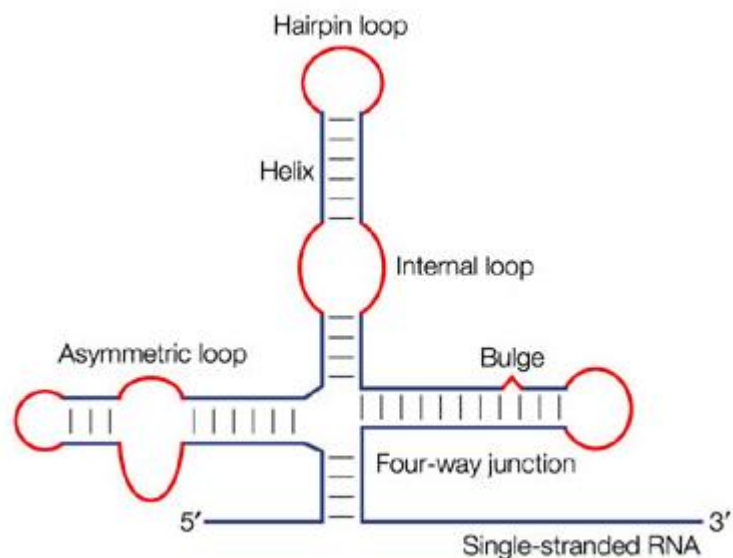


Figure 3: RNA building blocks
Typical RNA secondary structural elements in RNA. This figure has been adapted from Schroeder et al., 2004.

complementary, base paired nucleotide sequences of the same molecule interrupted by an unpaired loop. The loop itself consists of 3-8 nucleotides, though 4-5 nucleotides do form the most stable loops. Bulges are unpaired nucleotides, within a duplex, but found only on one strand. In contrast, internal loops are also unpaired nucleotides, within a duplex but found on both strands simultaneously (Moore 1999; Abrahams 1990). These can be either symmetric or a asymmetric internal loops. While duplexes are actively formed by Watson-Crick base pairing, tertiary interactions can be formed by both canonical and non-canonical base pairing interactions. In any case, formation of RNA secondary and tertiary structure is stabilized by metal ions.

2.1 Influence of mono- and divalent ions on RNA folding

Considering the structure of RNA and its main building blocks, a repeating pattern of negatively charged nucleotides is observed. Repulsion of negative charges needs to be overcome to allow RNA folding (Draper 2004). Hence, compaction - a pre-requisite of RNA folding - requires cations, which neutralize repulsion between nucleotides. While potassium is the most common monovalent ion, magnesium is the most common divalent ion assisting RNA in folding. Metal ions can interact in different ways with RNA. Some metal ions can interact diffusely, preventing destabilizing electrostatic interactions of the polyanionic backbone and mediating counterion-induced compaction. In other words folding of an RNA sequences into their secondary structure requires this

charge screening, mostly performed by monovalent ions. Forming the tertiary structure however depends additional metal ion-RNA interactions that support folding of specific RNA elements. These metal ions, which are mostly of divalent nature, bind to specific pockets formed within the RNA. Two site-specific interactions are possible. Outer sphere site-bound interactions refer to interactions between acidic protons of a water molecule, which are part of the hydrate shell of the Mg^{2+} ions, and oxygen or nitrogen atoms of RNA bases. Inner-sphere site bound interactions are known as direct interactions of Mg^{2+} and RNA elements. Typical ligands are oxygen atoms of phosphate groups or nitrogen atoms of nucleobases. Both site-specific interactions are mostly performed by divalent ions (Draper 2004).

Many RNAs do have defined metal ion binding motifs, often found in the major groove, in which an increased potential for repulsion between negatively charged phosphates occurs. One of the most intensively investigated RNA structure is that of the *Tetrahymena* group I intron. The P4-P6 domain of this group I intron shows, when correctly folded, a metal ion core (Cate et al. 1997). This core consists of five magnesium ions, which are bound to three helical junctions. Point mutation in one of these binding sites results in a loss of ion-RNA interaction and therefore in misfolding of the entire domain (Cate et al. 1997; Tinoco & Kieft 1997).

2.2 General RNA folding paradigms

Correct folding of an RNA sequence is a highly complex process. While RNA sequences belonging to the same phylogenetic family do only show very little sequence conservation, these molecules do fold into a very similar structure. On the other hand some RNAs have identical sequence, but fold into completely different tertiary structures (Schroeder et al. 2004). Due to the many factors that come into play during structure formation, the prediction of native RNA structure is very difficult, only by knowing the primary sequence (Michel et al. 2009; Schroeder et al. 2004).

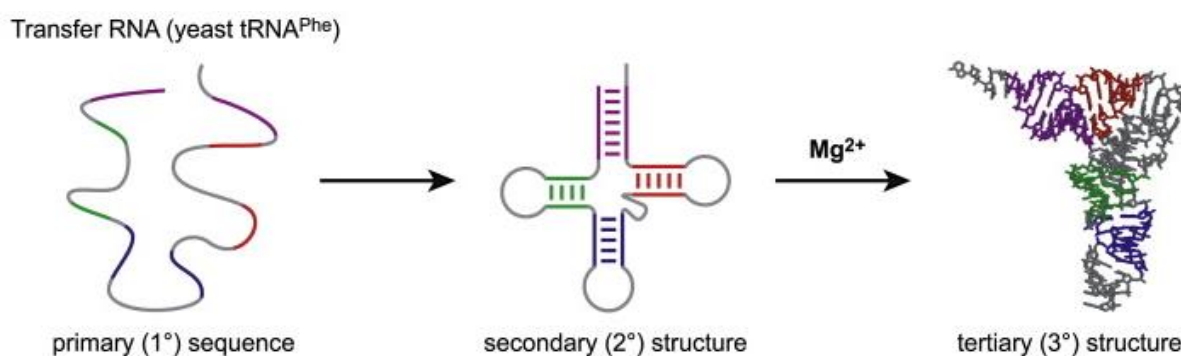


Figure 4: RNA folding hierarchy

Primary, secondary and tertiary structure of yeast tRNA demonstrating RNA folding hierarchy. This figure has been adapted from Silverman, 2008.

During the past years some general paradigms of RNA folding were derived based on a vast number of studies on structure formation of different RNA molecules (Schroeder et al. 2004). The most basic phenomenon is the hierarchy observed in RNA folding. This hierarchy is split into three levels, primary, secondary and tertiary structure (figure 4). In the first instance primary structure gives information about the nucleotide sequence and sequence motifs.

On the second level, primary sequence is folded into its secondary structure, which is based on Watson-Crick base pairs between nucleobases. The canonical type of base pairing occurs between the nucleobases adenine and uracil, and guanine and cytosine. Base-pairing between two nucleotides allows formation of RNA duplexes that are intervened by single-stranded regions. RNA-RNA helices do prefer A-form geometry, a right-handed helix, with a phosphate-phosphate distance of 5.9Å. This A-form helices are more tightly packed than B-form helices. This compact packing form is caused by the C3'-endo sugar pucker. Beside Watson-Crick base pairing, there are numerous interaction possibilities between two nucleobases. Each nucleobase does have three interaction sites, the Watson-Crick edge, the Hoogsteen edge and the sugar edge. Within these interaction sites, almost every constellation is possible in *cis* or *trans* orientation of the glycosidic bond. In total there are 12 possible binding types. Most RNA helices are antiparallel, meaning the 5' ends of two interacting helices point in different directions. RNA strands do not necessarily form duplexes.

The next level in RNAs hierarchical order is characterized by tertiary structures formed out of secondary structure via site specific binding of divalent metal ions and long range tertiary interactions. Common tertiary structure motifs are, for example, pseudoknots, tetraloop-receptor interactions, kissing loops or ribose zippers (Schroeder et al. 2004). The most dominant folding mechanism in tertiary structure is coaxial stacking. Coaxial stacking observes a principle, in which helices prefer interaction with nearest neighbours along a common axis. In other words, one helix is situated on top of another helix. Each transition goes along with an increased degree of compaction, with the largest reduction in radius induced by the counter-ion-induced compaction occurring during secondary structure formation. Another phase of compaction following the initial electrostatic collapse happens in the presence of Mg^{2+} and associated tertiary structure formation (Tinoco & Bustamante 1999).

2.3 RNA folding problem

RNA is known to fold hierarchically, meaning that secondary structure elements are quite stable, even without any tertiary interactions. This fact results in the so-called "RNA folding problem" (Herschlag 1995). Theoretically, RNA should tend to fold into a functional structure, which should be

favoured over any other possible conformation. On the one hand the native RNA structure is thermodynamically unstable, on the other hand RNA can become kinetically trapped in non-native interactions. Such misfolded elements are often very stable and thus long-lived, keeping the RNA in a misfolded, non-functional conformation (Herschlag 1995).

Even though the “RNA folding problem” exists both *in vitro* and *in vivo*, *in vitro* folding and *in vivo* folding do exhibit fundamental differences. Parameters like, temperature, metal ion concentration, ligands and concentration of denaturing reagents affect RNA strongly. Changing one of these parameters can shift the equilibrium between folded and unfolded species (Herschlag 1995; Zemora & Waldsich 2010; Schroeder et al. 2004).

In vitro folding of RNA can be supported by increasing metal ion concentration above physiological conditions

(Zemora & Waldsich 2010). Although *in vivo*, a cell is not able to increase metal ion concentrations to an extensive level and therefore needs alternative ways to deal with structural instabilities or the “RNA folding problem” in general.

The solution to this problem lies in protein-assisted folding, in which proteins help RNA to reach its native conformation (Schroeder et al. 2004). Cyt-18, for example, is a mitochondrial tyrosyl-tRNA synthetase, which assists in splicing of group I introns by binding to the conserved region P4-P6 and in turn stabilizing the catalytic core. This stabilization leads to recruitment of additional proteins, like DEAD-Box protein Cyt-19. Together, the two proteins facilitate splicing of their cognate group I introns (Chadee et al. 2010; Chen et al. 2004).

Another solution is found in case of the thymidylate synthase (*td*) pre-mRNA splicing, which depends on the ribosome for efficient splicing *in vivo* (Semrad & Schroeder 1998). Inhibiting translation via antibiotics or by introducing stop codons in the upstream exon results in misfolding at the 5' splice site and further to missplicing (Waldsich et al. 1998; Pichler & Schroeder 2002). In the absence of translation, the misfolded *td* pre-mRNA can also be refolded by proteins with RNA chaperone activity (Waldsich et al. 1998; Pichler & Schroeder 2002).

Often, folding of an RNA segment is not just an equilibrium between unfolded and native conformation. I-Anil, a maturase in *Aspergillus nidulans* mitochondria interacts with the unfolded

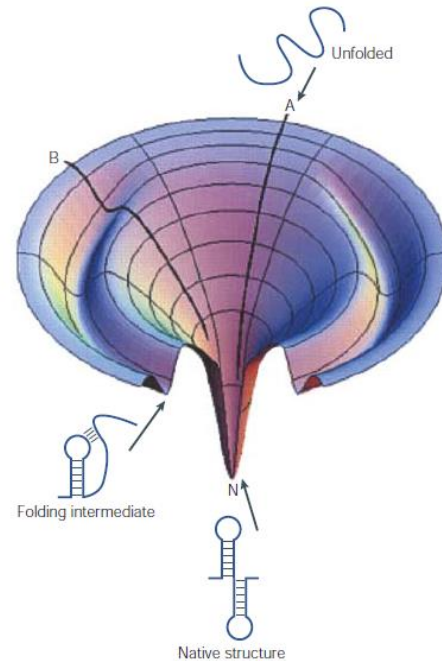


Figure 5: RNA folding landscape
Pathway A shows direct folding of unfolded RNA into its native conformation. Pathway B shows folding of unfolded RNA into its native structure via intermediate conformation. This figure has been adapted from Schroeder et al., 2004.

cytochrome-b pre-mRNA, forming an intermediate conformation. Only if the intermediate state is correctly folded, pre-mRNA is capable of forming its native conformation (Solem et al. 2002). Specifically folding of large RNAs do have a rugged free-energy landscape and are able to adopt various - intermediate - conformations, resulting in an heterogeneous RNA population (figure 5) (Woodson 2000; Treiber et al. 1998; Treiber & Williamson 2001). Thus large RNAs can follow parallel folding pathways from the unfolded to the native state containing different on- and sometimes off-pathway intermediates (Pan et al. 1997).

3. Group I introns

Group I introns are phylogenetically wide spread, found in lower eukaryotes and in plants as well as in bacteria. This dispersion leads to two theories that cover the origins of group I intron. The intron-early theory suggests that group I introns are ancient genetic elements, which got deleted in some evolutionary branches (de Souza et al. 1998; Koonin 2006). On the other hand, the intron-late theory suggests that self-splicing introns are mobile elements, able to be horizontally transferred between evolutionary neighbours (de Souza et al. 1998; Koonin 2006).

Together with RNase P, group I introns were one of the first RNAs that were proofed to have catalytic activity. Group I introns represent a large group of ribozymes, which are capable of catalysing their own excision during the splicing progress. Splicing is one of the most essential processes during RNA maturation. While Introns get excised, ligation of exons leads to the functional RNA (i.e. mRNA or ncRNA) (Winter et al. 1990; T R Cech 1990).

Generally, group I introns are divided into 14 structural subgroups (IA1-3, IB1-4, IC1-3, ID and IE1-3), which are characterized by their conserved sequences in the catalytic core and subgroup-specific peripheral elements (Vicens et al. 2008). Peripheral elements branch out from core helices (P2, P5, P6, P8 and P9) and function as stabilizing structures via tertiary long-range interactions with the core (figure 6) (Vicens & Cech 2006).

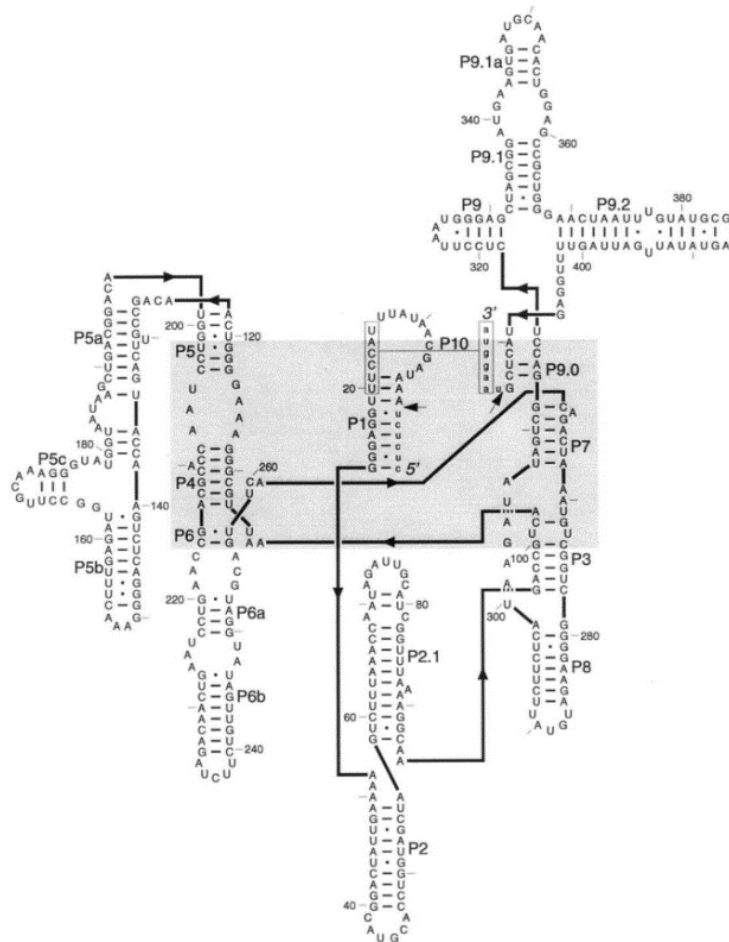


Figure 6: The secondary structure of the *Tetrahymena* group I intron, secondary structure. The P4-P6 domain is shown on the left hand side, P3-P9 domain is localized on the right hand side. The active site, including P1, is marked with a grey box in the centre of the structure. This figure has been adapted from Thomas R. Cech et al. 1994.

3.1 The splicing pathway of group I introns

Splicing of group I introns is a highly conserved, very precise process. The splicing reaction of group I introns occurs in two consecutive ester transfer reactions. To execute these two reactions, the RNA molecule needs to adopt a specific tertiary structure, including the correct positioning of the P1 stem formed by internal guide sequence (IGS) base paired to the upstream exon, thereby defining the 5' splice site. Specifically, the IGS is located at the 5' end of group I introns and forms a duplex of 4-7 nucleotides with the 3' end of the 5' exon. The number of hydrogen bonds between the base pairs in these duplex determines the binding strength. Mutation in the IGS may lead to reduced hydrogen bonds and therefore to dissociation of the sequences and missplicing. Increasing the number of hydrogen bonds via mutation results in stronger association and defects in intron release (Campbell & Cech 1996).

The splicing reaction itself is initiated by an endogenous guanosine nucleotide or an exogenous guanosine (=exoG) (Winter et al. 1990; T R Cech 1990). The 3'-OH of the guanosine makes a

nucleophilic attack on the phosphate between the last base of the 5' exon and the first base of the 5' end of the intron (figure 7a). After the transition state, the guanosine is attached to the 5' end of the intron, as the bond between the phosphate and the 3'-OH of the exon base is broken, resulting in a free 3'-OH of the 5' exon. Still, the upstream exon remains attached to the IGS (figure 7b) (Cech, 1990).

After a conformational change, the second ester transfer reaction follows. The new arisen nucleophile, which is the 3'-OH of the upstream exon, now attacks the phosphate of a highly conserved endogenous guanosine nucleotide at the 3' splice site (figure 7c). The bond between the terminal guanosine of the intron and the 3' exon is disrupted and the 5' exon is ligated to the 3' exon, resulting in a mature RNA sequence. The IGS releases the ligated exon and the intron is excised in a linear form. The splicing process is completed (figure 7d) (Cech, 1990).

In some cases the excised intron undergoes additional reactions or modifications. The *Tetrahymena* excised intron, for example, performs a circularization reaction, which is also catalysed by the intron itself. In another ester transfer reaction the 3'-OH of the conserved terminal guanosine attacks the phosphate at the 5' end of the intron, resulting in ligation and circularization of the molecule (Kruger et al. 1982; Vicens & Cech 2009).

Several experiments led to the assumption that two metal ions are essential for a successful splicing reaction. During the first ester transfer reaction, the first metal ion is bound to the 3'-OH of the guanosine cofactor, acting as nucleophile activator. The second metal ion is bound to the uridine of the wobble base pair G-U in P1 and functions as leaving group stabilizer. This reaction leads to binding of the first metal ion to the 3' oxygen atom of the uridine. In the second part of the splicing reaction, the two metal ions switch their roles. Additionally both metal ions serve as guidance for the nucleophilic attack at the 3' and 5' splice site phosphates (Steitz & Steitz 1993).

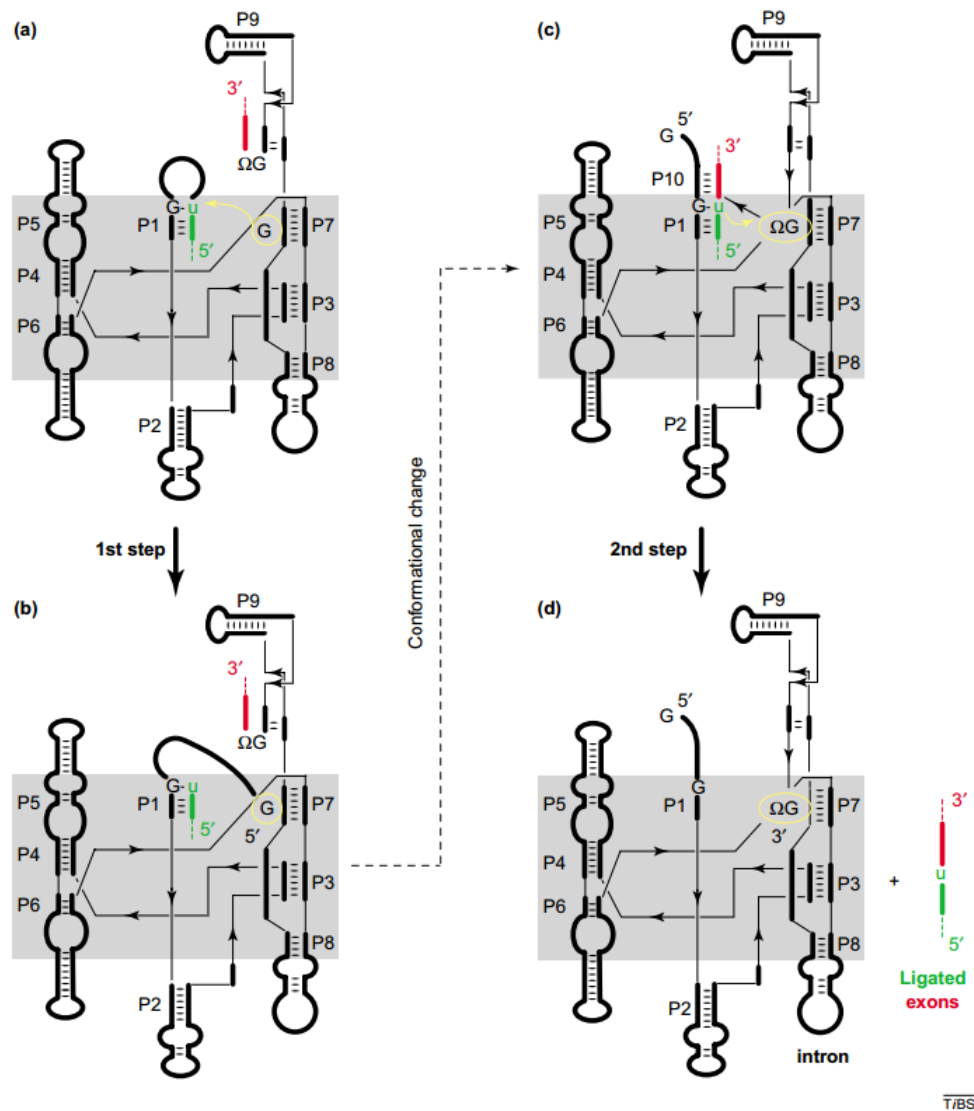


Figure 7: Splicing process of group I introns
 a) The yellow marked guanosine attacks the 5' splice site (5' exon marked in green).
 b) The first splicing step results in a free 3'OH of the 5' exon.
 c) ΩG (terminal guanosine) attacks the 3' splice site (3' exon marked in red).
 d) The second splicing step results in ligated exons and free intron
 This figure has been adapted from Vicens & Cech 2006.

3.2 The structural organization of group I introns

Correct splicing of group I introns requires the native conformation. Michel and Westhof were one of the first, who were able to predict structural elements of *Tetrahymena thermophila* group I intron, using comparative sequence analysis (Michel & Westhof, 1990).

Remarkably, not the primary sequence but the secondary structure is highly conserved in group I introns. Only 10% of the primary structure, which is the sequence, show similarities among all group I introns (Michel & Westhof 1990).

The secondary structure consists of nine duplex regions, P1-P9 (figure 8). P1 defines the 5' end of the intron. It contains the internal guide sequence, 4-7 nucleotides, which base pair with the last nucleotides of the upstream exon. This duplex assures that 5' splice site is defined and positioned correctly in the first step of splicing. Generally, the sequence of P1 is not conserved with exception of the last nucleotide in the internal guide sequence, a uracil, which wobble base pairs with a guanosine (Cech 1990). The Guanosine-Uracil base pair defines the 5' splice site, which is attacked by the exogenous guanosine in the first ester transfer reaction (Cech 1990). Similarly, in the second step of splicing P10 forms between the IGS and the very beginning of the 3' exon, thereby defining the 3' splice site (Cech 1990).

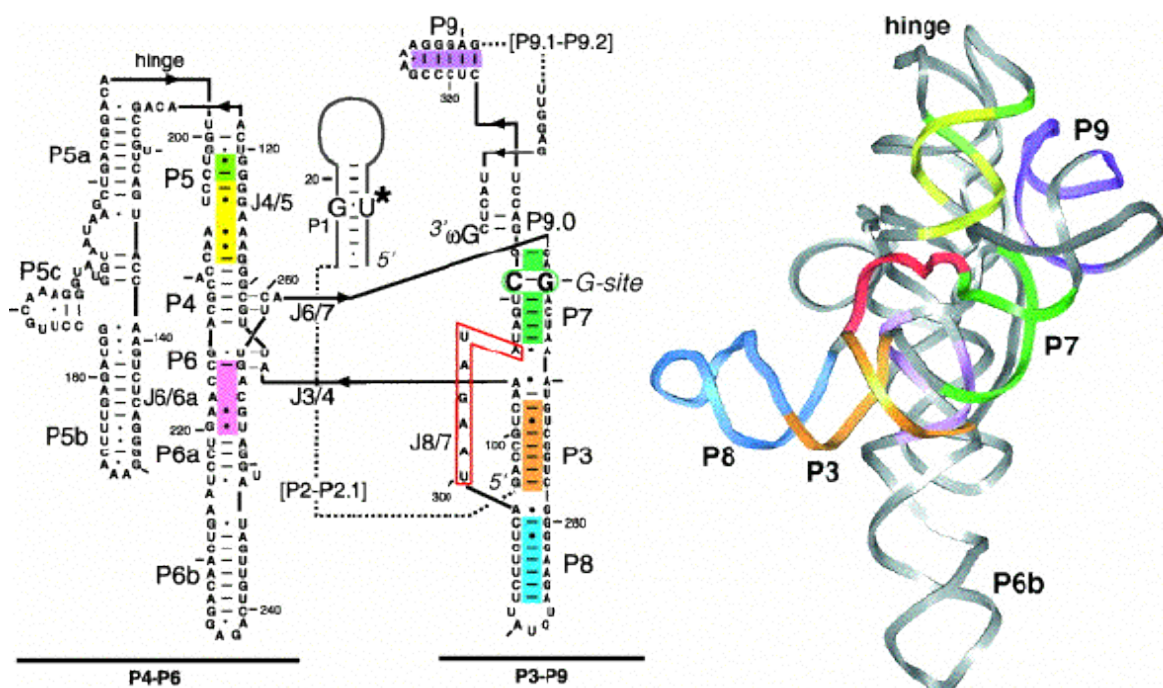


Figure 8: Secondary and tertiary structure of *Tetrahymena* group I intron
Secondary structure is shown at the left hand site, the crystalized structure at the right site of the figure. Colour scheme is the same in both parts of the figure. This figure has been adapted from Golden et al. 1998.

The 3' end of group I introns is found near P9. Similar to the 5' end, the 3' end shows no conservation, except for a single nucleotide, namely the terminal guanosine, referred to as Ω G. Ω G plays a key role in the second ester transfer reaction, during which it is bound to the G-binding site in stem P7. For exon ligation formation of P10 is essential, but also pairing of two nucleotides preceding Ω G with two residues adjacent to P7, thereby forming P9.0, are crucial for 2nd step of splicing (Cech, 1990).

Based on the common usage of guanosine cofactors among all group I introns, Michel et al. were the first, to propose suggested the existence of a G-binding site (Michel & Westhof, 1990). The fact that all group I introns share this characteristic led F. Michel to the assumption that the G-binding site has to be found in one of the conserved regions. In addition, the G-binding site should be positioned

proximal to the two guanosines, which participate in the two ester transfer reactions. The most promising region fulfilling all requirements was found in P7. P7 is a part of the intron core that is highly conserved and adjacent to the Ω G in P9. Mutational analysis confirmed that changing the base pair, G-C, beneath the semi-conserved bulge in P7 is in fact the G-binding site, as mutating G-C base pair into A-U base pair results in splicing inhibition (Cech 1990). In the wild type, on the other hand, G-C and guanosines are forming an isosteric base triple via hydrogen bonds, necessary for correct splicing. The Ω G•G₂₆₄-C₃₁₁ base triple is “sandwiched” in between three other base triples, formed between the P7 duplex and J6/7 and S8/7, respectively G₃₁₂-C₂₆₂•A₂₆₃, A₂₆₁•U₃₁₀-A₂₆₅ and A₃₀₆•G₃₀₉-C₂₆₆ (figure 9). This base stacking interactions allowing the guanosine to recognize the G-binding site (Guo et al. 2004).

Importantly, for G-binding and correct positioning of the substrate helices P1 and P10 to the active site needs to assemble, which depends on proper formation of the intron architecture, which is mainly dictated by its two major domains (Michel & Westhof 1990; Guo et al. 2004). The first

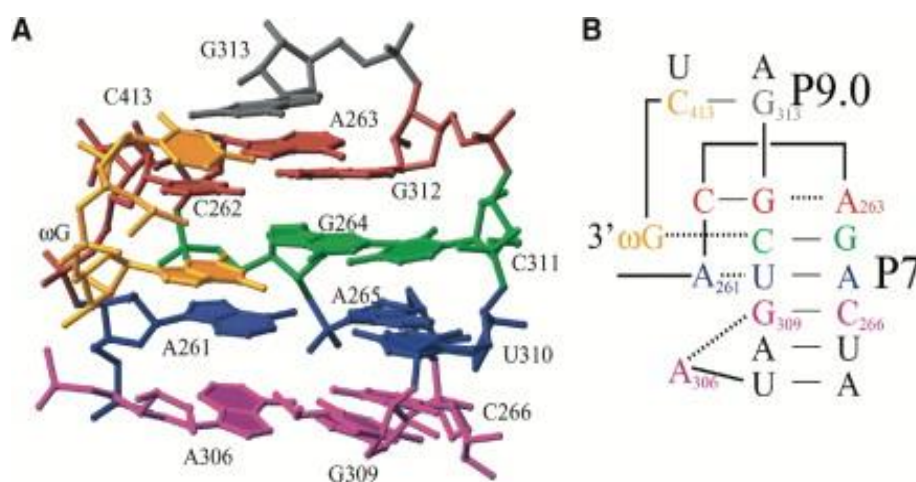


Figure 9: Guanosine binding site

- A) Base triple is formed by G₂₆₄-C₃₁₁ (green) and active ω G (yellow). Other base triples coloured in red, blue and magenta.
- B) Secondary structure of G-binding site. Colour code is the same as in a). Interactions are marked with dashed lines.

This picture has been adapted from Guo et al., 2004.

domain, called P4-P6, consists of the helical segments P4, P5, P6 and associated peripheral extension. Early folding experiments showed that the P4-P6 domain can fold into its tertiary structure, independently of the second major domain (Cate et al. 1996; Michel & Westhof 1990). The second major domain, termed P3-P9, consists of P3, P7, P8 and P9 helices and cannot assemble on its own (Cate et al. 1996; Michel & Westhof 1990). Adopting the correct tertiary structure of P3-P9 requires the presence of the P4-P6 domain (Michel & Westhof 1990). Hence, the P4-P6 domain works as structural stabilizer for the P3-P9 domain (Michel & Westhof, 1990).

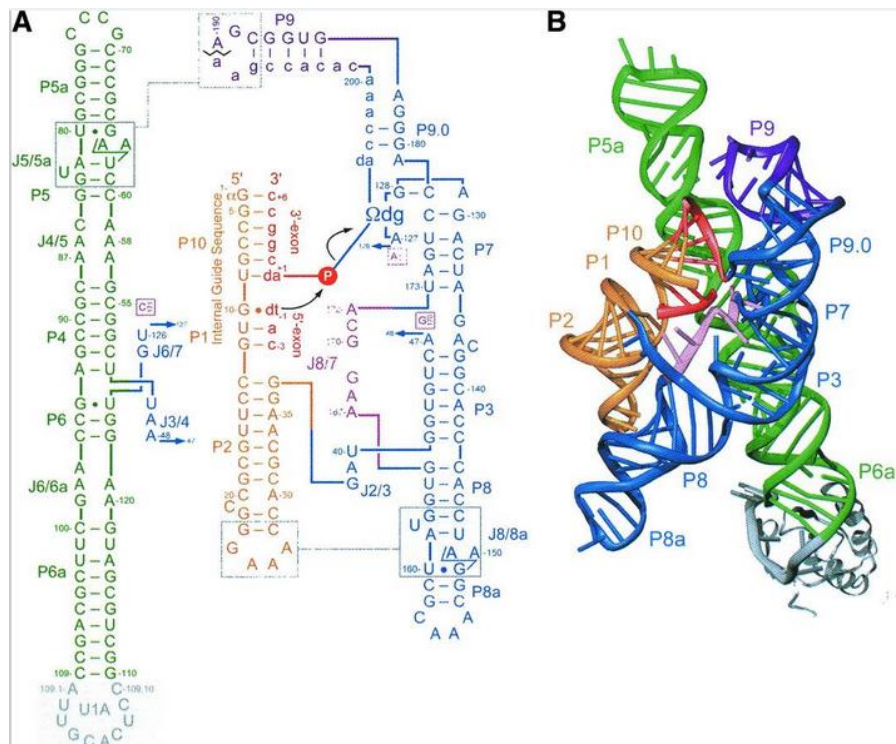


Figure 10: The secondary structure (A) and tertiary structure (B) of *Azoarcus* Ile-tRNA intron.

- A) The secondary structure of *Azoarcus*. The two major domains are labelled in green (P4-P6) and blue/purple (P3-P9). Splicing progress and its corresponding ligation reaction is indicated by black arrows.
- B) The tertiary structure of *Azoarcus*. The colour scheme follows that shown in part A. This figure was adapted from Adams, P.L 2004.

Helices are connected by 3-7 single-stranded nucleotides, called junctions. Similar to the duplexes, junctions do form specific structures, which are essential for correct folding and, in some cases, for successful substrate binding. The two major domains P4-P6 and P3-P9 are connected by J3/4 and J6/7. Base-triple interactions between these joining regions and P4 and P6 stabilize the scaffold and are essential for proper orientation of the major domains relative to each other (Cech 1990; Guo et al. 2004; Michel & Westhof 1990). The main helices of the P4-P6 domain are coaxially stacked and the P3-P9 domain wraps around the P4-P6 domain, forming a cleft into which the substrate helix (P1 or P10) dock into (Michel & Westhof 1990; Cech 1990; Pan & Woodson 1999). The core structure, formed by domain P4-P6 and P3-P9, is stabilized by long-range tertiary interactions (Cech 1990; Guo et al. 2004; Michel & Westhof 1990). Among these is the conserved tetraloop-receptor interaction between L9 and P5 (Guo et al. 2004; Michel & Westhof 1990), while other long-range substrates are subgroup specific. For example, in the *Tetrahymena* intron the 3' terminal P9.1 and P9.2 extensions stabilize the core structure, whereas the kissing loop is formed in the bI5 intron (Woodson 2005). Importantly, junctions J8/7 and J4/5 are positioned for direct interaction with P1. J8/7 is one of the very few nucleotide sequence that shows a high degree of conservation (Michel & Westhof 1990; Cech 1990; Pan & Woodson 1999; Guo et al. 2004). This conserved primary sequence interacts in P3-

P7, which contains the G-binding site, and P1, harbouring the 5' splice site and is thus critical for active site formation (Thomas R Cech 1990; Guo et al. 2004; Michel & Westhof 1990).

The asymmetric internal loop between P4 and P5 (J4/5, J5/4) forms two non Watson-Crick base pairs (A•A). This geometry is essential for the formation of hydrogen bonds between one adenine of each strand of the tandem A•A and the guanine of the wobble base pair G•U at the 5' splice site (A₅₈ and A₈₇ in *Azoarcus*, A₅₆ and A₈₃ in *Staphylococcus aureus* bacteriophage Twort) (figure 10 and 11) (Vicens & Cech 2006).

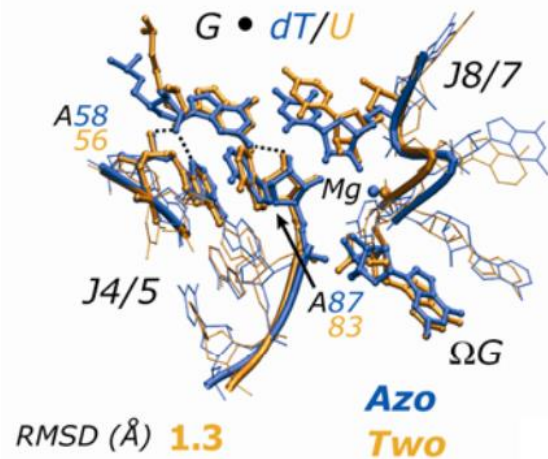


Figure 11: Interactions between J4/5 and the 5' splice site. Non Watson-Crick base pairs between J4/5 and 5' splice site are labelled in blue (*Azoarcus*) and yellow (*Staphylococcus aureus* bacteriophage Twort). This figure has been adapted from Vicens & Cech 2006.

Beside these conserved domains, the *Tetrahymena* group I intron contains the P5abc extension, which is only found in subgroup IC1 and IC2. Other subgroups lack this P5abc element, but instead have other additional structural elements (Cate et al. 1996). These peripheral elements stabilize the active conformation. In 1996, Cate et al. were able to establish a high resolution crystal structure (2.8Å) of the P4-P6 domain of the *Tetrahymena thermophila* group I intron. This crystal structure revealed how folding into the native conformation might be achieved (Cate et al. 1996).

The duplex P5a contains an asymmetric A-rich bulge, which maintains a certain distance to P4 (Cate et al. 1996). This bulge seems to play a key role in the architecture of P4/P6, as its deletion causes disorder and misfolding of the P4-P6 domain. Also found in the P4-P6 domain is a canonical 11 nucleotide long motif in P6a that acts as receptor for the GAAA tetraloop L5b. The GAAA tetraloop L5b docks in the minor groove of P6a at a 30° angle (Cate et al. 1996). Together, the GAAA loop and the A-rich bulge, are responsible for holding the halves of P4-P6 together (Cate et al. 1996).

3.3 Folding of group I introns

In 1998 Woodson and Brenowitz were the first, to obtain a deep insight into the folding process of the self-splicing group I intron of *Tetrahymena thermophila* (Sclavi et al. 1998). Using radiolysis of water with a synchrotron x-ray beam revealed the hydroxyl radical-accessible surface of the *Tetrahymena* group I intron with a resolution in 10 milliseconds (figure 12) (Sclavi et al. 1998). These experiments showed that RNA secondary structures fold in a time scale of 10^{-5} to 10^{-4} seconds, while

the tertiary structures fold in a time scale of 10^{-2} to 10^{-1} seconds (Sclavi et al. 1998). Resolving non-native structures and refolding them takes approximately 0.1 to 1 second (Sclavi et al. 1998).

The Mg^{2+} rich P5abc domains are folding independently of P4-P6, indicating the formation of a metal ion “core” (Cate et al. 1997; Sclavi et al. 1998). This is followed by folding of the P4-P6 domain. Complete folding of P4-P6 takes only a few seconds (Sclavi et al. 1998). Folding of P3-P9 occurs after formation of the P4-P6 domain. Tertiary interaction between those two major domains stabilize the P3-P9 structure (Sclavi et al. 1998; Cech et al. 1994; Doherty & Doudna 1997; Lagerbauer et al. 1994). The two major domains are connected and stabilized by interaction with the P2, P2.1 and P9.1 domains (Lehnert et al. 1996). The domains P2-P2.1 and P9.1-P9.2 wrap around the ribozyme and therefore interact with the two central domains (Lehnert et al. 1996; Sclavi et al. 1998; Doherty & Doudna 1997). Most of the tertiary interactions are formed within 10 seconds (Sclavi et al. 1998). However, the folding process from unfolded to active ribozyme, with P3 and P7 folding last, takes minutes (figure 12) (Sclavi et al. 1998).

While secondary structures are already formed at 42°C with no Mg^{2+} , the final folding with tertiary interactions can only occur with a sufficient amount of divalent metal ions (Sclavi et al. 1998).

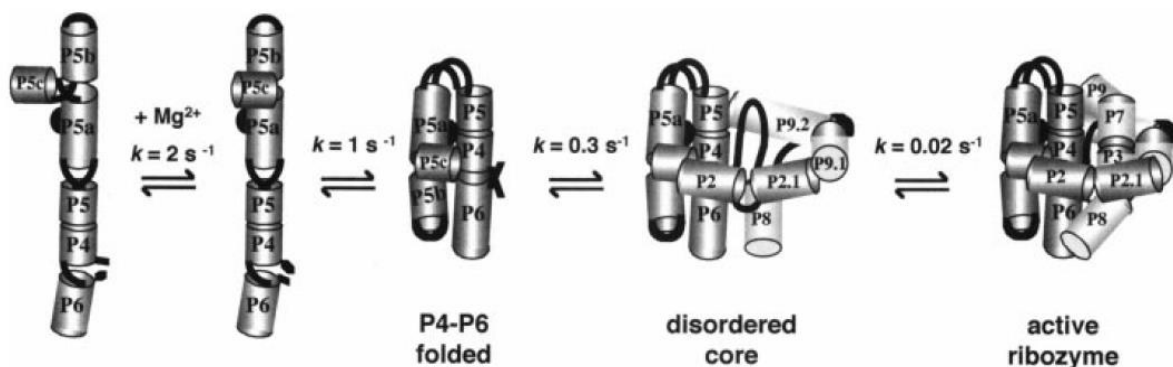


Figure 12: The folding process of the *Tetrahymena thermophila* ribozyme.

Addition of Mg^{2+} initiates the folding process starting with the P5a-P5c domain. Tertiary interactions with P4-P6 allow formation of the P3-P9 domain. The P2, P2.1, P9.1 and P9.2 wraps around the disordered core and stabilizes the ribozyme.

This figure has been adapted from Sclavi et al. 1998.

4. RNA binding proteins and their role in RNA folding

In the last decades, thousands of experiments showed the endless functional abilities of RNA. Although, *in vivo*, not a single RNA was found that worked completely independent, without any help of a protein. RNA binding proteins (RBP) cover a group of proteins, which interact with RNA to form ribonucleoprotein complexes (RNPs). Given that RNA is transcribed in the nucleus and transported into the cytoplasm, RNA binding proteins can be found in nucleus as well as in cytoplasm. Functions of RBPs are highly diverse, including RNA biogenesis, stability, transport and many more (Glisovic et al. 2008). Considering this diversity in function, RBPs also differ in their affinity and

specificity to RNA. This allows a very specific assembly of RNPs during RNA maturation and function, according to the specific circumstances (Glisovic et al. 2008).

Although there are hundreds of different RNA binding proteins, many of them share certain RNA-binding domains. Some of the most common RNA-binding domains are the K-homology domain, the RGG domain (arginine, glycine, glycine), the zinc finger, the RRM domains, the Piwi/Ago domain or the dsRBD, among others (Schroeder et al. 2004). Often RBPs do have more than one RNA-binding domain. It is estimated that more than 5% of eukaryotic genes encode proteins with the ability to bind RNA (Glisovic et al. 2008). This fact may be explained by the tremendous importance of post-transcriptional regulation in eukaryotes (Glisovic et al. 2008).

RBPs can be divided into two groups, non-specific and specific RNA binding proteins. While specific RBPs do show high affinity to their cognate RNAs, non-specific RBPs bind and interact with low affinity to a large number of target RNAs. However, the classification into these two groups is often controversial (Glisovic et al. 2008; Schroeder et al. 2004). Recently, Jankowsky and Guenther proposed that specific RNA binding proteins do favour certain RNA sequences (Guenther et al. 2013). Non-specific RBPs work in very similar ways, with the exception that the cell does not express their specific RNA sequence. Therefore, non-specific RBPs bind to available RNAs with a similar sequence to their ideal sequence, suggesting that both, specific and non-specific proteins, work with the same biochemical principle (Guenther et al. 2013). However, the more widespread opinion supports the idea of a classification into non-specific and specific RNA binding proteins.

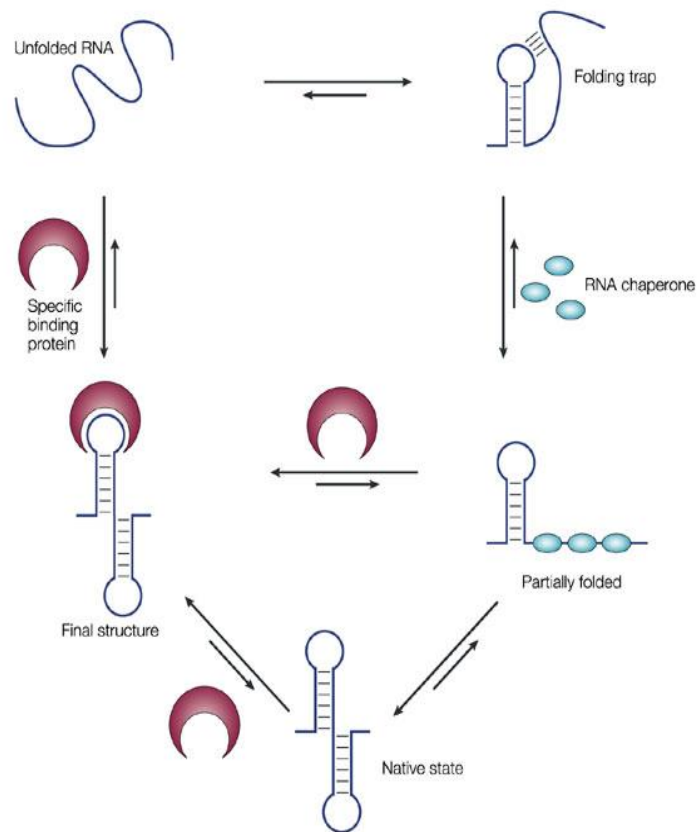
4.1 RNA cofactors and chaperones facilitate RNA structure formation

A large group of non-specific RNA binding proteins is covered by proteins with RNA chaperone activity (Weeks 1997; Waldsich et al. 2002; Herschlag et al. 1994). RNA chaperone activity refers to the ability of a protein to that assist in RNA folding by resolving kinetic traps (Weeks 1997; Waldsich et al. 2002; Herschlag et al. 1994). RNA often adopts stable, but non-native and in turn non-functional conformations. To escape from these kinetic traps, RNA chaperones destabilize the misfolded RNA, thereby resolving the inactive conformation and giving the RNA a chance to refold (figure 13) (Rajkowitsch et al. 2007; Schroeder et al. 2004; Weeks 1997; Waldsich et al. 2002). Proteins with RNA chaperone activity are involved in many different biological processes such as transport, replication or protein complex assembling (Rajkowitsch et al., 2007). RNA chaperone activity does not require an external energy source, such as ATP (Mayer et al. 2007; Rajkowitsch et al. 2007). Generally, the interaction between the RNA and the RNA chaperone is mainly based on electrostatic interactions, which are characterised by low specificity and weak binding (Schroeder et al. 2004).

Numerous RNA chaperones were identified to date, but their primary cellular function and protein structure are very diverse and the mechanism of action has only been characterized for a few RNA chaperones (Rajkowitsch et al. 2007). For example, RNA chaperones are heterogeneous found within abundant family of nuclear ribonucleoproteins (hnRNPs), which are known to interact during gene transcription (Bomsztyk et al. 2004; Marfatia et al. 2003) and within the family of cold shock proteins (CSPs) that specifically stimulate transcription as well as translation at low temperatures (Schroeder et al. 2004). Nevertheless, RNA

chaperones share some common features. Mutational analysis of StpA, an *E. coli* protein with its primary function in transcription regulation, showed that reducing its RNA binding affinity, leads to an increased RNA chaperone activity and therefore to destabilization of RNA (Mayer et al. 2007). On the other hand, increasing RNA binding affinity of proteins with chaperone activity results in RNA stabilization (Schroeder et al. 2004; Mayer et al. 2007; Waldsich et al. 2002).

Specific RNA binding proteins, also called RNA cofactors, are proteins that recognize specific RNA elements. Like RNA chaperones, RNA cofactors help RNA to reach its native conformation. However, RNA cofactors do not destabilize kinetically trapped RNAs, but support folding of thermodynamically unstable RNAs into its active form. Furthermore, RNA cofactors need to remain associated with the RNA molecule to maintain its conformation. Some cofactors, like Cyt18, LtrA or Cbp2 are known to lower the required Mg^{2+} concentration (Zemora & Waldsich 2010). Cyt18, the *Neurospora crassa* aminoacyl-tRNA synthase, assists in group I intron splicing (Zemora & Waldsich 2010). By stabilizing the catalytically active conformation of the intron, Cyt18 is known to guide RNA during structure formation. Mutational analysis also showed that Cyt18 is able to rescue intron structures suffering from increased instability (Zemora & Waldsich 2010).



Nature Reviews | Molecular Cell Biology

Figure 13: Influence of specific and non-specific RNA binding proteins on RNA folding. Specific binding proteins help folding of unfolded RNA in its native state. RNA chaperones help resolving trapped RNA molecules and refolding to their native state. This figure has been adapted from Schroeder et al.

4.2 DEAD-box proteins assist RNA in folding

Some conformational changes in RNA require energy. A large protein family, which binds and hydrolyses ATP resulting in nucleic acid structure changes, are DEAD-box proteins. DEAD-box proteins belong to the superfamily 2 RNA helicases (SF2). This class of protein is found in prokaryotes as well as in eukaryotes. Their ability of ATP hydrolysis is used for RNA helicase activity (figure 14). This double-strand separation mediates RNA folding, structural rearrangement and RNP remodelling (Jarmoskaite & Russell 2011; Jankowsky 2011).

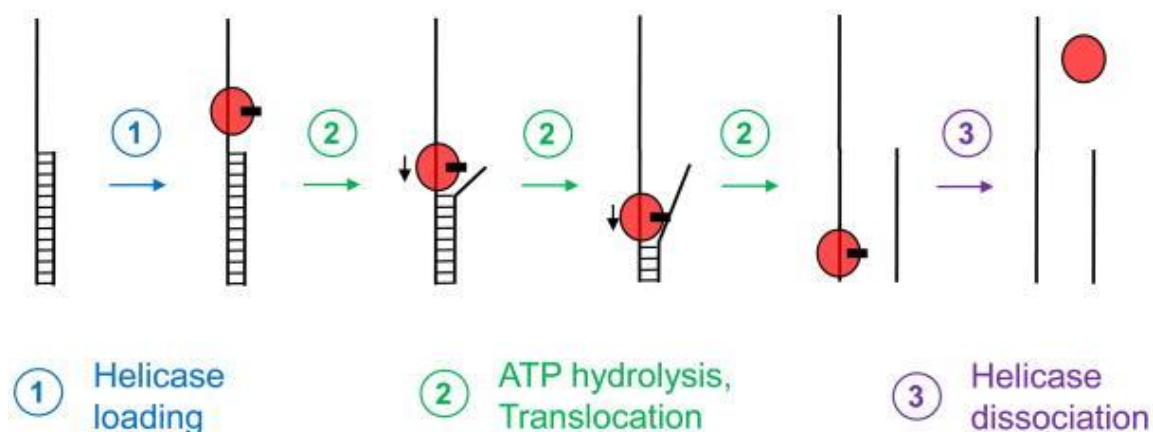


Figure 14: The working process of helicases.

Black lines indicate RNA/DNA strands. Red circle represents helicase with bound ATP (black rectangle). RNA/DNA double strand is loaded with the helicase. ATP hydrolysis leads to strand separation. The helicase dissociates after the completed strand separation. This picture was adapted from E. Jankowsky 2011.

Their structure is highly conserved, consisting of a core region with two recombinase A-like domains (Linder & Jankowsky 2011a). Domain 1 is found close to the helical N-terminus. It contains motif Q, I, II and III, which are responsible for ATP binding and hydrolysis and motifs Ia, Ib and Ic, used for RNA-binding. Domain 2, located at the C-terminal end, also harbours ATP hydrolysis motifs (VI and Va) and RNA binding motifs (IV, IVa and V) as well. Noteworthy, motif II is characterized by the conserved amino acid sequence aspartate-glutamate-alanine-aspartate (DEAD) (Jarmoskaite & Russell 2011). Although DEAD-box proteins show helicase activity, helices longer than 15 nucleotides cannot be unwound. Furthermore, helices longer than 25 nucleotides are not even recognized by DEAD-box helicases (Jarmoskaite & Russell, 2011). However, this inefficiency does not present a problem, considering that RNA rarely has duplexes longer than 10 base pairs. Still, due to their low processivity, DEAD-box proteins are not able to unwind more stable secondary structures (Jarmoskaite & Russell 2011).

In contrast to RNA chaperones, DEAD-box proteins recognize specific RNA elements such as secondary structures or 3'/5' overhangs preceding the duplex and require ATP function (Jarmoskaite & Russell 2011). Only a few helicases work unidirectional, are able to remove bound proteins and

work in a processive manner (Rajkowitsch et al. 2007). In addition to two RecA-like domains, these proteins contain more domains, assisting in substrate recognition and unwinding (Linder & Jankowsky 2011b). More helicases are represented by the non-processive helicase family. Non-processive helicases dissociate more often. Thus, these are far more less efficient in unwinding longer segments (Rajkowitsch et al. 2007).

5. Two proteins are necessary to promote bI5 splicing in yeast mitochondria

5.1 The yeast mitochondrial group I intron bI5

Evolution brought thousands and thousands of organism with unfathomable diversity. Despite this variety, there is one property that is shared by all organisms, the need of energy to develop and grow. Many organisms use a specific pathway called, the electron transport chain (ETC) for gaining energy. In eukaryotes ETC is established by an electrochemical proton gradient for synthesising adenosine triphosphate (ATP). One essential molecule of this pathway is cytochrome b, a subunit of the coenzyme QH₂-cytochrome c reductase, which catalyses the reaction of dihydroquinone and ferri-cytochrome c to quinone, ferro-cytochrome c and protons. These protons are used to generate the electrochemical proton gradient and in turn ATP.

In *Saccharomyces cerevisiae*, cytochrome b is a mitochondrial encoded protein, which is transcribed as pre-mRNA composed of 5 introns and 6 exons (Gampel & Tzagoloff 1987). Excision of the introns is essential for obtaining a functional protein. The terminal intron is called bI5 (figure 15). bI5 belongs to the autocatalytic group IA introns (Partono & Lewin 1990). In its natural form bI5 has a length of 966 nucleotides, with many adenine and uracil-rich regions. While the catalytic core is conserved among all group I introns, the peripheral elements differ. In contrast to the *Tetrahymena thermophila* group I intron, bI5 lacks the P5abc domain, but has additional peripheral elements P7.1, P7.2 and P9.1. The natural bI5 construct is also characterized by additional large insertions in L1, L6, L6b and L8. These insertions are not part of the catalytic core. Therefore, deletion of these three peripheral extensions does not influence the splicing efficiency (Weeks & Cech 1995).

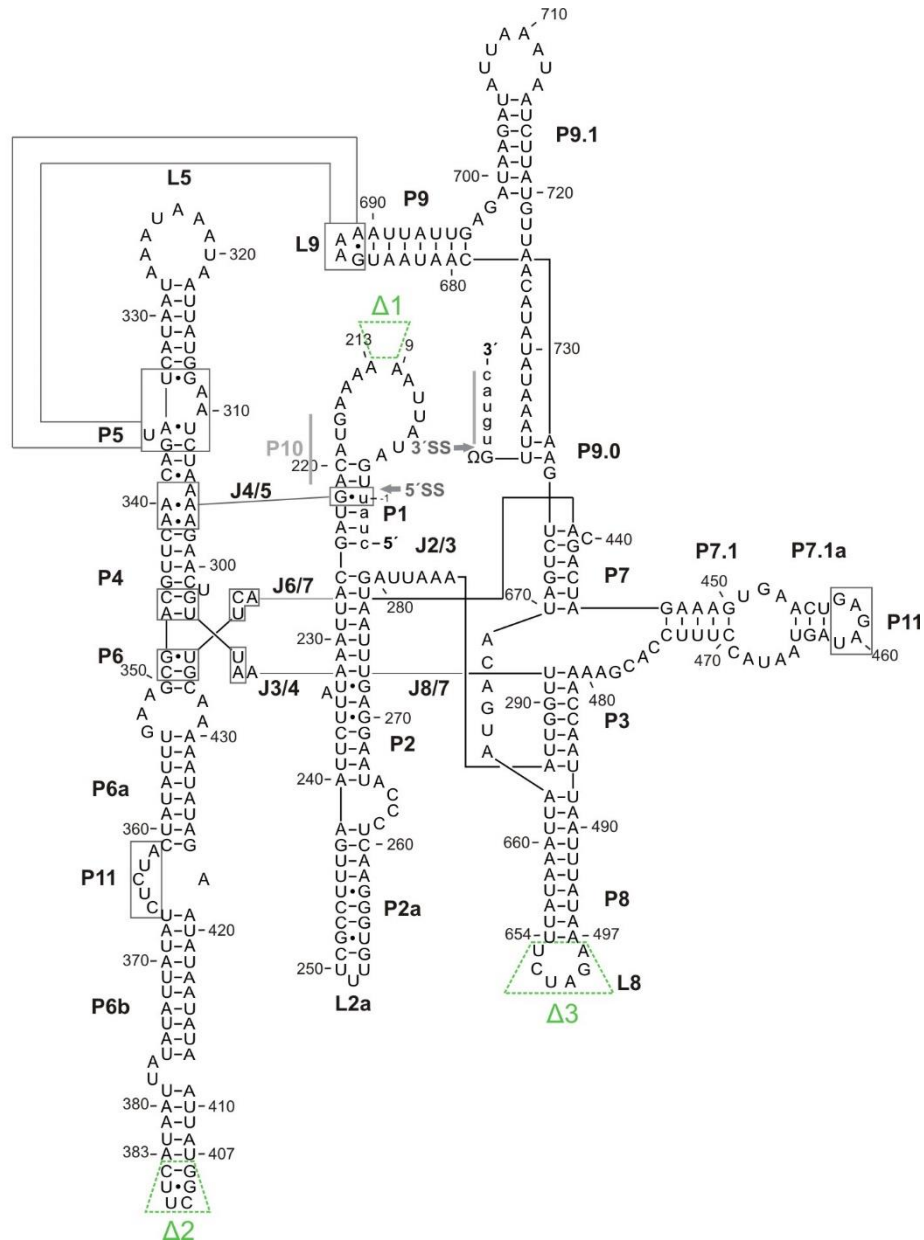


Figure 15: The secondary structure of bI5.

$\Delta 1$, $\Delta 2$ and $\Delta 3$ indicate truncations, which were made for simplifying further *in vitro* experiments. $\Delta 1$ lost 204 nucleotides, $\Delta 2$ 24nts and $\Delta 3$ 157nts. “P” indicates paired regions, while “J” indicates junction regions. A pseudoknot is found in P11 (L7.1a and J6a/6b). Dark grey lines indicate a tetraloop-receptor interaction between P9 and P5. Also labelled in dark grey, the interactions between the non-Watson-Crick base pair A•A and G•U wobble base pair at the 5' splice site. This figure has been adapted from Sachsenmaier 2014.

Although bI5 is a self-splicing intron, it requires some cofactors to execute the splicing reaction efficiently *in vivo* and *in vitro* (Gampel & Tzagoloff 1987; Gampel & Cech 1991). *In vitro*, bI5 can fold into its native structure with help of a high concentration of magnesium ions, in the absence of assisting proteins (Gampel & Tzagoloff 1987; Gampel & Cech 1991). *In vivo*, the presence of the cofactors Cbp2 and Mss116p is necessary to reach the native form of bI5 (Weeks & Cech 1995; Séraphin et al. 1987). Notably, in the presence of the splicing cofactor Cbp2, the Mg^{2+} ion

concentration can be significantly lowered to near-physiological amount to allow efficient splicing *in vitro* (Weeks & Cech 1995).

5.2 Splicing cofactor Cbp2

Efficient splicing of bI5 is achieved by forming its native structure. *In vitro*, bI5 does not necessarily require protein cofactors, but can successfully reach its native conformation by a sufficient non-physiological concentration of metal ions. *In vivo*, however, native conformation of bI5 is reached in a different way. Physiological conditions provide much less metal ions, assuming that bI5 needs a stabilized RNA cofactor. Cbp2 is the nuclear-encoded cytochrome b pre-mRNA splicing cofactor that assists bI5 during splicing reactions (McGraw & Tzagoloff 1983). Given that bI5 splice both at high metal ion concentration and at low Mg^{2+} in the presence of Cbp2 *in vitro* lead to the assumption that Cbp2 does not directly contribute to the splicing reaction and instead assists bI5 in adopting its native conformation (McGraw & Tzagoloff 1983; Weeks & Cech 1995). Inactivating Cbp2 via mutation resulted in deficiency of the respiratory chain (Gampel & Cech 1991). Splicing of other introns of cytochrome b pre-mRNA was not influenced in the *cbp2*-deficient yeast strain suggesting that Cbp2 serves only as splicing cofactor for bI5 (Gampel & Cech 1991). Tirupati and Lewin proved via mutational analysis that the interaction site of Cbp2 with bI5 are located at its N-terminus. Mutating specific amino acids lead to reduced or complete loss of function (Tirupati et al. 1999).

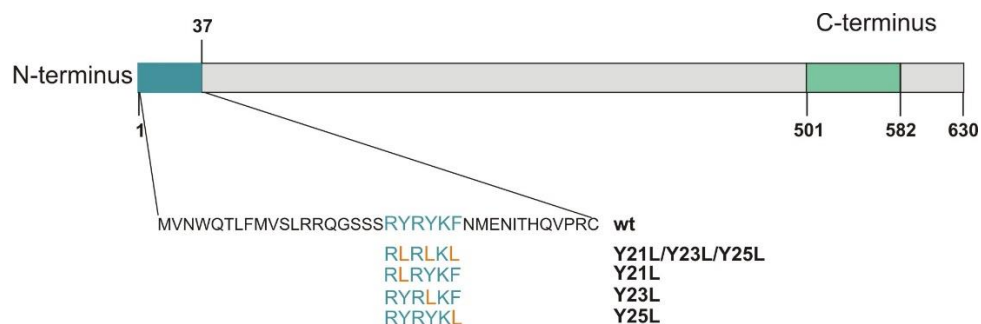


Figure 16: Primary sequence of Cbp2.

The aromatic amino acids lysin (K), arginine (R) and aromatic amino acids at the N-terminus represent the RNA binding site proved by mutational analysis by Tirupati and Lewin. This figure has been adapted from Tirupati et al. 1999.

Cbp2 consists of 630 amino acids residues, with a total molecular weight of 73,67kDa. With 89 basic amino acids and 75 acidic amino acids, Cbp2 has an overall positive charge and contains in addition numerous aromatic amino acids. The basic as well as the aromatic amino acids are both prone to interact with RNA (figure 16) and distributed over the entire primary structure of Cbp2. Notably, Cbp2 does not share any homology with other proteins and as such does not contain any conserved motifs.

Group I introns are capable of catalysing their own excision during the splicing process. Two consecutive ester transfer reactions result in ligated exons and a free intron. However, for a successful splicing reaction, self-splicing introns need to adopt native conformations. The fifth intron of yeast cytochrome b pre-mRNA is bI5, which belongs to the group I subgroup IA. Splicing of bI5 requires assembly of ribonucleoprotein (RNP) enzyme (Weeks & Cech 1996). In case of bI5 this RNP is composed out of the intron itself and the splicing cofactor Cbp2. Under near-physiological metal ion concentrations (7mM Mg^{2+}), bI5 is able to collapse to a near-native state (McGraw & Tzagoloff 1983; Weeks & Cech 1995). Importantly, formation of a collapsed intermediate is facilitated by Mg^{2+} ions (McGraw & Tzagoloff 1983; Weeks & Cech 1995). Cbp2 is then able to capture this near-native conformation, leading to the formation of the native, splicing-competent state (Weeks & Cech 1995; Weeks & Cech 1996). Although Cbp2 is not required for establishing the initial tertiary structure, it is necessary for stabilizing the native conformation and enhances the splicing rate constant by an order of magnitude (Weeks & Cech 1996).

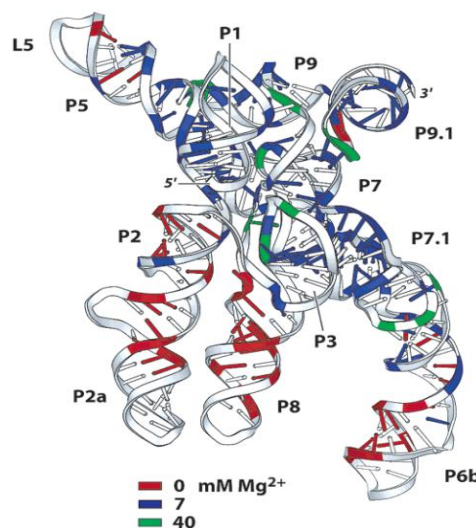


Figure 17: Folding of bI5 core with different magnesium concentrations
Red, blue and green coloured backbone or bases (adenosines) indicate protection of 2'-amine acylation and N1 methylation with different magnesium concentrations. This figure has been adapted from Chamberlin & Weeks 2003.

However, the pathway of achieving this native structure can differ *in vitro* and *in vivo*. *In vitro* experiments demonstrated that bI5 can fold into its native structure without RNA binding proteins, such as Cbp2 or Mss116p, as high concentrations of Mg^{2+} can compensate the absence of Cbp2 and allow native structure formation and in turn splicing (Weeks & Cech 1995; Weeks & Cech 1996; McGraw & Tzagoloff 1983). In case of bI5, the optimal splicing efficiency is achieved at $\sim 50\text{mM}$ Mg^{2+} , in the absence of assisting proteins (Weeks & Cech 1995; Gampel & Tzagoloff 1987). However, metal ions alone do not initiate splicing reactions. Even under high Mg^{2+} concentration conditions, guanosine cofactors are required for starting the splicing process. Under near-physiological

conditions, 7mM Mg^{2+} , bI5 requires Cbp2 for stabilization of near-native state, in which secondary and part of tertiary structure are formed, allowing formation of the native state. (figure13) (Weeks & Cech 1995; Weeks & Cech 1996; McGraw & Tzagoloff 1983).

5.3 The structure and function of the DEAD-box helicase Mss116p

The yeast protein Mss116p belongs to the helicase superfamily 2. It is a DEAD-box helicase, which binds and hydrolyses ATP in order to unwind short RNA duplexes (S  raphin et al. 1987).

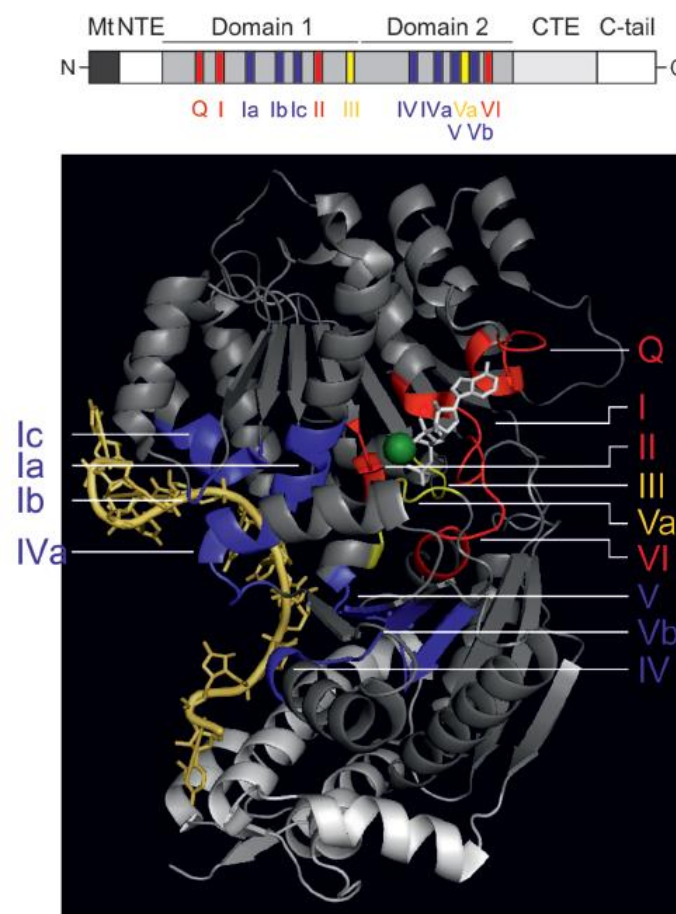


Figure 18: DEAD-box protein Mss116p

Different motifs are shown in different colours. Blue: RNA binding, red: ATP binding and hydrolysis, yellow: connection between ATPase activity and RNA binding. Dark grey represents domain 1 and 2 of Mss16p, light grey CTE. RNA is coloured in yellow and AMPNP (non-hydrolysable ATP analog) in white. Green sphere represents magnesium ion. This figure has been adapted from Sachsenmaier & Waldsich 2013.

Mss116p shows a DEAD-box protein characteristic structure (Huang et al. 2005). The helical core consists of two RecA-like domains with at least eleven conserved motifs (Del Campo & Lambowitz 2009; Huang et al. 2005; Liebeg et al.; Sachsenmaier & Waldsich 2013). The N-terminal domain 1 starts with motif Q, which, together with motif I, forms a binding pocket that recognizes the adenine base of ATP. Motif II and III are responsible for hydrolysing the bound ATP. The adjacent motif Ia, Ib, and Ic are known as RNA binding motifs. The C-terminal domain 2 harbours the RNA binding motifs

IV, IVa, V and Vb together with QxxR, and ATP binding motifs VI and Va (Sachsenmaier & Waldsich 2013). The SAT motif (motif III) serves as connector between ATP binding, ATP hydrolysis and RNA binding. Besides the helicase core, some DEAD-box proteins, like Mss116p, have a non-conserved C-terminal extension (CTE) (Huang et al. 2005; Del Campo & Lambowitz 2009). Among DEAD-box proteins, this domain is variable in sequence and structure. Although CTEs are believed to participate in substrate interaction, the mechanism is not fully understood (Mallam et al. 2012; Del Campo & Lambowitz 2009; Huang et al. 2005; Liebeg et al.).

In the absence of ATP, Mss116p exhibits an open conformation, in which the two helical core domains are moved away from each other (figure 19) (Del Campo & Lambowitz 2009). The presence of ATP results in cooperative binding of ATP and RNA, resulting in a collapsed conformation (Mallam et al. 2012)

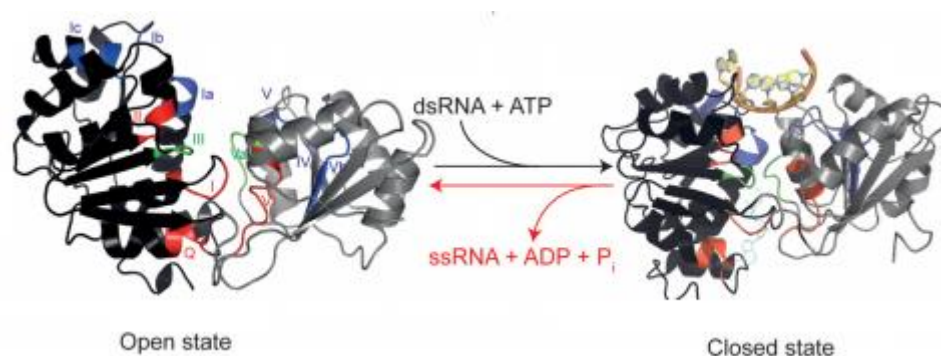


Figure 19: Conformational changes in DEAD-box helicases.

The DEAD-box protein YxiN is shown in the open and closed conformation. With binding of ATP the affinity for RNA is increased and the protein is in closed state. Hydrolysis of ATP leads to conformational changes resulting in a low affinity for RNA and the protein being in an open state. RNA binding motifs are coloured in blue, the ATP binding site in red and motifs mediating the communication between RNA binding and ATP binding/hydrolysis in green. This figure has been adapted from Samatanga & Klostermeier 2014.

The crystal structure of Mss116p in complex with ssRNA revealed that Mss116p has five to six nucleotides interacting with the backbone of a single-stranded RNA (Del Campo & Lambowitz 2009; Mallam et al. 2012). While the helicase domains are conserved among DEAD-box proteins, the sequence in RNA binding motifs has lower conservation (Del Campo & Lambowitz 2009; Mallam et al. 2012). This is reasonable, because RNA binding motifs mostly interact with the RNA sugar-phosphate backbone. The mechanism of unwinding of dsRNA is not fully understood yet. Structural analysis by Mallam & Lambowitz (Mallam et al. 2012) suggests that the central base pair of the dsRNA is disrupted by the conserved post-II region in domain 1. Formation of the closed helicase conformation leads also to a bend of one RNA strand, which is induced by motif Ib and a second bend involved by the interaction of the RNA with the non-conserved C-terminal extension (Fedorova et al. 2010; Del Campo & Lambowitz 2009; Mallam et al. 2012). Importantly, the observed bent conformation of the ssRNA is incompatible with the A form geometry of an RNA duplex. Thus, it has been proposed that

bending of the RNA contributes to unwinding (Huang et al. 2005; Zingler et al. 2010; Sachsenmaier & Waldsich 2013). However, the full mechanism remains unclear.

Mss116p is a mandatory factor in both group I and group II introns. However knocking out *mss116* results in complete loss of splicing of ai5 γ , a group II intron, but only in a reduced splicing activity of bl5, a group I intron (Sachsenmaier & Waldsich 2013). This suggests that Mss116p has a distinct mechanism for promoting group II introns (ai5 γ) and group I introns (bl5) (Sachsenmaier & Waldsich 2013). The role of Mss116p in either RNA folding pathway is not fully understood. However, due to the lack of Cbp2 to discriminate between misfolded and correctly folded RNA, Mss116p might assist in this process (Sachsenmaier & Waldsich 2013).

Mutation experiments showed that ATP-binding and hydrolysis play a key role in Mss116p's function. Mutating the ATP hydrolysis motif, abolished mitochondrial splicing (Huang et al. 2005; Zingler et al. 2010; Sachsenmaier & Waldsich 2013). However, sufficient duplex unwinding does not require ATP hydrolysis, but is achieved by ATP binding (Liu et al. 2008). ATP hydrolysis is only required for Mss116p turnover (Henn et al. 2008).

6. Mss116p and Cbp2 cooperate to facilitate bl5 folding in vivo

In vitro Cbp2 is sufficient to promote efficient bl5 splicing, while other proteins are required in yeast mitochondria. As discussed earlier, Mss116p is a mandatory factor in all mitochondrial group II and partially in group I introns. However, the specific interactions of Mss116p with the group I intron bl5 and its cofactor Cbp2 remain unclear. Possibly, Mss116p might assist Cbp2 to reach and stabilize the near native conformation of bl5. The binding of the two proteins may occur hierarchically or in a competition for the binding site. Another possible interaction of Mss116p might occur with non-native conformations. Precursor mRNA is bound to Cbp2 and forms a stable, kinetically trapped, non-native structure. Mss116p helps to resolve this conformation, which leads to the collapsed and further to the near-native conformation (figure 21). Conceivably, Mss116p and Cbp2 could also work independently. While Mss116p helps resolving kinetically trapped conformations and assists in reaching the near-native core, Cbp2 captures this state and finalizes the folding process of bl5.

Recently, the first insights into the role of Mss116p and Cbp2 in bl5 folding in vivo was obtained (Sachsenmaier 2014). Knocking out *cbp2* leads to a loss of splicing activity in yeast mitochondria

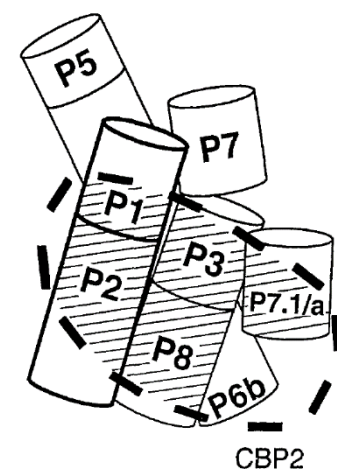


Figure 20: Assembly of the bl5/Cbp2 complex

Dashed line indicates bl5 surface bound to Cbp2. This picture has been adapted from Weeks & Cech, 1996.

(Weeks & Cech 1995). Also Mss116p is not able to compensate for Cbp2 (Sachsenmaier 2014). Knocking out Mss116p, but still having active Cbp2, results in a 55% loss of splicing activity, which leads to the assumption that Mss116p rather assists during the bI5 Cbp2-facilitated splicing (Sachsenmaier 2014). Structural analysis showed that stem P8 of bI5 is not formed in the absence of Cbp2. This suggests that Cbp2 might bind to P8 and facilitates Watson-Crick base pairing (Sachsenmaier 2014). Cbp2 might also stabilize stem P1 in later steps of folding, which might be necessary for P1 docking to the catalytic core of bI5 (Sachsenmaier 2014). Native structures around the G-binding site are also only formed in the presence of Cbp2 (Sachsenmaier 2014).

The knock-out of *mss116p* reveals only minor changes in the structure of bI5. While the modification pattern of bI5 is similar in *cbp2*- and *mss116p*-knockout strains at the Cbp2-binding site in P7.1, the P8 stem forms correctly in absence of Mss116p. Also, stem P1 forms independently of Mss116p (Sachsenmaier 2014). Further structural analysis suggests that Mss116p might assist Cbp2-facilitated bI5 folding by resolving misfolded structures at the 5' splice site (Sachsenmaier 2014). While the intron core is formed properly in the *mss116p* knock-out strain, the active site and P1 docking do not occur correctly (Sachsenmaier 2014). The fact that in *mss116p* knock-out strain bI5 splicing is reduced to 55%, this suggests that a population of 55% of bI5 requires Mss116p for proper splicing. If bI5 is kinetically trapped or splicing is slowed down without Mss116p remains unclear. On the one hand, Mss116p is known to inhibit splicing of *Tetrahymena* LSU intron, because of partial unfolding (Yang & Jankowsky 2006; Halls et al. 2007). This supports the theory that Mss116p resolves kinetically trapped conformations. On the other hand, some DEAD-box helicases are known to work as RNases by releasing protein - pre-mRNA interactions (Schroeder et al. 2004). Thus, Mss116p might disrupt the binding of Cbp2 and bI5, to allow further folding processes (Sachsenmaier 2014).

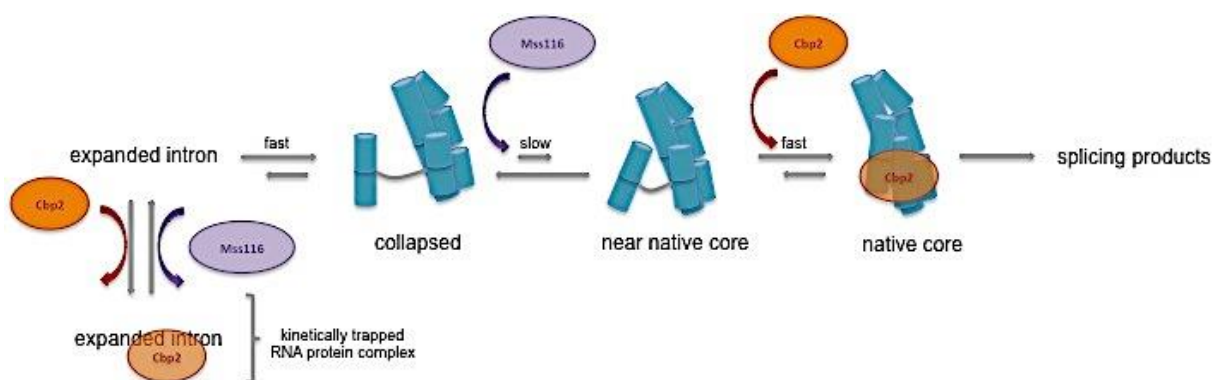


Figure 21: The protein assisted folding pathway of bI5 in vivo.

Interaction of Cbp2 with the expanded intron can lead to a stable, but kinetically trapped conformation. Mss116p might help to resolve this non-native structure. Without interaction of Cbp2, bI5 is able to reach the collapsed state and further the near-native state in presence of Mss116p. This near-native conformation is captured by Cbp2 and folding processed gets finalized. This figure has been adapted from Sachsenmaier 2014.

Scientific aims of the project

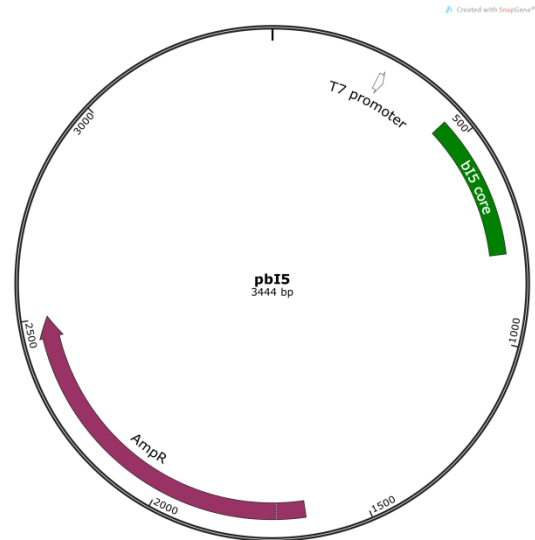
The last decade was a period of prosperity in RNA research. Still, many RNA functions remain unknown. However, to fulfil its function, RNA has to be folded properly. But, prior to the focus on RNA folding, it is necessary to determine RNA structural elements and their interactions (Schroeder et al. 2004). In this project we investigated the *S. cerevisiae* mitochondrial group I intron bI5 and its way from unfolded to folded, splicing-competent state. *In vivo* bI5 requires two splicing cofactors to reach its native conformation, Mss116p and Cbp2 (Gampel & Tzagoloff 1987; Weeks & Cech 1995). While the DEAD-box helicase Mss116p assists in the folding process of group I and group II introns, Cbp2 is just required for group I introns (Gampel & Tzagoloff 1987; Weeks & Cech 1995; Fedorova et al. 2010; Huang et al. 2005; Liebeg et al.; Solem et al. 2006). *In vitro*, however, proper bI5 folding can be achieved by the addition of near-physiological Mg^{2+} concentrations and Cbp2, but not Mss116p. To understand the *in vivo* interactions of proteins with pre-mRNA, it is necessary to define the roles of both proteins during the splicing and folding process of bI5. Therefore, we aimed at understanding the role of either protein in stimulating bI5 splicing and at characterising their dissociation constant to bI5. As such, we expect to shed light into whether RNP assembly depends on a strict order of events and the obtained information is required for proceeding with structural analysis of bI5.

Materials and Methods

1. Plasmids

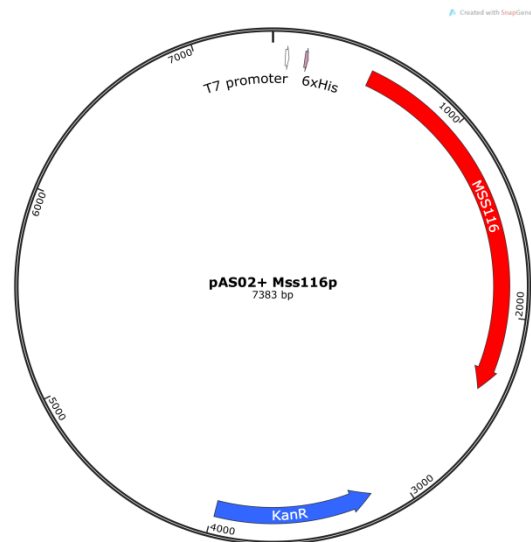
pbI5

The plasmid pbI5 was kindly provided by K. M. Weeks (University of North Carolina, Chapel Hill, USA). It contains a truncated variant of the bI5 intron, as some peripheral elements were deleted and the shortened intron is flanked by exonic sequences (Weeks & Cech 1995). Despite these deletions, the truncated bI5 can still form its native conformation. While the wild-type sequence counts 966 nucleotides, this shorter version consists of only 368 nucleotides (Weeks & Cech 1995). In the truncated bI5 207 nucleotides were removed from L1 and 23 nucleotides from L6b. L6b was closed with a tetraloop C(UUCG)G. Additionally, L8 lacks nucleotides 502-653 and was closed with AGAUCU.



pAS02

The plasmid pAS02 harbours the ORF of Mss116p, of which the MLS (=amino acid 1-37) was deleted (Debeljak 2013). It therefore was used for recombinant protein expression in Rosetta™ 2(DE3)pLysS Singles™ (Novagen®).



2. Strains

Rosetta™ 2(DE3)pLysS Singles™ Competent Cells Novagen®

These competent cells were obtained from Novagen®. They were used for eukaryotic protein expression. Rosetta™ 2 strain is an *E. coli* BL21 derivative, which supplies tRNAs for 7 rare codons on a chloramphenicol-resistant plasmid and the T7 RNA pol has been integrated into the *E. coli* genome under the control of *plac*. Thus, the expression of the recombinant protein is induced by IPTG which allows expression of the T7 RNA pol which in turn transcribes the *MSS116* gene.

Genotype: $F^- ompT hsdS_B(r_B^- m_B^-) gal dcm$ (DE3) pLysSpRARE2³ (CamR®)

E. coli DH5α

E. coli DH5α were used for transformation to propagate the plasmid.

Genotype: $F^- \Phi 80/lacZ\Delta M15 \Delta(lacZYA-argF) U169 recA1 endA1 hsdR17 (rK^-, mK^+) phoA supE44 \lambda^- thi-1 gyrA96 relA1$

3. Transformation in Escherichia coli DH5α

100μL competent DH5α cells were thawed on ice. 50ng of *pbl5* were mixed with competent cells and incubated on ice, for 30 minutes followed by a heat shock at 42°C for 1 minute. After 20 minutes on ice again, 1mL of pre-warmed LB Medium was added to the sample. Following a 60 minutes incubation step at 37°C followed, the sample was centrifuged at 4000 rpm for 1 minute. The supernatant was removed and the cell pellet was resuspended in 150μL LB and the suspension was plated on LB amp plates.

Required solutions

LB medium

5g NaCl

5g yeast extract

10g tryptone

Fill up to 1L with ddH₂O and autoclave.

LB-amp-plates

5g NaCl

5g yeast extract

10g tryptone

15g agar

Fill up to 1L with ddH₂O and autoclave.

After cooling, add 1mL 1000 x ampicillin [f.c. 0.1mg/mL]. The solution is poured in petri dishes. Store plates at 4°C after solidification.

4. Midi prep

To extract and purify plasmid DNA from *E. coli* DH5α cells the Pure Yield™ Plasmid Midiprep System from Promega was used, according to the manufacturer's protocol with the following exception

To achieve a higher DNA concentration the purified plasmid was precipitated as follows:

1μl Glycogen [10mg/mL]
 2μL 0.5M EDTA pH 8.0
 2.5 x vol. EtOH/0.3M NaOAc

The sample was stored at -20°C for at least 1 hour. After centrifugation (4°C with full speed for 30 minutes) the supernatant was discarded and the pellet was dried at room temperature for 10 minutes. The pellet was resuspended in 15μl ddH₂O.

Required solutions

EtOH/0.3M NaOAc
 0.5M EDTA pH 8.0
 Glycogen [10mg/mL]
 3M NaOAc pH 5.5

5. Restriction digest

For the *in vitro* transcription a linearization of pbl5 was necessary. Therefore the plasmid was processed with a restriction digest with XbaI as restriction enzyme.

100μg psbl5
 12μL 10 x NEBuffer 4
 1.2μL 100 x BSA
 7μL XbaI (20U/μL)
 Fill up to 120μL with ddH₂O

To get rid of the enzyme, a phenol-chloroform extraction was performed followed by precipitation (see Material and Methods 5.).

Required solutions

10 x NEBuffer 4

100 x BSA

*Xba*I (20U/ μ L)**6. Phenol-chloroform purification**

The aqueous DNA sample was purified with an equal volume of TE-saturated phenol mixed 1:1 with CI was added to the DNA sample. After vortexing, the tube was centrifuged for 5 minutes at 15.000xg. The aqueous phase was transferred into a new tube. An equal volume of chloroform:isoamyl alcohol (CI) (24:1) was added, vortexed and centrifuged for 5 minutes at 15.000xg. The aqueous phase was again transferred into a new tube.

For optimum yield, a back-extraction of the original organic phase was performed. First, an equal volume of 1x TE was added to the organic phase. After vortexing and centrifugation, the aqueous phase was transferred in a new tube and extracted with CI. Afterwards aqueous phase was combined with that other one and precipitated.

1 μ L glycogen [10mg/mL]2 μ L 0.5M EDTA pH 8.0

2.5 x vol. EtOH/0.3M NaOAc

The sample was stored at -20°C for at least 1 hour and afterwards centrifuged at 4°C for 30 minutes (full speed). After discarding the supernatant, the pellet was dried at room temperature for 10 minutes. In a final step, the pellet was resuspended in 15 μ L ddH₂O.

Required solutionsTE buffer

10mM Tris-HCl pH 8.0

1mM EDTA pH 8.0

TE-saturated phenol

Chloroform:isoamyl alcohol solution (24:1)

1x TE (10mM Tris-HCl pH 8.0/1mM EDTA pH 8.0)

Ethanol p.a.

3M NaOAc pH 5.5

Glycogen [10mg/mL]

0.5M EDTA pH 8.0

7. In vitro transcription

7.1 In vitro transcription - method 1

In vitro transcription was performed for synthesizing RNA, which later was used for splicing and filter binding assays. *In vitro* transcription was performed with the MEGAscript® T7 Transcription Kit from Life Technologies, according to the manufacturer's protocol. Instead of recommended 20µL reaction mix, 40µL were assembled.

7.2 In vitro transcription - method 2

In vitro transcription was performed for synthesizing RNA, which later was used for filter binding assays. *In vitro* transcription was performed according to the following protocol:

2.5µg	linearized pbl5	
5µL	10 x TRA buffer	
0.5µL	1M DTT	
3µL	100mM ATP	
3µL	100mM GTP	
3µL	100mM CTP	
3µL	100mM UTP	
1µL	RNase Inhibitor [40U/µL]	
4µL	T7 RNA Polymerase (home-made)	
Fill up to 50µL with ddH ₂ O		

Incubate the reaction mix 37°C for 3 hours at. To digest the DNA template 2µL DNase I RNase-free [40U/µL] were added and the sample was kept at 37°C for 15 minutes.

Required solutions

10 x TRA buffer

400µL	1M Tris-HCl pH 7.5	[f.c. 400mM]
260µL	1M MgCl ₂	[f.c. 260mM]

30µL 1M Spermidine [f.c. 30mM]

Fill up to 1mL with ddH₂O. Store at -20°C.

1M DTT

100mM ATP/GTP/CTP/UTP

DNase RNase-free [40U/µL]

RNase Inhibitor [40U/µL]

T7 RNA Polymerase (home-made)

7.3 Transcript purification

To remove the enzymes, excess nucleotides, small RNA fragments and buffer components, the sample has been purified. The purification was performed with the MEGAclean™ Transcription Clean-Up Kit from Life Technologies, according to the manufacturer's protocol.

7.4 RNA body labelling – method 1

Body labelling was accomplished by incorporating α -P³²-UMP during transcription of bI5. The transcribed RNA was later used for splicing assays. Transcription was performed via MEGAscript® T7 Transcription Kit according to the manufacturer's protocol.

7.5 RNA body labelling – method 2

Body labelling was accomplished by incorporating α -P³²-UMP during transcription of bI5. The transcribed RNA was later used for splicing assays. Transcription was performed according to the following protocol:

2.5µg linearized pbI5

5µL 10 x TRA buffer

0.5µL 1M DTT

3µL 100mM ATP

3µL 100mM GTP

3µL 100mM CTP

1.5µL 100mM UTP

1.5µL α -P³²-UTP [10µCi/µL] [3000Ci/mmol]

1 μ L RNase Inhibitor [40U/ μ L]
 4 μ L T7 RNA Polymerase (home-made)
 Fill up to 50 μ L with ddH₂O.

Incubate the reaction mix at 37°C for 1.5 hours at 37°C. To digest the DNA template 2 μ L DNase I RNase-free [40U/ μ L] were added and the sample was kept at 37°C for 15 minutes.

Required solutions

10 x TRA buffer

400 μ L 1M Tris-HCl pH 7.5 [f.c. 400mM]
 260 μ L 1M MgCl₂ [f.c. 260mM]
 30 μ L 1M Spermidine [f.c. 30mM]
 Fill up to 1mL with ddH₂O. Store at -20°C

1M DTT

100mM ATP/GTP/CTP/UTP

α -P³²-UTP [10 μ Ci/ μ L] [3000Ci/mmol]

T7 RNA Polymerase (home-made)

RNase Inhibitor [40U/ μ L]

DNase I RNase-free [40U/ μ L]

1M Spermidine [f.c. 30mM]

7.6 RNA end labelling

Radioactive 5'end labelling of a transcript first requires dephosphorylation of the 5'-phosphate. Subsequently the γ -P³² phosphate group of γ -P³²-ATP is transferred onto the 5'OH end of dephosphorylated RNA. For removal of the 5'-phosphate, the following protocol was used.

300pmol bI5 RNA
 2 μ L Alkaline phosphatase [1U/ μ L]
 120 μ L ME buffer

The sample was incubated at 37°C for 30 minutes. After adding 30 μ L 3M NaOAc pH 5.0 and 100 μ L ME buffer, a phenol extraction was performed. 250 μ L water-saturated phenol was added, vortexed and centrifuged for 5 minutes at 20.000xg. The aqueous phase was transferred into a new tube and

250µL chloroform:isoamyl alcohol (24:1) was added. After vortexed, the sample was centrifuged at 20.000xg for 5 minutes. The received aqueous phase was again transferred into a new tube and kept on ice. To increase the final yield, a back extraction was performed with the organic phase. As such, 30µL 3M NaOAc pH 5.0 and 210µL ME buffer were added to the initial organic phase. After vortexing, the sample was centrifuged at 20.000xg for 5 minutes. The aqueous phase was transferred into a new tube. A CI purification step followed. The two aqueous phases were combined precipitated.

1µl Glycogen [10mg/mL]
 2µL 0.5M EDTA pH 8.0
 2.5 x vol. EtOH/0.3M NaOAc

The sample was stored at -20°C for at least 1 hour and afterwards centrifuged at 4°C for 30 minutes (full speed). After discarding the supernatant, the pellet was dried at room temperature for 10 minutes. In a final step, the pellet was resuspended in 10µL ME buffer and concentration was measured.

5' End labelling of the dephosphorylated transcript was made, according to the following protocol:

1µL 10µM dephosphorylated bI5 RNA
 7µL γ -P³²-ATP [10µCi/µL] [6000Ci/mmol]
 1µL 10 x PNK buffer
 1µL T4 polynucleotide kinase [10U/µL]

The sample was incubated at 37°C for 30 minutes.

For purification 10µL ME buffer were added. To remove excess γ -P³²-ATP illustra MicroSpin G-25 columns were used, according to the manufacturers protocol (GE Healthcare).

Required solutions

ME buffer

10mM MOPS pH 6.0
 1mM EDTA pH 8.0

Phenol, water-saturated

Chloroform:isoamyl alcohol solution (24:1)

3M NaOAc pH 5.0

Ethanol p.a.

0.5M EDTA pH 8.0

10xPNK NEB buffer

γ -P³²-ATP [10 μ Ci/ μ L] [6000Ci/mmol]

glycogen [10mg/mL]

Alkaline phosphatase [1U/ μ L]

T4 polynucleotide kinase [10U/ μ L]

8. Protein expression and purification

8.1 Expression

A single colony of *E. coli* Rosetta 2(DE3) plysS containing pAS02 was inoculated in 5mL LB-medium with kanamycin [f.c. 50 μ g/mL]. The culture was incubated on a rotary shaker at 37°C o/n. The next day, 0.75mL of the o/n culture was transferred into 1.5L LB-medium with kanamycin [f.c. 50 μ g/mL] and incubated at 37°C till an optical density of 0.5 was reached. The optical density was measured by a UV/VIS spectrophotometer (Hitachi U-2000 Spectrophotometer). Typically, after 5 hours, the culture attained the required optical density. The protein expression was then induced with 750 μ L freshly made 0.5mM IPTG. The culture was incubated on a vigorous shaker at 18°C o/n. The next day, cells were harvested by centrifugation at 4°C for 20 minutes at (6.500 x g). The supernatant was discarded away and the remaining pellet was frozen at -80°C for 30 minutes. After freezing the cells, the pellet was resuspended in 25mL lysis buffer. For improved cell lysis, lysozyme [10mg/mL] was added and the sample was incubated on ice for 30 minutes. Additionally the cells were sonicated 6 times for 10 seconds. Subsequently, the sample was centrifuged at 10.000 x g, 4°C for 30 minutes. For SDS-PAGE analysis, 20 μ L of the obtained supernatant were removed and mixed with 80 μ L SDS-PAGE sample buffer. The pellet (cell debris) was resuspended in 5mL lysis buffer, 20 μ L thereof were removed and mixed with 80 μ L SDS-PAGE sample buffer. Both aliquots were stored at -20°C.

8.2 Purification

To facilitate protein purification, the recombinant protein was fused with a polyhistidine-tag (6xHis), which has high affinity to nickel ions. This characteristic was used for purification of the tagged Mss116p using a Ni-NTA sepharose column. First 1mL Ni-NTA beads were washed with 15mL lysis buffer. Therefore the beads were mixed with the buffer and centrifuged for 10 minutes at maximum speed. While the supernatant was discarded, the washed beads were mixed with the cell lysate.

After 1 hour on the rotary shaker at 4°C, the mixture was loaded on a polypropylene column (20mL capacity). The matrix was washed six times with 1mL wash buffer I, six times with 1mL wash buffer II and finally eluted six times with 1mL elution buffer. Each obtained fraction was collected in a separate tube, 10µL of each fraction were removed and mixed with 10µL SDS-PAGE sample buffer. Eventually, all samples were loaded onto a SDS-PAGE and ran at 140V for 1 hour. Gels were stained with Coomassie blue staining solution for 10 minutes, followed by 30 minutes destaining with destaining solution 1. Further destaining was done with ddH₂O for several hours. Afterwards the gel was dried under vacuum and at 80°C.

8.3 Removal of the 6xHis-tag

The fractions containing the highest protein amount were combined and their solubility was increased by adding the following solution:

4µL 1M DTT [f.c. 1mM]
 8µL 0.5M EDTA pH 8.0 [f.c. 50mM]
 400µL 0.5M L-Arginine [f.c. 50mM]
 400µL 0.5M L-Glutamine [f.c. 50mM]
 400µL 99% glycerol [f.c. 10%]

The 6xHis-tag was cleaved by SUMO protease.

4mL Mss116p solution
 100µL +salt buffer
 100µL –salt buffer
 20µL SUMO protease [1U/µL]

The cleavage reaction was performed at 4°C o/n. To check the cleavage efficiency, samples before and after cleavage were ran on a SDS-PAGE. Finally, the cleaved SUMO-tag was removed by centrifugation with Amicon Ultra Ultracel – 30K tubes (10 minutes, 5.200 x g). The protein concentration was measured by Bradford assay. The protein was then aliquoted and stored at -80°C.

Required solutions

LB Medium

5g NaCl
 5g yeast extract
 10g tryptone
 Fill up to 1L with ddH₂O and autoclave.

Kanamycin [50mg/mL]

1M IPTG

Lysis Buffer

20mL binding buffer

1mL 1M imidazole

Fill up to 100mL with ddH₂O and adjust pH to 8.0 with 3M KOH.

Wash buffer I

20mL binding buffer

5mL 1M imidazole

Fill up to 100mL with ddH₂O and adjust pH to 8.0 with 3M KOH.

Wash buffer II

20mL binding buffer

10mL 1M imidazole

Fill up to 100mL with ddH₂O and adjust pH to 8.0 with 3M KOH.

Elution buffer

20mL binding buffer

25mL 1M imidazole

Fill up to 100mL with ddH₂O and adjust pH to 8.0 with 3M KOH.

SDS-PAGE sample buffer

10mL 0.5M Tris-HCl pH 8.0

10mL glycerol

10mL 10% SDS

10mg bromophenol blue

β-mercaptoethanol [f.c. 5%]

Solubility increasing solution

4μL 1M DTT [f.c. 1mM]

8μL 0.5M EDTA pH 8.0 [f.c. 50mM]

400μL 0.5M L-Arginine [f.c. 50mM]

400μL 0.5M L-Glutamine [f.c. 50mM]

400μL glycerol [f.c. 10%]

+salt buffer

500mM Tris-HCl pH 8.0

2% igepal (NP-40)

1.5M NaCl

10mM DTT

-salt buffer

500mM Tris-HCl pH 8.0

2% igepal (NP-40)

10mM DTT

SUMO protease [1U/ μ L] (Invitrogen)

Staining solution

50% Methanol

10% Acetic acid

0.25% Coomassie Brilliant Blue R350

Destaining solution

5% Methanol

7.5% Acetic Acid

9. ATPase assay

	-RNA	+RNA	Neg. control
Mss116p [f.c. 250nM]	X μ L	X μ L	X μ L
11.53 μ M bI5 [f.c. 0.5 μ M]	-	2.6 μ L	2.6 μ L
Proteinase K [800mAnsonU/ μ L]	-	-	1 μ L
RNase Inhibitor [40U/ μ L]	1.5 μ L	1.5 μ L	1.5 μ L
Incubate at 30°C for 10'			
1M Hepes, pH 7.5 [f.c. 40mM]	2.4 μ L	2.4 μ L	2.4 μ L
10mM DTT [f.c. 0.63mM]	3.78 μ L	3.78 μ L	3.78 μ L
ddH ₂ O	up to 51 μ L		
Incubate at 30°C for 10'			
10mM ATP [f.c. 1mM]	6 μ L	6 μ L	6 μ L
20mM MgCl ₂ [f.c. 1mM]	3 μ L	3 μ L	3 μ L

After initiating the reaction with ATP/Mg²⁺, 5 μ L aliquots of the samples were removed at the following time points: 0, 10, 20, 30, 40, 45, 60 and 90 minutes. These 5 μ L were then diluted with 45 μ L ddH₂O. The total amount of 50 μ L were further used with Malachite Green Phosphate Detection Kit from R&D Systems according to the manufacturer's protocol. The optical density that increased with the amount of hydrolysed ATP was determined by TECAN Infinite® Reader F500. The absorbance was plotted vs. time and the kinetic progress curve was fit to a single exponential equation using Kaleidograph.

Required solutions

1M Hepes pH 7.5

1M DTT

10mM ATP

20mM MgCl₂

Proteinase K [800mAnsonU/ μ L]

RNase Inhibitor [40U/ μ L]

10. Splicing assay

10.1 Adding Cbp2 to the unfolded bI5

	pos. control	neg. control	10nM Cbp2
bI5	0.25 μ L	0.25 μ L	0.25 μ L
0.1 x TE	14 μ L	14 μ L	14 μ L
90°C for 1 min.			
Put on ice for 2 min.			
Add			
10x reaction buffer I	-	2 μ L	-
10x reaction buffer II	2 μ L	-	2 μ L
RNase inhibitor [40U/ μ L]	2 μ L	2 μ L	2 μ L
100nM Cbp2	-	-	2 μ L
Protein storage buffer	2 μ L	2 μ L	-
Incubate sample on 35°C for 30 min.			
Add			
20mM GTP	1 μ L	1 μ L	1 μ L
After defined time points, take 1 μ L of sample and treat as follows:			
Add			
Proteinase K [800mAnsonU/ μ L]	1 μ L	1 μ L	1 μ L
Incubate sample for 1 min.			
Add			
Stop buffer	3 μ L	3 μ L	3 μ L
Store samples at -20°C.			

Splicing reaction was stopped at 0, 15, 30, 45 seconds and minute 1, 1.5, 2, 2.5, 3, 5, 10, 15, 30 and 60. Splice products are resolved on a 5% denaturing PAGE (23W, 45min). The gel was dried under vacuum and at 80°C. Afterwards the gel was exposed to a phosphor imager screen o/n. After scanning of the screen with a Typhoon TP10 phosphor imager, the gel was analysed with Image Quant TL v7. After normalization the fraction of the linear intron and of the pre-RNA were plotted

versus time. The kinetic progress curve was fit to single exponential or linear equations using Kaleidagraph.

10.2 Adding Cbp2 and Mss116p or KCl to the unfolded bI5

	10nM Cbp2 + 100nM Mss116p	10nM Cbp2 + 50mM KCl
bI5	0.25μL	0.25μL
0.1 x TE	12μL	12μL
	90°C for 1 min.	
	Put on ice for 2min.	
Add		
10x reaction buffer II	2μL	2μL
RNase inhibitor [40U/μL]	2μL	2μL
100nM Cbp2	2μL	2μL
1μM Mss116p	2μL	-
500mM KCl	-	2μL
	Incubate sample on 35°C for 30 min.	
Add		
20mM GTP	1μL	1μL
After defined time points, take 1μL of sample and treat as follows:		
Add		
Proteinase K [800mAnsonU/μL]	1μL	1μL
	Incubate sample for 1 min.	
Add		
Stop buffer	3μL	3μL
	Store samples at -20°C.	

10.3 Adding Cbp2 and varying Mss116p concentrations to the unfolded bI5

	25nM Cbp2 + 25nM Mss116p	25nM Cbp2 + 50nM Mss116p	25nM Cbp2 + 100nM Mss116p
bI5	0.25µL	0.25µL	0.25µL
0.1 x TE	12µL	12µL	12µL
	90°C for 1 min.		
	Put on ice for 2min.		
Add			
10x reaction buffer II	2µL	2µL	2µL
RNase inhibitor [40U/µL]	2µL	2µL	2µL
250nM Cbp2	2µL	2µL	2µL
250nM Mss116p	2µL	-	-
500nM Mss116p	-	2µL	-
1µM Mss116p	-	-	2µL
	Incubate sample on 35°C for 30 min.		
Add			
20mM GTP	1µL	1µL	1µL
After defined time points, take 1µL of sample and treat as follows:			
Add			
Proteinase K [800mAnsonU/µL]	1µL	1µL	1µL
	Incubate sample for 1 min.		
Add			
Stop buffer	3µL	3µL	3µL
	Store samples at -20°C.		

10.4 Adding various Mss116p concentrations to the bI5/Cbp2 complex

	25nM Cbp2 + 25nM Mss116p	25nM Cbp2 + 50nM Mss116p	25nM Cbp2 + 100nM Mss116p
bI5	0.25µL	0.25µL	0.25µL
0.1 x TE	12µL	12µL	12µL
90°C for 1 min.			
Put on ice for 2min.			
Add			
10x reaction buffer II	2µL	2µL	2µL
RNase inhibitor [40U/µL]	2µL	2µL	2µL
250nM Cbp2	2µL	2µL	2µL
Incubate sample on 35°C für 30 min.			
250nM Mss116p	2µL	-	-
500nM Mss116p	-	2µL	-
1µM Mss116p	-	-	2µL
Incubate sample on 35°C for 30 min.			
Add			
20mM GTP	1µL	1µL	1µL
After defined time points, take 1µL of sample and treat as follows:			
Add			
Proteinase K [800mAnsonU/µL]	1µL	1µL	1µL
Incubate sample for 1 min.			
Add			
Stop buffer	3µL	3µL	3µL
Store samples at -20°C.			

10.5 Adding Cbp2 to the bI5/Mss116p complex

	25nM Cbp2 + 25nM Mss116p	25nM Cbp2 + 50nM Mss116p	25nM Cbp2 + 100nM Mss116p
bI5	0.25µL	0.25µL	0.25µL
0.1 x TE	12µL	12µL	12µL
	90°C for 1 min.		
	Put on ice for 2min.		
Add			
10x reaction buffer II	2µL	2µL	2µL
RNase inhibitor [40U/µL]	2µL	2µL	2µL
250nM Mss116p	2µL	-	-
500nM Mss116p	-	2µL	-
1µM Mss116p	-	-	2µL
	Incubate sample on 35°C for 30 min.		
250nM Cbp2	2µL	2µL	2µL
	Incubate sample on 35°C for 30 min.		
Add			
20mM GTP	1µL	1µL	1µL
After defined time points, take 1µL of sample and treat as follows:			
Add			
Proteinase K [800mAnsonU/µL]	1µL	1µL	1µL
	Incubate sample for 1 min.		
Add			
Stop buffer	3µL	3µL	3µL
	Store samples at -20°C.		

Reaction sample was separated on 5% PAGE. Radioactive signals were detected by storage phosphor screens.

Required solutions

0.1 x TE-buffer

1mM Tris-HCL pH 8.0

0.1mM EDTA pH 8.0

10 x Reaction buffer I

500mM Hepes

500mM KCl

400mM MgCl₂

10 x Reaction buffer II

500mM Hepes

500mM KCl

70mM MgCl₂

RNase Inhibitor (40U/μl, Promega)

20mM GTP

Proteinase K [800mAnsonU/μL]

Stop buffer

Solution 1

400μL 50% sucrose

100μL 10xTBE

500μL ddH₂O

Solution 2

4mL formamide

1mL solution 1

Solution 3

500μL 0.5M EDTA pH8

4500μL solution 2

5% denaturing Acrylamide solution

210g 7M UREA

62.5mL 40% acrylamide/bisacrylamide solution (19:1)

50mL 10xTBE

10 x TBE

540g Tris base [f.c. 890mM]
 275g boric acid [f.c. 890mM]
 29.2g EDTA [f.c. 20mM]
 Fill up to 5L with ddH₂O

TEMED

10% APS

11. PAGE

11.1 SDS PAGE

4% Stacking Gel

3.83mL	ddH ₂ O
0.625mL	1.5M Tris-HCl pH 6.8
50μL	10% SDS
485μL	30% Acrylamide/bisacrylamide (37.5:1)
50μL	10% APS
5μL	TEMED

10% Separating Gel

4.87mL	ddH ₂ O
2.5mL	1.5M Tris-HCl pH 8.8
100μL	10% SDS
2.48mL	30% Acrylamide/bisacrylamide (37.5:1)
100μL	10% APS
10μl	TEMED

After assembling the glass plates, the separating gel was poured between the plates. To ensure smooth surface, EtOH was poured on top of the separating gel. After polymerization the EtOH was removed, the stacking gel was poured between the glass plates and a comb was put in. After polymerization of the stacking gel, the comb was removed, the gel was placed into the chamber, the electrodes were attached and the chambers were filled with 1 x GTS as running buffer.

Required solutions

1.5M Tris-HCL pH 6.8

1.5M Tris-HCL pH 8.8

10% SDS

30% Acrylamide-solution (37.5:1) solution

TEMED

Ethanol p.a.

10 x GTS

60g Tris base [f.c. 250mM]

288g glycine [f.c. 1.92M]

20g SDS [f.c. 1%]

11.2 Continuous denaturing PAGE

Continuous denaturing Polyacrylamide gel electrophoresis was used for separating splice products. Therefore 30mL 5% Acrylamide solution, 30μL TEMED and 300μL 10% APS. The solution was poured between glass plates separated by a thin spacer (0.7mm) and polymerized for at least one hour. Afterwards the gel was set up and pre-heated by running it at 25W for half an hour. After rinsing the wells with 1 x TBE buffer the reaction samples were loaded into the wells. The gels ran at 25W for 45 minutes. After disassembling the glass plates, the gel was dried for one hour via a vacuum gel dryer. Radioactive signals were detected by storage phosphor screens (GE Healthcare), scanned and visualized with Image Quant.

Required solutions

5% denaturing acrylamide solution

210g 7M Urea

62.5mL 40% acrylamide/bisacrylamide solution (19:1)

50mL 10 x TBE

Fill up with ddH₂O to 500mL.

10% APS

TEMED

10 x TBE

540g Tris base [f.c. 890mM]
 275g boric acid [f.c. 890mM]
 29.2g EDTA [f.c. 20mM]
 Fill up to 5L with ddH₂O

12. Filter binding assay

Filter binding assays were used for determining the binding constants of the proteins to RNA. As such a constant amount of RNA was incubated with increasing concentration of protein followed by separation via the filter binding. RNA was received by *in vitro* transcription of pbl5 (see Material and Methods 6.1). The obtained RNA was purified with MEGAclean™-96 Transcription Clean-Up Kit (see Material and Methods 6.3). The transcript was dephosphorylated, purified and end-labelled (see Material and Methods 6.4 - 6.6). End-labelled RNA was used for the following filter binding assays.

12.1 Adding increasing concentrations of Cbp2 or Mss116p to the unfolded bl5

	Cbp2	Mss116p	neg. control
RNA [f.c. 100pM]	0.5µL	0.5µL	0.5µL
0.1 x TE	10µL	10µL	10µL
	90°C for 1 min.		
	Put on ice for 2min.		
Add			
10x reaction buffer II	1.5µL	1.5µL	1.5µL
RNase inhibitor [40U/µL]	1.5µL	1.5µL	1.5µL
10 x Cbp2 [f.c. 0-100nM]	1.5µL	-	-
10 x Mss116p [f.c. 0-400nM]	-	1.5µL	-
10 x BSA [f.c. 0-1µM]	-	-	1.5µL
	Incubate sample on 35°C für 30 min.		
	Apply sample immediately to the filter binding apparatus (see 11.4).		

12.2 Adding increasing concentrations of Mss116p to the Cbp2/bI5 complex and vice versa

	10nM Cbp2 + 0-400nM Mss116p	100nM Mss116p + 0-100nM Cbp2
RNA [f.c. 100pM] 0.1 x TE	0.5µL 10µL	0.5µL 10µL
	90°C for 1 min.	
	Put on ice for 2min.	
Add		
10x reaction buffer II	1.5µL	1.5µL
RNase inhibitor [40U/µL]	1.5µL	1.5µL
100nM Cbp2	1.5µL	-
10 x Cbp2 [f.c. 0-100nM]	-	1.5µL
1µM Mss116p	-	1.5µL
10 x Mss116p [f.c. 0-400nM]	1.5µL	
	Incubate sample on 35°C für 30 min.	
	Apply sample immediately to the filter binding apparatus (see 11.4.).	

12.3 Adding various concentrations of Cbp2 to bI5 folded at different concentrations of KCl or Mss116p storage buffer and vice versa

	10nM Cbp2 + 0-400mM KCl	200mM KCl + 0-100nM Cbp2	Mss116p Protein storage buffer + 0-100nM Cbp2
RNA [f.c. 100pM] 0.1 x TE	0.5µL 10µL	0.5µL 10µL	0.5µL 10µL
90°C for 1 min.			
Put on ice for 2min.			
Add			
10x reaction buffer II	1.5µL	1.5µL	1.5µL
100nM Cbp2	1.5µL	-	-
10 x Cbp2 [f.c. 0-100nM]	-	1.5µL	1.5µL
2µM KCl	-	1.5µL	-
10 x KCl [f.c. 0-400mM]	1.5µL	-	-
Mss116p			
Protein storage buffer	-	-	1.5µL
Incubate sample on 35°C for 30 min.			
Apply sample immediately to the filter binding apparatus (see 11.4.).			

12.4 Assembly of the Bio-Dot apparatus

Filter binding assays were performed with Bio-Dot apparatus from Bio-Rad. The apparatus was assembled according to the manufacturer's protocol. The upper part of the apparatus (part 1, figure 17) contains a 96 well plate, in which the reaction samples are pipetted. Part 2 is a plastic support, which serves as platform for membranes. Part 3 and part 4 building the vacuum chamber. Attaching a vacuum pump to part 4 leads to depression and results in pull-down of the samples onto the membranes.

Before usage the membranes are equilibrated in binding buffer. These membranes are positioned in between part 1 and part 2. For the performed filter binding assays two membranes were used (not seen in figure 17). The upper Nitrocellulose membrane (Amersham Hybond-N, GE Healthcare) selects for RNA bound to a protein. The lower positively charged Nylon membrane (Amersham Hybond-XL, GE Healthcare) filters unbound RNA. Radioactive signals were detected by exposing both dried membranes to storage phosphor screens o/n. After scanning the screen, the data were analysed using Image Quant T2 v7. The fraction of RNP was plotted vs. the protein concentration and fit to a 1:1 binding isotherm based on the equation using Kaleidograph.

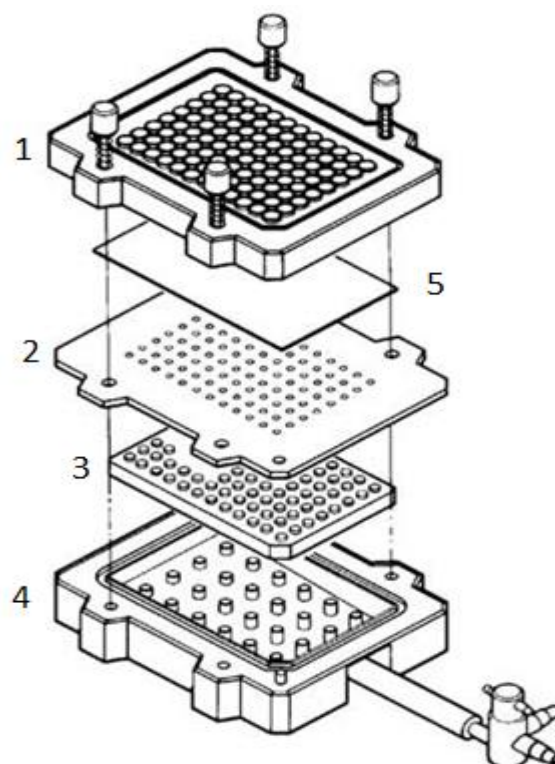


Figure 22: Bio-Dot apparatus

Part 1: 96 well plate

Part 2: plastic support as platform for membranes

Part 3/4: vacuum chamber with attached valve for de/activating vacuum

Part 5: Nitrocellulose and pos. charged nylon membrane.

Required solutions

0.1 x TE buffer

1mM Tris-HCL pH 8.0

0.1mM EDTA pH 8.0

ME buffer

10mM MOPS pH 6.0

1mM EDTA pH 8.0

10 x Reaction buffer I

500mM Hepes

500mM KCl

400mM MgCl₂

10 x Reaction buffer II

500mM Hepes

500mM KCl

70mM MgCl₂

Protein storage buffer

50mM Tris-HCl pH 7.5

1mM DTT

300mM KCl

10% Glycerol

Phenol, water saturated

Chloroform:Isoamyl alcohol solution (24:1)

3M NaOAc pH 5.0

3M KCl

Ethanol p.a.

0.5M EDTA pH 8.0

10xPNK NEB buffer

γ-P³²-ATP [10μCi/μL]

Glycogen [10mg/mL]

Recombinant RNasin® Ribonuclease Inhibitor (40U/μl, Promega)

Alkaline Phosphatase (1U/μL)

Results

1. ATPase assays

The yeast protein Mss116p belongs to the family of DEAD-box helicases (Huang et al. 2005). DEAD-box helicases are known for binding and hydrolysing ATP in order to unwind RNA (S  raphin et al. 1987; Huang et al. 2005). Noteworthy, Mss116p shows increased ATPase activity in the presence of RNA (Solem et al. 2006; Halls et al. 2007). ATPase assays were performed to determine the activity of recombinantly expressed Mss116p. For this approach, the Malachite Green Phosphate Detection Kit from R&D Systems was used. The Malachite green phosphate detection kit is based on the reaction between malachite green, molybdate and inorganic phosphate. This complex formation can be measured with a spectrophotometer at 620nm. Because ATPase activity of Mss116p results in free inorganic phosphate, whose concentration can be measured by complex formation, the ATPase activity directly correlates with absorbance of the complex.

The ATPase activity is significantly stimulated in the presence of bI5 compared to that in the absence of RNA. As a negative control, proteinase K was added to degrade Mss116p and consequently no ATPase activity was detectable.

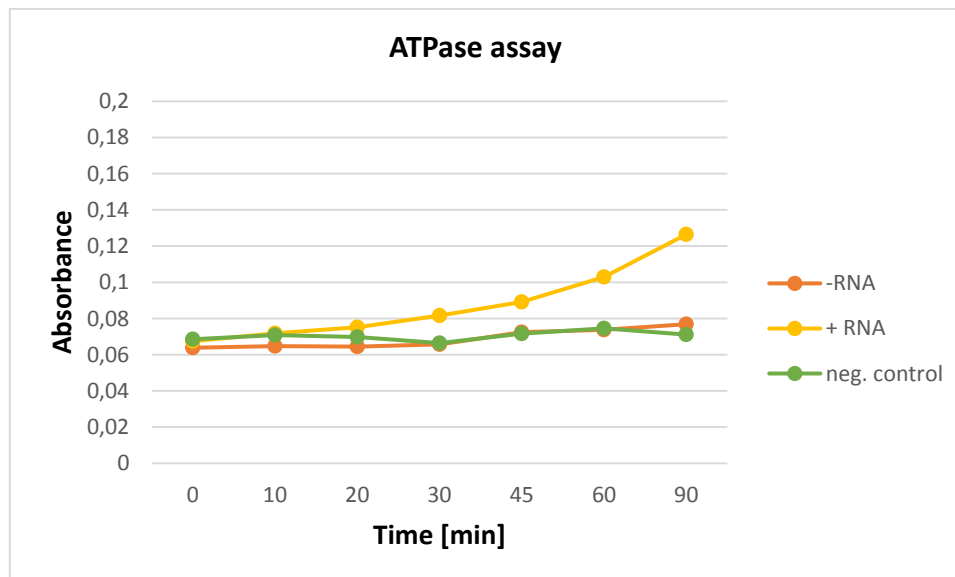


Figure 23: ATPase activity of Mss116p
The ATPase activity is represented by the conversion of ATP to ADP + free phosphate.

1.1 Activity of various Mss116p batches

As expected, Mss116p only shows significant ATPase activity in the presence of RNA (figure 20). In fact, in the absence of the bI5 RNA, the ATPase activity is reduced to background levels, comparable to the negative control (figure 20). Comparing ATPase activity with earlier experiments carried out in

our laboratory, we expected an absorbance of 0.18 after 90 minutes when performing the ATPase with Mss116p in the presence of bI5. Surprisingly the observed activity and in turn the absorbance was lower than expected (0.13).

Nevertheless, this assay proved useful in determining whether recombinant Mss116p is active.

Therefore, the ATPase activity of various batches of recombinantly expressed and purified Mss116p that were prepared by Stefan Handl and myself were compared to select the best protein preparation for subsequent experiments. While most batches showed efficient ATP hydrolysis in the presence of bI5 (batch B, C and D), some batches were inactive (batch A and E; figure 21).

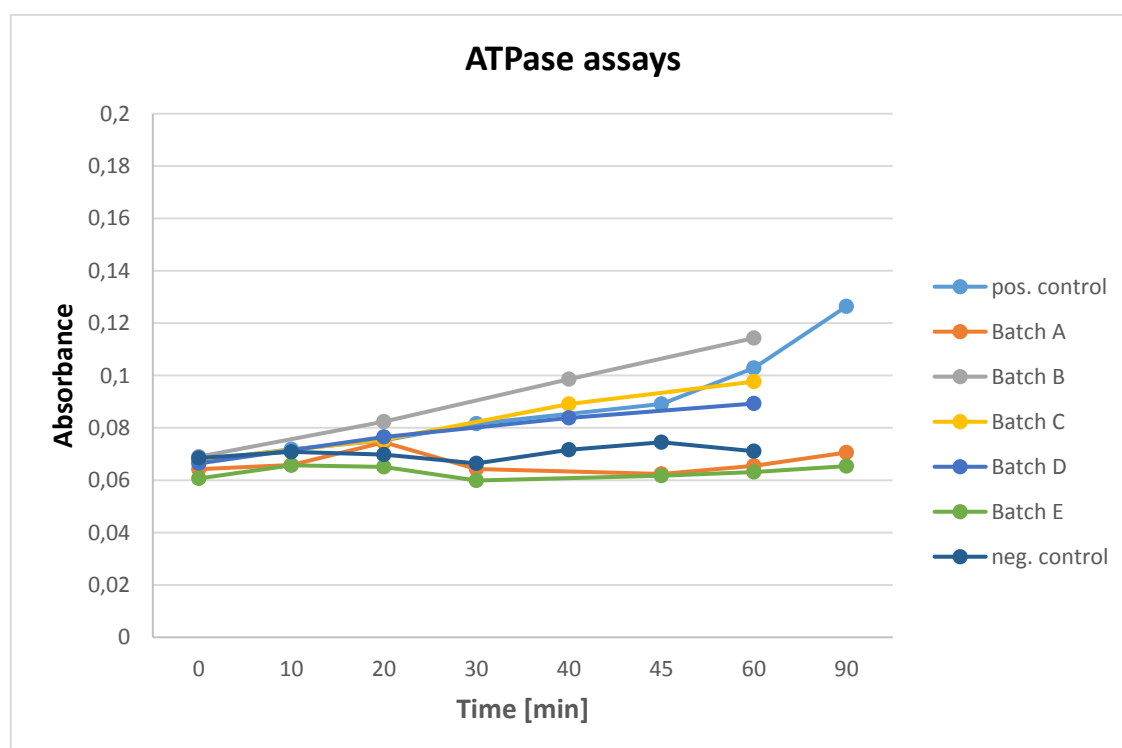


Figure 24: ATPase activity of various Mss116p batches

Comparison of ATPase activity of different Mss116p batches, shown at the right hand site. Batch A-E were created at the University of Vienna, the Pyle protein were received from A. Pyle (Yale University).

Although all batches showed low activity, it is unlikely that all proteins are of insufficient quality, as these showed comparable activity to the positive control, a Mss116p batch obtained from the Pyle lab (Yale University). One possible explanation for low absorbance is the malfunction of the Malachite Green Phosphate Detection Kit, which would explain similar behaviour of all batches (B-D) including the positive control. Besides, it cannot be ruled out that the spectrophotometer did not work properly and reflected wrong results. In case of batch A & E, it is likely that Mss116p was inactivated during purification, as their activity was reduced to background levels, as observed in the negative control. Thus, batches B, C and D were used for further experiments.

2. Influence of Cbp2 and Mss116p on splicing efficiency of bI5

bI5 belongs to group I introns, autocatalytic RNAs that facilitate their own excision from the pre-mRNA during the splicing reaction. *In vivo* bI5 requires assistance of two proteins, Cbp2 and Mss116p, to reach its native structure and in turn to self-splice. *In vitro*, however, bI5 is capable of splicing either at high Mg^{2+} concentration or at low Mg^{2+} concentration in the presence of Cbp2. To examine the influence of Cbp2 and Mss116p on the splicing efficiency of bI5 *in vitro* splicing assays were performed.

Splicing products

During a successful splicing reaction of bI5 pre-mRNA, five products will be formed. The first transesterification leads to formation of a free 5' exon and 3' exon still ligated to the intron. The second ester transfer reaction results in ligation of 5' and a 3' exon and a free intron, either in linear or circular form. For all splicing assays the bI5 ribozyme, the clone which was kindly provided by K. Weeks (University of North Carolina), was used. The bI5 ribozyme (344nt) is flanked by exon sequences (173nt, 45nt); thus the pre-RNA consists of 562 nucleotides. Hence, the following splicing products are formed:

1. Products of the first step of splicing
 - 5' exon (173 nucleotides)
 - 3' exon attached to the linear intron (389 nucleotides)
2. Products after the 2nd step of splicing
 - Ligated exons (218 nucleotides)
 - Linear intron (344 nucleotides)
 - Circular intron (344 nucleotides)

After resolving the splicing products all are detectable, except for the 3' exon. With a length of 45nts, the 3' exon ran out of the gel.

As positive control, bI5 was incubated with 40mM Mg^{2+} , at which bI5 is able to form its native structure without assisting proteins (Weeks & Cech 1995; Weeks & Cech 1996; McGraw & Tzagoloff 1983). Therefore bI5 is found to self-splice efficiently. In fact, after 60 minutes barely any pre-RNA is left and only linear and circular intron as well as ligated exons are observed (figure 23). The negative control was performed at a Mg^{2+} concentration of 7mM in the absence of proteins. At these near-physiological conditions bI5 is only capable of collapsing to the near-native state but, does not fold to its native conformation and therefore cannot self-splice (figure 23). Interestingly, some splicing assays show splicing activity in negative controls, containing 7mM Mg^{2+} , indicating that a small

population of bI5 is folded into its native conformation, even under near-native ion conditions, but without assisting proteins. However, this phenomenon was only observed rarely. In contrast to the positive control, the pre-mRNA remained unspliced and thus constant in negative control (figure 23) Figure 22 displays all observed rate constants we calculated after the performed splicing assays, at which pre-mRNA decay was followed.

		$k_{\text{obs}} [\text{min}^{-1}]$	$1/k_{\text{rel}}$
Cbp2 is added to the unfolded bI5 - RNA complex	25nM Cbp2	0.41 ± 0.03	1
	10nM Cbp2	0.64 ± 0.03	1.5
	10nM Cbp2 + 50mM KCl	0.55 ± 0.02	2
Cbp2 and Mss116p are added concomitantly to the unfolded bI5 - RNA	25nM Cbp2 + 25nM Mss116p	0.97 ± 0.15	1.3
	25nM Cbp2 + 50nM Mss116p	1.07 ± 0.16	2.4
	25nM Cbp2 + 100nM Mss116p	1.90 ± 0.18	4.7
Mss116p is added to the native Cbp2 - bI5 complex	25nM Cbp2 + 25nM Mss116p	0.76 ± 0.05	1.9
	25nM Cbp2 + 50nM Mss116p	0.95 ± 0.14	2.3
	25nM Cbp2 + 100nM Mss116p	1.60 ± 0.15	3.9
Cbp2 is added to the Mss116p - bI5 complex	25nM Mss116p + 25nM Cbp2	1.05 ± 0.16	2.6
	50nM Mss116p + 25nM Cbp2	1.09 ± 0.18	2.6
	100nM Mss116p + 25nM Cbp2	1.68 ± 0.25	4.1

Figure 25: Observed rate constant of bI5 splicing under various reaction conditions. k_{obs} was derived from pre-mRNA decay. The average and standard deviation were calculated for three independent experiments.

2.1 Cbp2 stimulates efficient splicing of the bI5 ribozyme *in vitro*

We first examined the influence of Cbp2 alone on splicing of bI5 and therefore incubated 10nM Cbp2 with unfolded bI5 RNA in the presence of 7mM Mg^{2+} (figure 26).

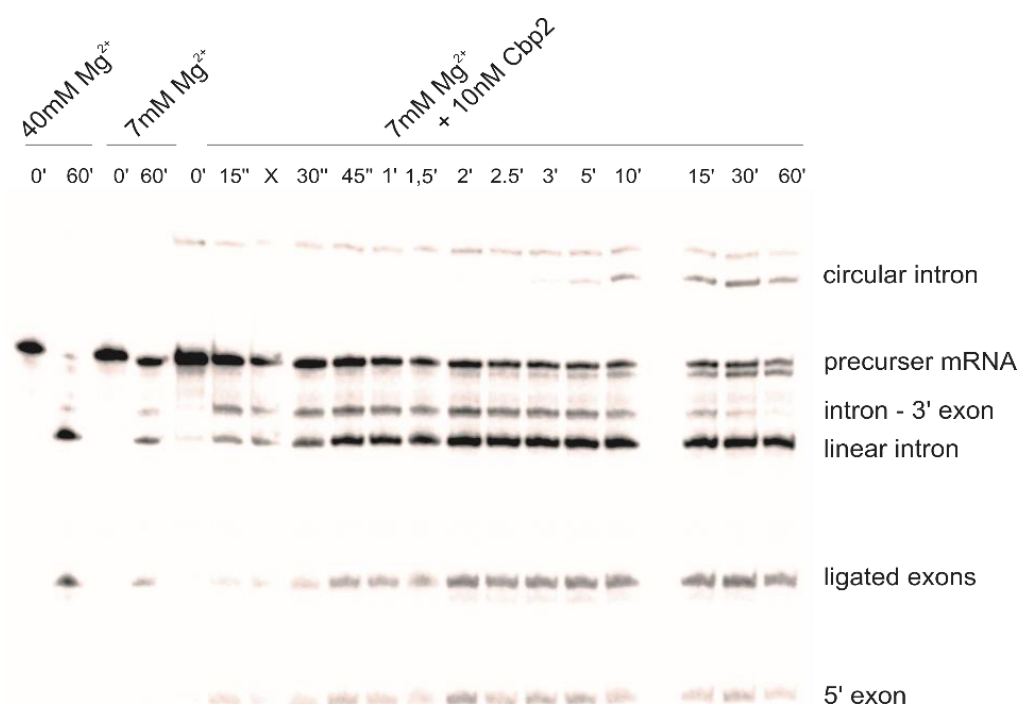


Figure 26: Cbp2 promotes splicing of bI5 at near-physiological conditions. As positive control folding of bI5 with 40mM Mg^{2+} is shown (lanes 1 and 2). For negative control 7mM Mg^{2+} in absence of the protein was used (lanes 3 and 4).

As positive control, the bI5 pre-RNA was folded at 40mM Mg^{2+} (lanes 1 and 2). In case of the negative control, bI5 was folded at 7mM Mg^{2+} only (lanes 3 and 4). Cbp2-assisted bI5 folding was provided by adding Mg^{2+} ions (7mM) and Cbp2 (10nM) concomitantly to the unfolded pre-RNA. As seen in figure 23, efficient splicing is already achieved by addition of 10nM Cbp2 and near-physiological Mg^{2+} ion concentrations. While time point 0' shows mainly pre-mRNA, at 15'' already the first splicing products can be seen. The amount of pre-mRNA continuously decreases over time due to the consecutive splicing steps. While the signal strength of linear intron still ligated to the 3' exon is first increasing, it decreases after minute 2. This is reasonable, considering that the intermediate is further processed into the final splicing products. A similar observation is made for the 5' exon. The first splicing step leads to a free 5' exon, resulting evolution of free 5' exon. The following second splicing step ligates both exons, reducing the amount of free 5' exon. The amount of final splicing products, ligated exons and linear intron, are continuously increasing. Although the linear intron can undergo an additional transesterification reaction, namely the circularization. After 2 minutes, a new band on top of the pre-mRNA band appears. This slow migrating band refers to the circular intron, which is formed due to a transesterification reaction at the free intron ends.

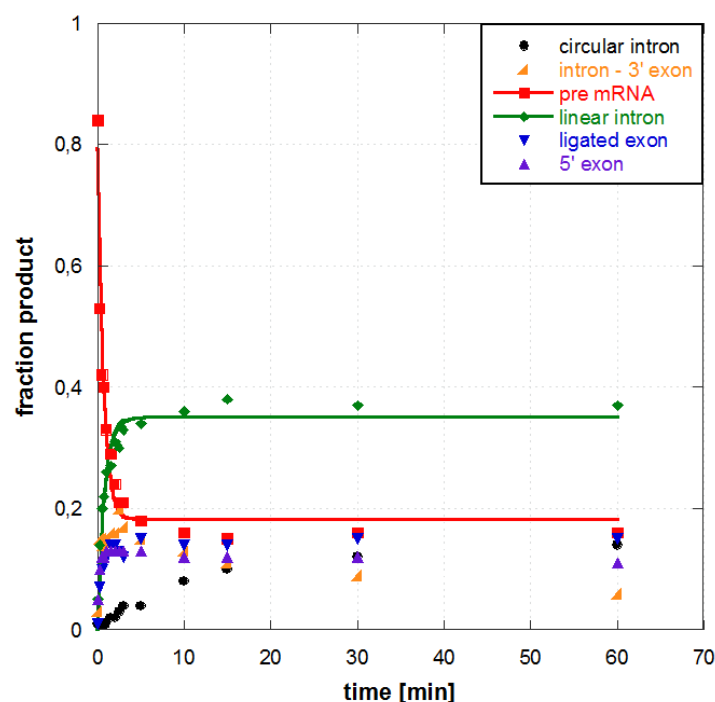


Figure 27: Kinetic progress curve of bI5 self-splicing in the presence of 10nM Cbp2.

Decay of pre-mRNA (red) and increase of the linear intron (green) were fit to single exponential equations, yielding a k_{obs} of $0.63 \pm 0.04 \text{ min}^{-1}$ and $1.5 \pm 0.15 \text{ min}^{-1}$, respectively.

The fraction of each splice product was plotted versus time, allowing the pre-mRNA decay and linear intron evolution to be fit to single-exponential equations (figure 24). Based on three independent experiments an average observed rate constant for decay of pre-mRNA (k_{obs}) of $0.64 \pm 0.03 \text{ min}^{-1}$ was obtained in the presence of 10nM Cbp2.

2.2 Salt influence on bI5 splicing efficiency

Many protein-nucleic acid interactions are heavily influenced by salt concentrations. While some organisms such as *Pyrococcus woesei* exist under high temperature and high salt conditions (O'Brien et al. 1998), others suffer under high salt concentrations, resulting in destabilized protein-nucleic acid interactions (Butcher et al. 1994). As Cbp2 contains a vast number of positive charges distributed over the entire primary structure of the protein, it was of interest to investigate the influence of salt on bI5 Cbp2 binding. Thus, we performed a splicing assay in the presence of 10nM Cbp2 and moderate ion concentration (50mM KCl) concomitantly (figure 25).

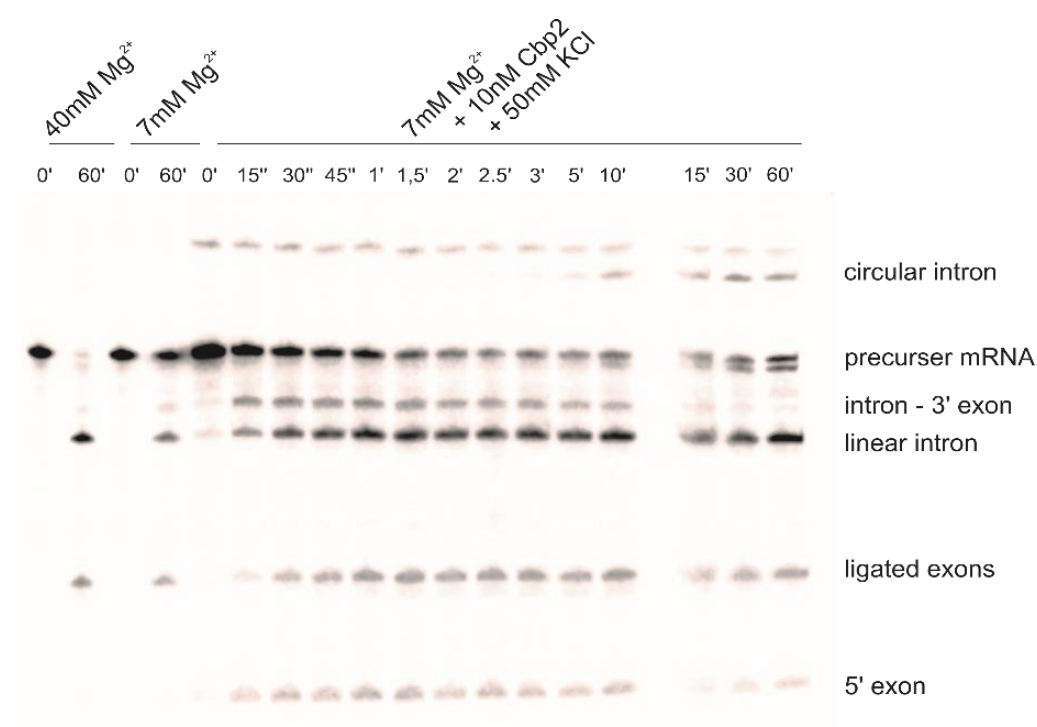


Figure 28: A moderate monovalent ion concentration does not significantly influence *bl5* splicing stimulated by Cbp2. Influence of 25mM Cbp2 and 50mM KCl on folding of pre-RNA in presence of 7mM Mg^{2+} . As positive control folding of *bl5* with 40mM Mg^{2+} is shown (lanes 1 and 2). For negative control 7mM Mg^{2+} in absence of the protein was used (lanes 3 and 4).

Adding 50mM KCl to the Cbp2-promoted *bl5* splicing reaction results in an average k_{obs} of 0.55 ± 0.02 [min^{-1}] (figures 28-29). Comparing the Cbp2-promoted *bl5* splicing efficiency in the absence and presence of 50mM KCl revealed very similar k_{obs} , indicating that the moderate monovalent ion concentration does not compete with Cbp2 for *bl5* binding.

This result is of great importance, as in the subsequent experiments a similar amount of KCl is added together with Mss116p, as it is part of the respective storage buffer.

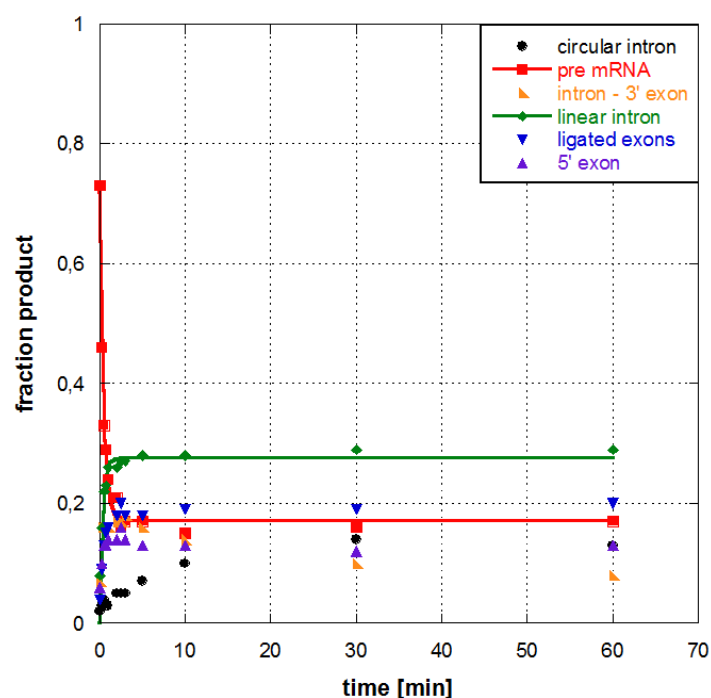


Figure 29: Kinetic progress curve of bI5 self-splicing in the presence of 10nM Cbp2 and 50mM KCl. Decay of pre-mRNA (red) and increase of the linear intron (green) were fit to single exponential equations, yielding a k_{obs} of $0.50 \pm 0.05 \text{ min}^{-1}$ and $3.01 \pm 0.6 \text{ min}^{-1}$, respectively.

2.3 Mss116p enhances the Cbp2-assisted bI5 splicing activity

Yeast Mss116p is known to assist mitochondrial group I introns during the self-splicing reaction *in vivo* (S  raphin et al. 1987; Zingler et al. 2010). In case of the bI5 intron, the knockout of mss116 reduces splicing of this intron to 50%, while the *cbp2* knockout abolishes bI5 splicing (Sachsenmaier & Waldsich 2013). Therefore, it is of interest to reveal whether Mss116p enhances Cbp2-assisted bI5 splicing *in vitro* as well. As such, both Cbp2 and Mss116p were added at different molar ratios to the unfolded bI5 RNA (figures 30-35).

In the presence of equimolar ratio of Cbp2 and Mss116p as well as at 2x excess of Mss116p relative to Cbp2 the splicing activity is only 2-fold increased, from $0.41 \pm 0.03 \text{ min}^{-1}$ to $0.97 \pm 0.15 \text{ min}^{-1}$ and $1.07 \pm 0.16 \text{ min}^{-1}$, respectively (figures 30-33). In contrast, adding 4x molar excess of Mss116p over Cbp2 to the bI5 splicing reaction results in a k_{obs} of $1.90 \pm 0.18 \text{ min}^{-1}$. And thus in a 4.7-fold enhancement (figures 32-33).

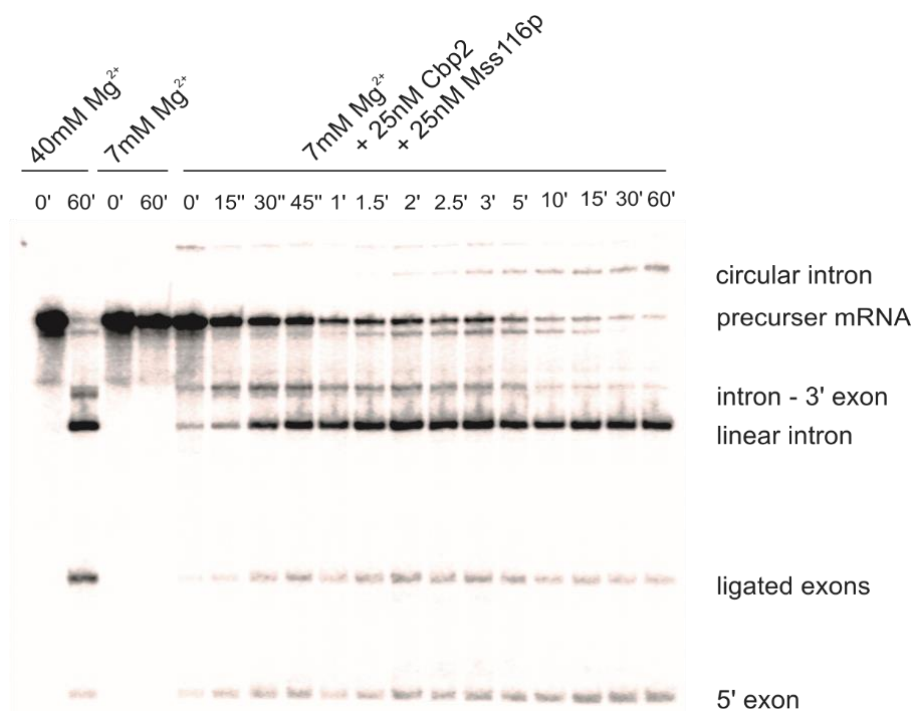


Figure 30: 25nM Cbp2 and 25nM Mss116p promote splicing of *bI5* at near-physiological conditions. As positive control folding of *bI5* with 40mM Mg^{2+} is shown (lanes 1 and 2). For negative control 7mM Mg^{2+} in absence of the protein was used (lanes 3 and 4).

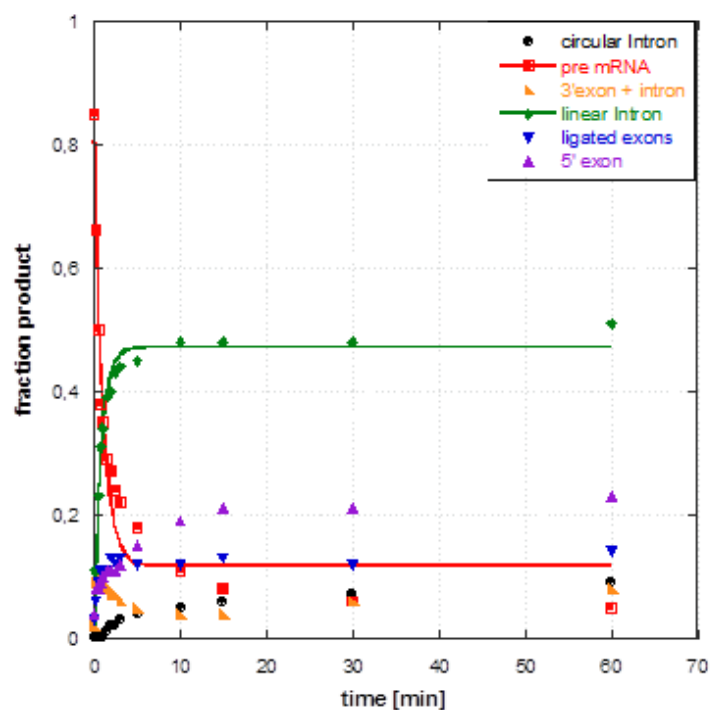


Figure 31: Kinetic progress curve of *bI5* self-splicing in the presence of 25nM Cbp2 and 25nM Mss116p. Decay of pre-mRNA (red) and increase of the linear intron (green) were fit to single exponential equations, yielding a k_{obs} of $0.96 \pm 0.14 \text{ min}^{-1}$ and $1.23 \pm 0.16 \text{ min}^{-1}$, respectively.

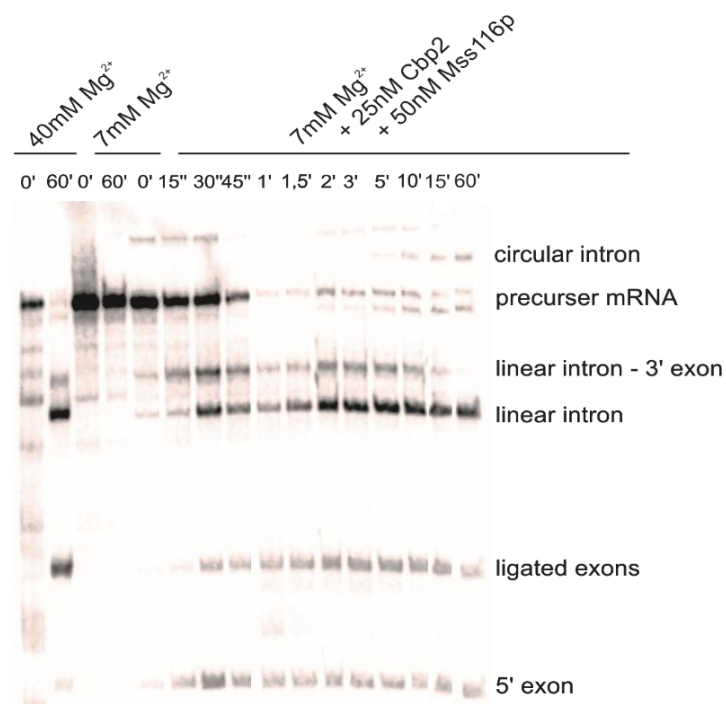


Figure 32: 25nM Cbp2 and 50nM Mss116p promote splicing of bI5 at near-physiological conditions. As positive control folding of bI5 with 40mM Mg^{2+} is shown (lanes 1 and 2). For negative control 7mM Mg^{2+} in absence of the protein was used (lanes 3 and 4).

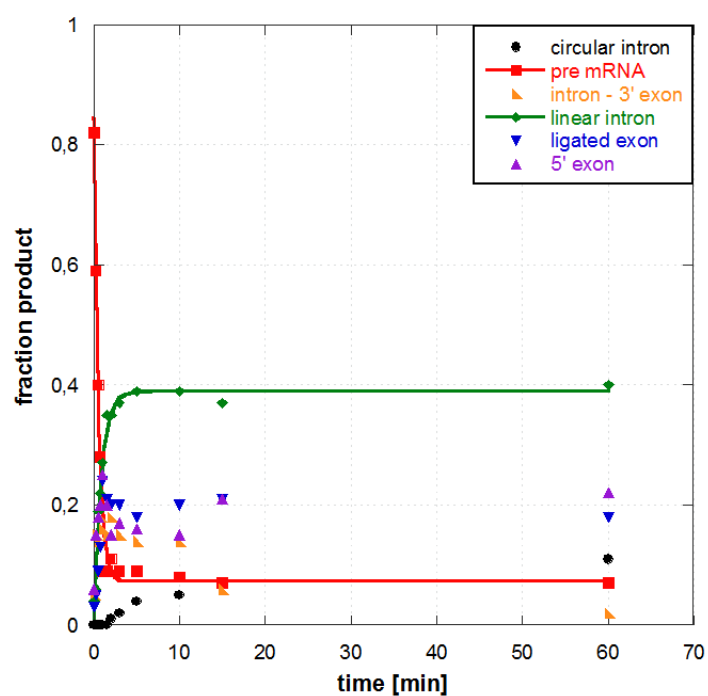


Figure 33: Kinetic progress curve of bI5 self-splicing in the presence of 25nM Cbp2 and 25nM 50nM Mss116p. Decay of pre-mRNA (red) and increase of the linear intron (green) were fit to single exponential equations, yielding a k_{obs} of $0.77 \pm 0.04 \text{ min}^{-1}$ and $1.19 \pm 0.11 \text{ min}^{-1}$, respectively.

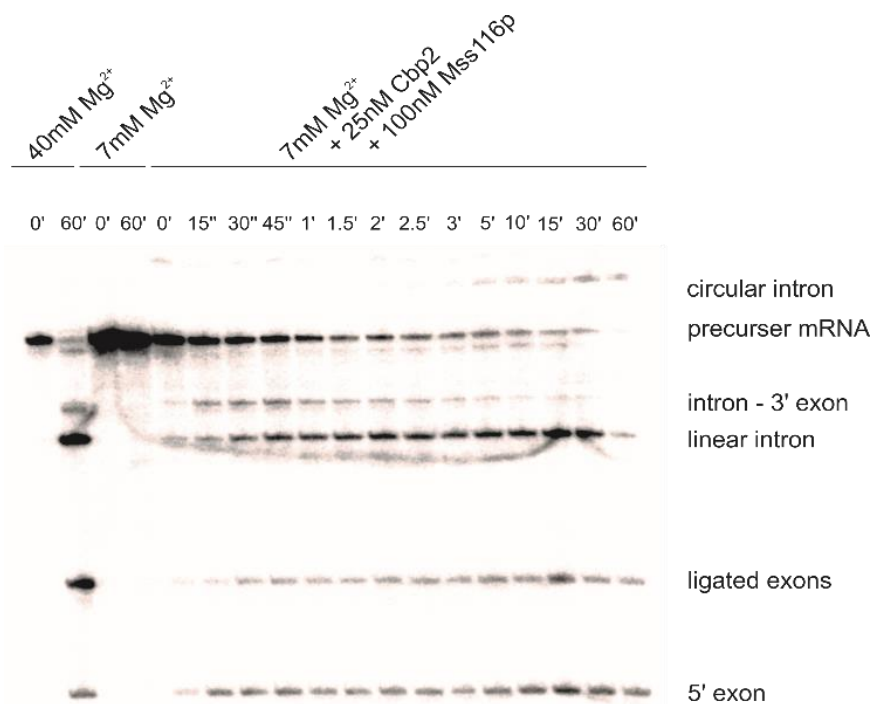


Figure 34: 25nM Cbp2 and 100nM Mss116p promote splicing of bI5 at near-physiological conditions. As positive control folding of bI5 with 40mM Mg^{2+} is shown (lanes 1 and 2). For negative control 7mM Mg^{2+} in absence of the protein was used (lanes 3 and 4).

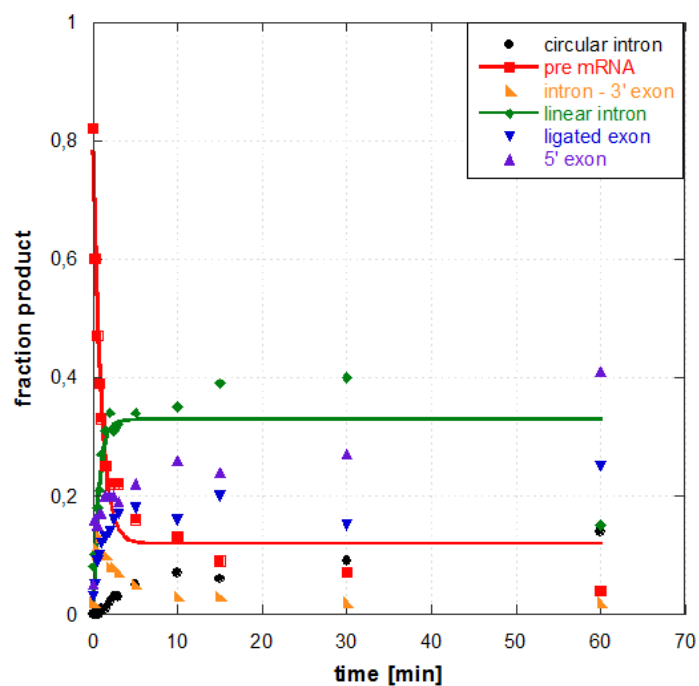


Figure 35: Kinetic progress curve of bI5 self-splicing in the presence of 25nM Cbp2 and 25nM 50nM Mss116p. Decay of pre-mRNA (red) and increase of the linear intron (green) were fit to single exponential equations, yielding a k_{obs} of $1.81 \pm 0.16 \text{ min}^{-1}$ and $1.58 \pm 0.51 \text{ min}^{-1}$, respectively.

2.4 bI5 does not have hierarchical order for Cbp2 and Mss116p

K. Weeks and T. Cech found out that Cbp2 and bI5 form a complex, in order to fulfil self-splicing reaction (Weeks & Cech 1996). Even though Mss116p is known to assist this process *in vivo*, it is still unknown, how Mss116p interacts with the Cbp2-bI5 complex. For example, does Mss116p need to act on bI5 prior to Cbp2 binding? Alternatively, Mss116p might be required to resolve a kinetically trapped bI5 – Cbp2 complex. Similarly, Mss116p could play a role in rapid Cbp2 turnover, among many other possible modes of action. As such, we first formed the native Cbp2-bI5 complex and subsequently added Mss116p at different molar ratios to the Cbp2 protein.

In the presence of an equimolar ratio of Cbp2 and Mss116p as well as at 2x excess of Mss116p relative to Cbp2 the splicing activity is only 1.9-2.3-fold increased, from $0.41 \pm 0.03 \text{ min}^{-1}$ to $0.76 \pm 0.05 \text{ min}^{-1}$ and $0.95 \pm 0.14 \text{ min}^{-1}$, respectively (figures 36-39). In contrast, adding 4x molar excess of Mss116p over Cbp2 to the bI5 splicing reaction results in a k_{obs} of $1.60 \pm 0.15 \text{ min}^{-1}$, and thus in a 3.9-fold enhancement (figures 40-41).

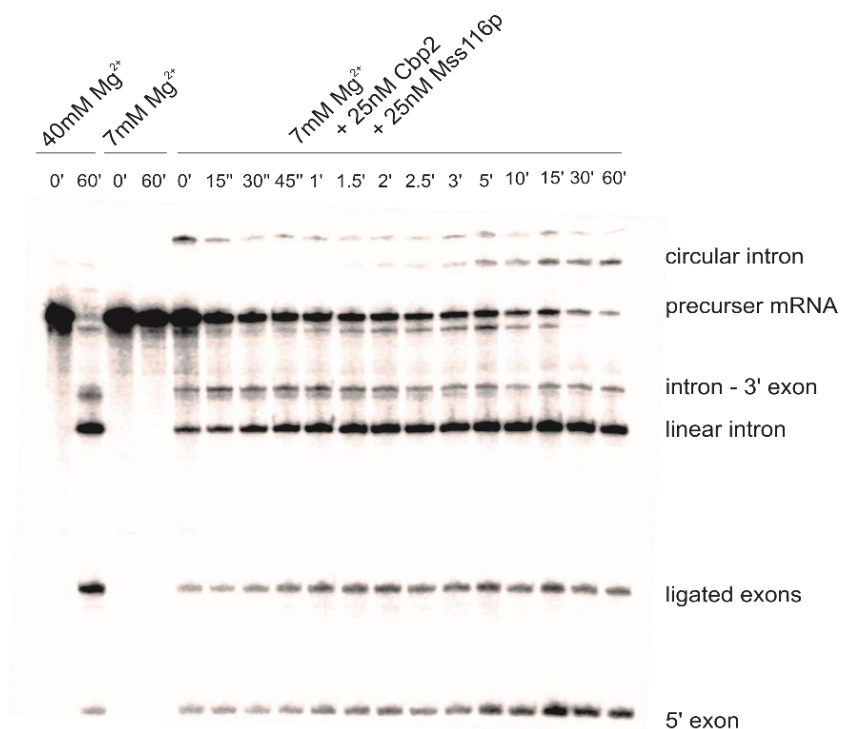


Figure 36: 25nM Mss116p promote splicing of a preformed Cbp2 - bl5 complex at near-physiological conditions. As positive control folding of bl5 with 40mM Mg^{2+} is shown (lanes 1 and 2). For negative control 7mM Mg^{2+} in absence of the protein was used (lanes 3 and 4).

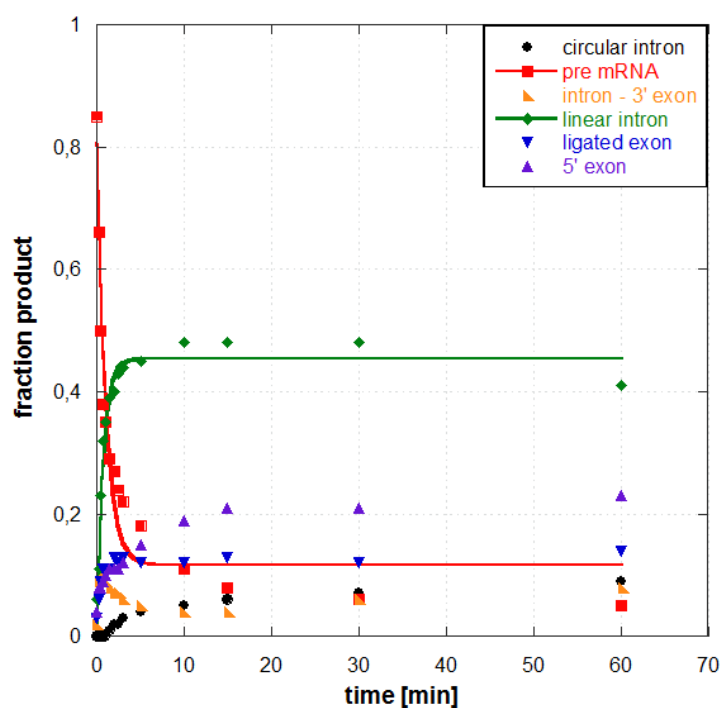


Figure 37: Kinetic progress curve of preformed Cbp2- bl5 complex self-splicing in the presence of 25nM Mss116p. Decay of pre-mRNA (red) and increase of the linear intron (green) were fit to single exponential equations, yielding a k_{obs} of $0.68 \pm 0.05 \text{ min}^{-1}$ and $1.38 \pm 0.14 \text{ min}^{-1}$, respectively.

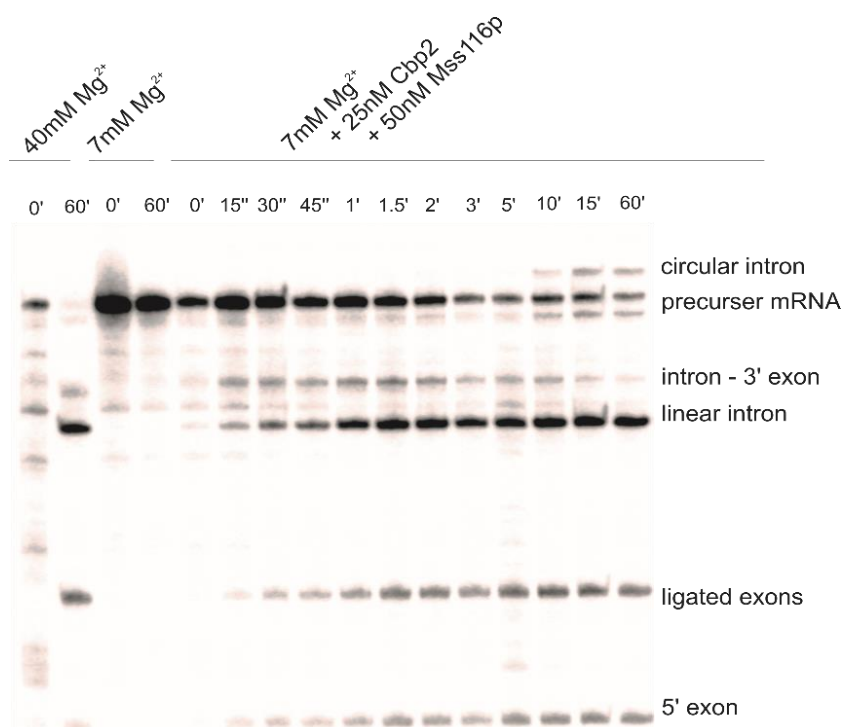


Figure 38: 50nM Mss116p promote splicing of a preformed Cbp2 - bI5 complex at near-physiological conditions. As positive control folding of bI5 with 40mM Mg^{2+} is shown (lanes 1 and 2). For negative control 7mM Mg^{2+} in absence of the protein was used (lanes 3 and 4).

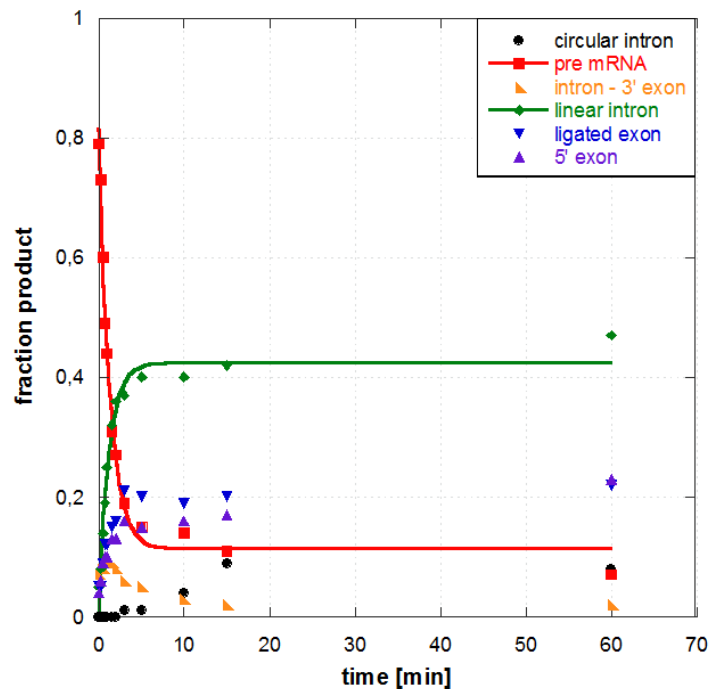


Figure 39: Kinetic progress curve of preformed Cbp2- bI5 complex self-splicing in the presence of 50nM Mss116p. Decay of pre-mRNA (red) and increase of the linear intron (green) were fit to single exponential equations, yielding a k_{obs} of $0.77 \pm 0.08 \text{ min}^{-1}$ and $0.85 \pm 0.08 \text{ min}^{-1}$, respectively.

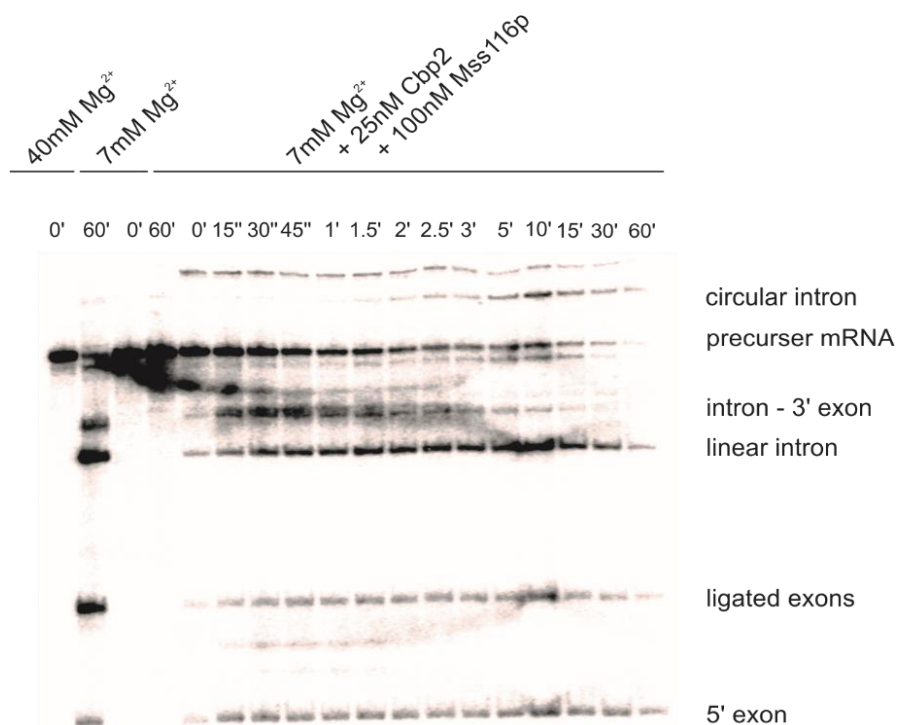


Figure 40: 100nM Mss116p promote splicing of a preformed Cbp2 - bI5 complex at near-physiological conditions. As positive control folding of bI5 with 40mM Mg^{2+} is shown (lanes 1 and 2). For negative control 7mM Mg^{2+} in absence of the protein was used (lanes 3 and 4).

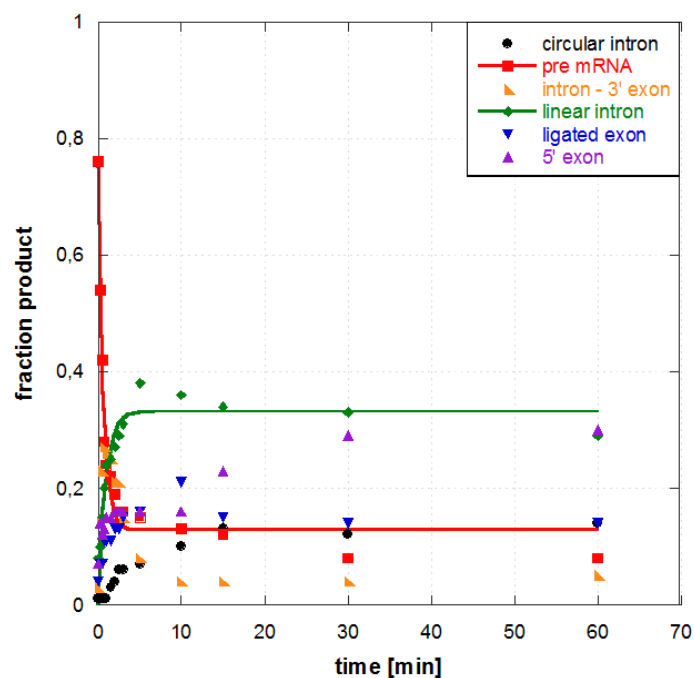


Figure 41: Kinetic progress curve of preformed Cbp2- bI5 complex self-splicing in the presence of 100nM Mss116p. Decay of pre-mRNA (red) and increase of the linear intron (green) were fit to single exponential equations, yielding a k_{obs} of $1.55 \pm 0.16 \text{ min}^{-1}$ and $1.2 \pm 0.24 \text{ min}^{-1}$, respectively.

As Mss116p is able to further stimulate Cbp2-assisted bl5 splicing, both when added to the unfolded bl5 – RNA or the preformed Cbp2 – bl5 complex, we were interested to understand if it is even more beneficial to bl5 folding to have Mss116p act on bl5 prior to forming the Cbp2 – bl5 complex. As such bl5 splicing was again tested at different Mss116p – Cbp2 protein ratios (figures 42-47). In the presence of an equimolar ratio of Cbp2 and Mss116p as well as at 2x excess of Mss116p relative to Cbp2 the splicing activity is 2.6-fold increased, from $0.41 \pm 0.03 \text{ min}^{-1}$ to $1.05 \pm 0.16 \text{ min}^{-1}$ and $1.09 \pm 0.18 \text{ min}^{-1}$, respectively (figures 42-45). In contrast, adding 4x molar excess of Mss116p over Cbp2 to the bl5 splicing reaction results in a k_{obs} of $1.68 \pm 0.25 \text{ min}^{-1}$ and thus in a 4.1-fold enhancement (figures 46-47).

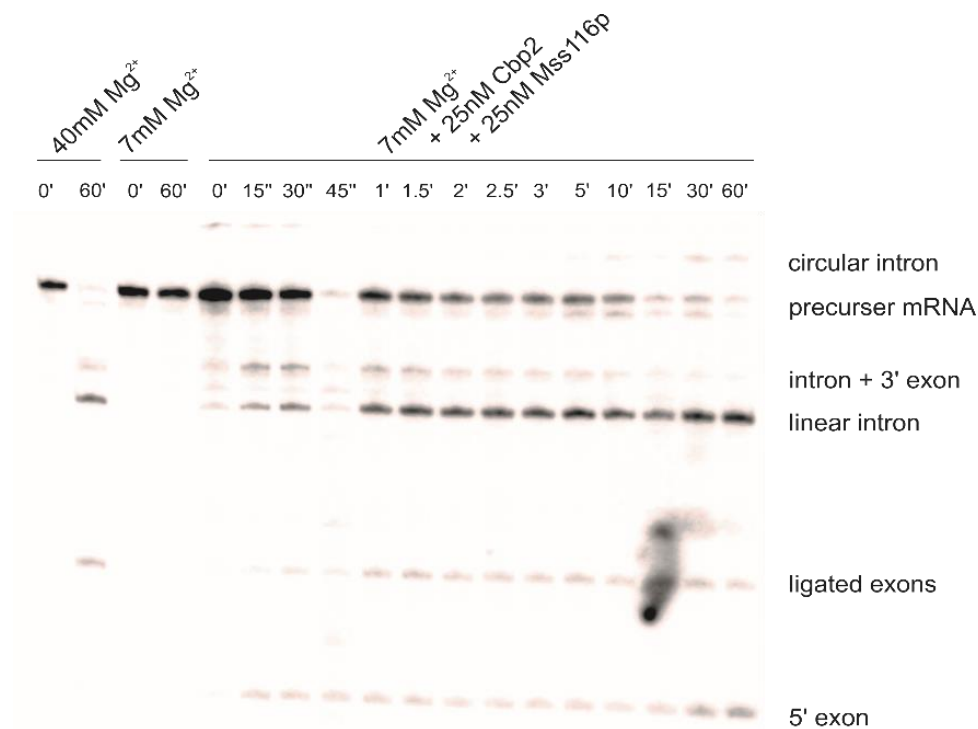


Figure 42: 25nM Cbp2 promote splicing of the preformed Mss116p - bl5 complex using 25nM Mss116p at near-physiological conditions. As positive control folding of bl5 with 40mM Mg^{2+} is shown (lanes 1 and 2). For negative control 7mM Mg^{2+} in absence of the protein was used (lanes 3 and 4).

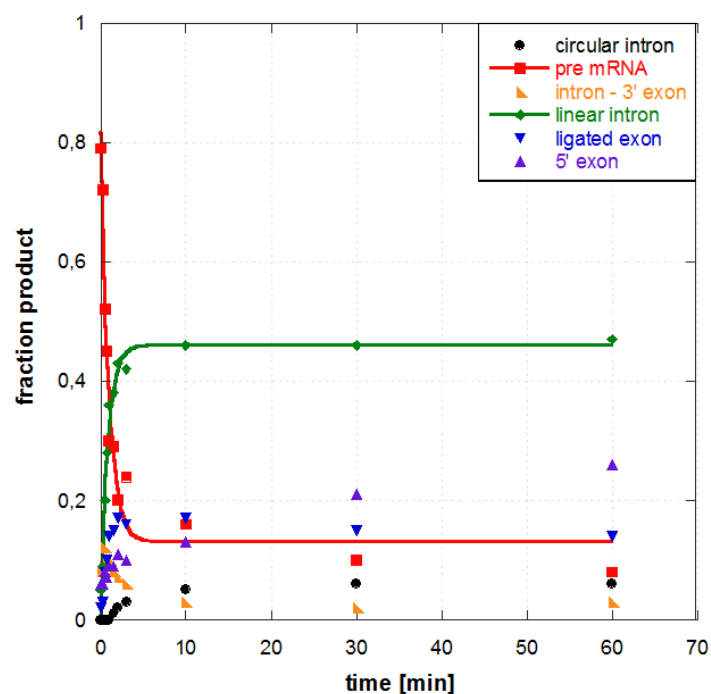


Figure 43: Kinetic progress curve of preformed Mss116p - bl5 complex, using 25nM Mss116p, self-splicing in the presence of 25nM Cbp2. Decay of pre-mRNA (red) and increase of the linear intron (green) were fit to single exponential equations, yielding a k_{obs} of $1.10 \pm 0.16 \text{ min}^{-1}$ and $1.23 \pm 0.11 \text{ min}^{-1}$, respectively.

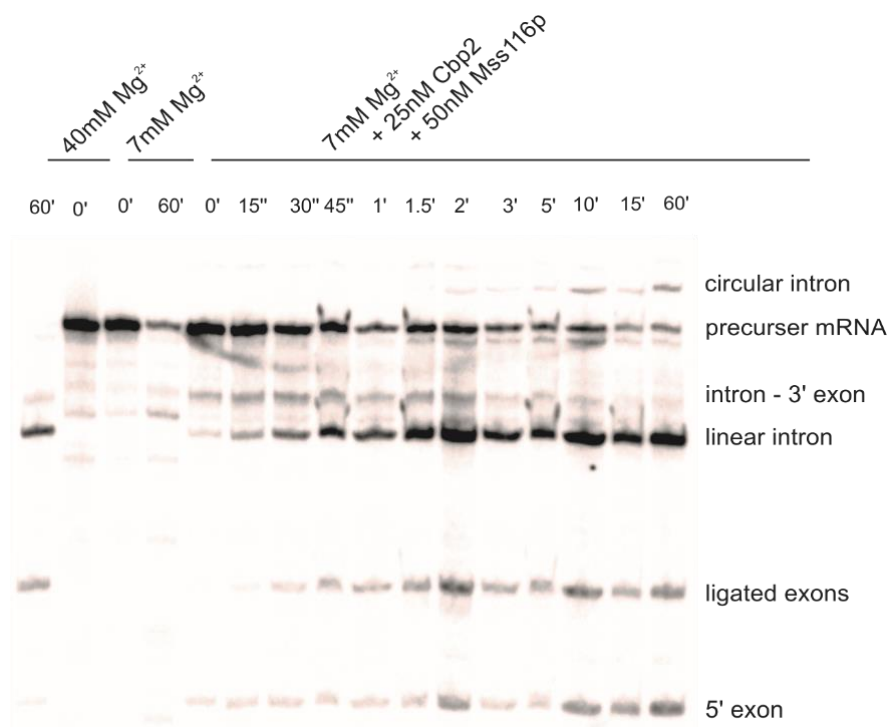


Figure 44: 25nM Cbp2 promote splicing of the preformed Mss116p - bl5 complex using 50nM Mss116p at near-physiological conditions. As positive control folding of bl5 with 40mM Mg^{2+} is shown (lanes 1 and 2). For negative control 7mM Mg^{2+} in absence of the protein was used (lanes 3 and 4).

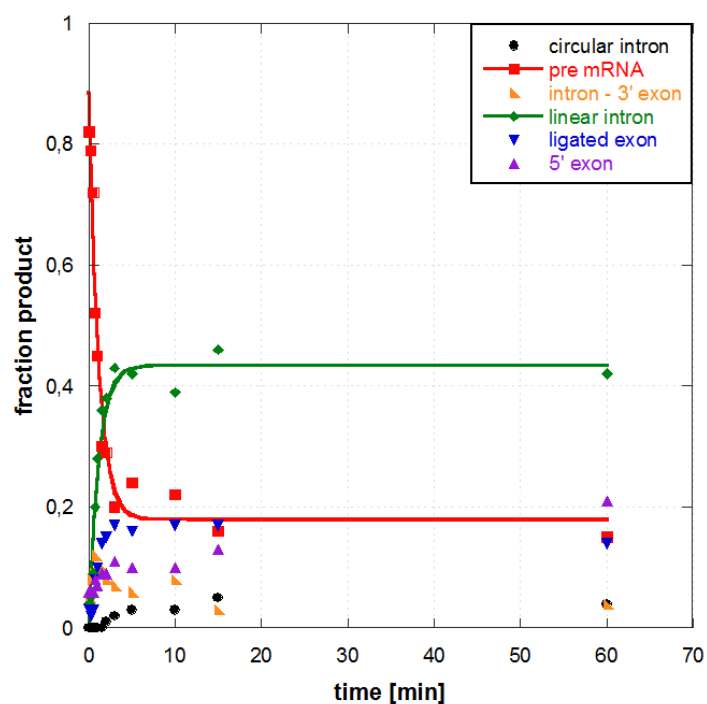


Figure 45: Kinetic progress curve of preformed Mss116p - bl5 complex, using 50nM Mss116p, self-splicing in the presence of 25nM Cbp2. Decay of pre-mRNA (red) and increase of the linear intron (green) were fit to single exponential equations, yielding a k_{obs} of $0.91 \pm 0.13 \text{ min}^{-1}$ and $0.90 \pm 0.12 \text{ min}^{-1}$, respectively.

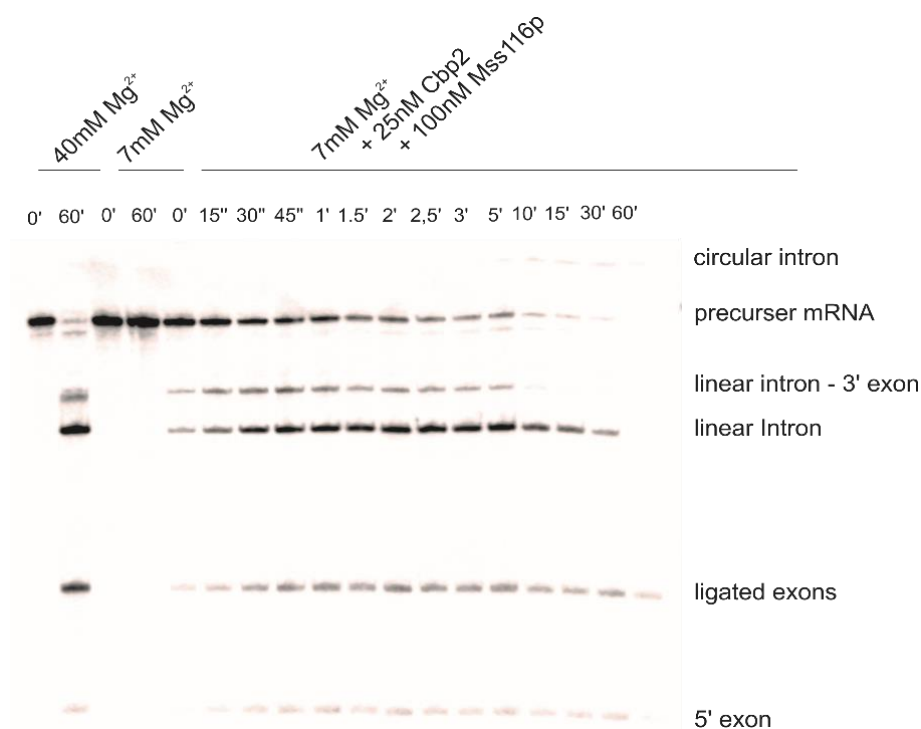


Figure 46: 25nM Cbp2 promote splicing of the preformed Mss116p - bI5 complex using 100nM Mss116p at near-physiological conditions. As positive control folding of bI5 with 40mM Mg^{2+} is shown (lanes 1 and 2). For negative control 7mM Mg^{2+} in absence of the protein was used (lanes 3 and 4).

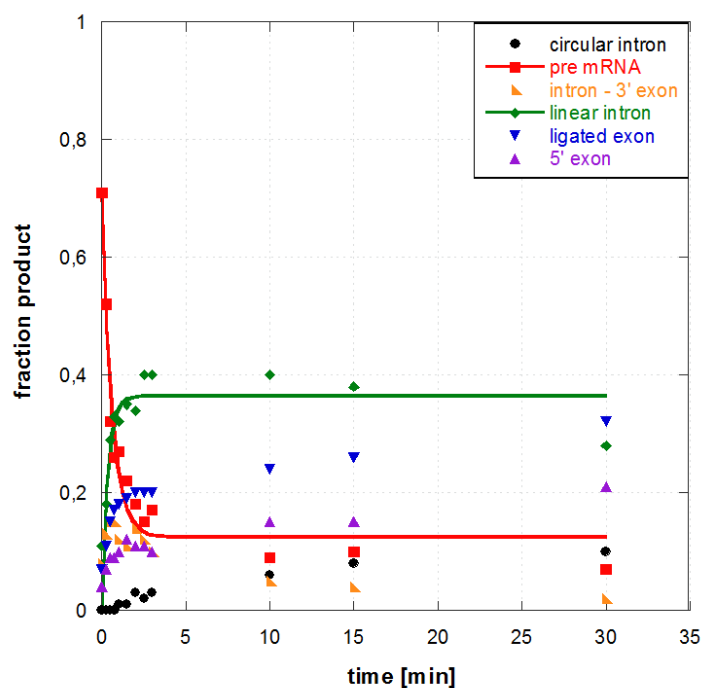


Figure 47: Kinetic progress curve of the preformed Mss116p - bI5 complex, using 100nM Mss116p, self-splicing in the presence of 25nM Cbp2. Decay of pre-mRNA (red) and increase of the linear intron (green) were fit to single exponential equations, yielding a k_{obs} of $1.64 \pm 0.25 \text{ min}^{-1}$ and $2.86 \pm 0.79 \text{ min}^{-1}$, respectively.

3. Determining the dissociation constant of Cbp2 and Mss116p to bI5

To get more insight into the interactions between Cbp2, Mss116p and bI5, structural analysis is necessary. In order to perform informative structural analysis such as SHAPE or DMS - probing, the dissociation constants of the proteins to bI5 have to be determined. The dissociation constant describes the affinity of a protein and a ligand. It is defined as the concentration of a protein, at which half of the ligand binding sites are occupied. The smaller the dissociation constant, the higher the affinity of protein and ligand is. To determine the K_d of either protein to the bI5 intron, which was folded to the near-native state prior to complex formation, the RNA was incubated at increased protein concentration. The complex was separated from the unbound RNA by filter binding (figures 48-64).

		K_d [nM]	$1/k_{rel}$ [min ⁻¹]
Each protein was added separately to unfolded bI5 RNA	0-100nM Cbp2	3.03nM ± 0.3	1
	0-400nM Mss116p	24.5nM ± 5.1	8.1
	0-1μM BSA	n.a.	n.a.
Mss116p is added to Cbp2 - bI5 complex	10nM Cbp2 0-400nM Mss116p	40.2nM ± 4.6	13.3
Cbp2 is added to Mss116p - bI5 complex	100nM Mss116p 0-100nM Cbp2	n.a.	n.a.
KCl is added to the Cbp2 - bI5 complex	10nM Cbp2 0-400mM KCl	n.a.	n.a.
Cbp2 is added to unfolded bI5 under high salt conditions	200mM KCl 0-100nM Cbp2	n.a.	n.a.
Cbp2 is added to unfolded bI5	0-100nM Cbp2 Mss116p PSB	17.25nM ± 5.7	5.7

Figure 48: Observed dissociation constants of proteins to bI5

3.1 Cbp2 binds with high affinity to bI5

In vitro, Cbp2 is a must for efficient splicing of bI5 at near-physiological conditions. Thus, the K_d of Cbp2-bI5 complex was determined first. For first approximations, we decided to go for a Cbp2 concentration range of 0nM-500nM (data not shown). These early filter binding assays suggested that the dissociation constant of Cbp2 is rather low. Therefore we reduced Cbp2 concentration range to 0nM-100nM (figure 49).

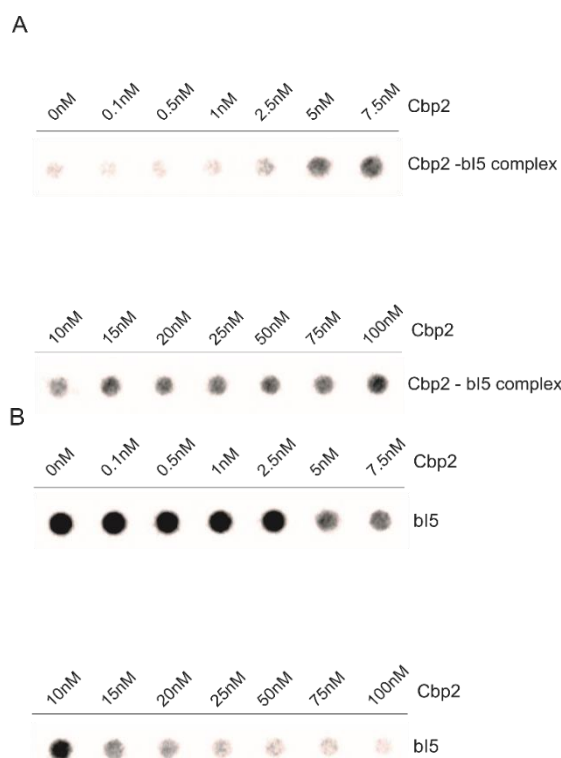


Figure 49: Determining the binding constant of Cbp2 to the bI5 intron.

A) The nitrocellulose selects for bI5 bound to Cbp2.

B) The positively charged nylon membrane selects for unbound bI5.

As shown in figure 49, the constant increase of Cbp2 concentrations, up to 100nM, leads to a stronger signal for the Cbp2-bI5 complex while that of the unbound bI5 decreased.

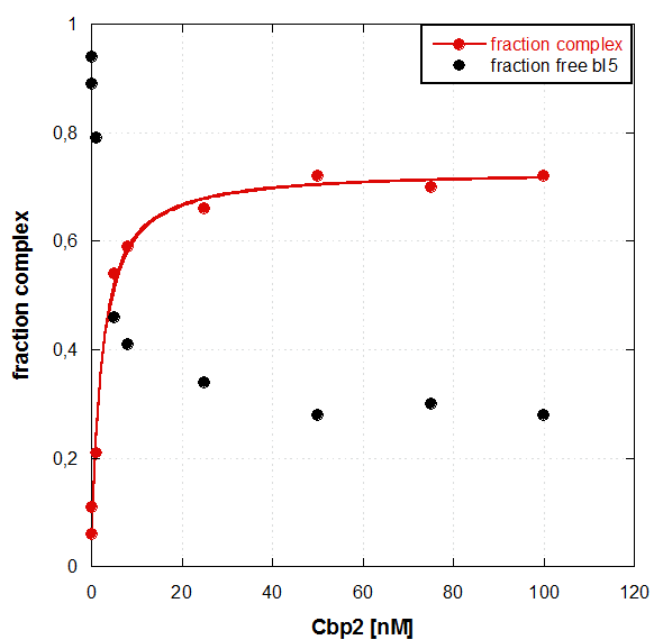


Figure 50: Binding curve of Cbp2 to the bI5 intron.

The fraction of complex (red) of the fraction of unbound bI5 (black) was plotted against the protein concentrations and fit to a 1:1 binding isotherm.

The observed K_d of Cbp2 to bI5 was 3.03 ± 0.3 nM with an amplitude of 0.73 ± 0.04 . The amplitude describes the maximal fraction of complex. These data correlate well with the previously published K_d for the bI5-Cbp2 complex, revealing a K_d of 1.0 ± 0.3 nM (Weeks & Cech 1995).

3.2 Mss116p has a K_d to bI5 in the nM range

The DEAD-box helicase is necessary to stimulate splicing of all yeast mitochondrial introns including bI5 (Huang et al. 2005). So far, it however remains enigmatic how Mss116p interacts with the bI5 intron. To obtain a first insight on the Mss116p-bI5 complex, we determined the dissociation constant of the DEAD-box helicase to bI5. For first filter binding assays with Mss116p, we used a protein concentration range of 0nM-100nM (data not shown). As the saturation point was not reached, the Mss116p concentration range was increased to 0nM-400nM (figure 51). As shown in figure 51, with increasing Mss116p concentrations, more and more of the Mss116p complex formed, while the signal of the unbound bI5 RNA decreased. We observed a K_d 24.5 ± 5.1 nM with an amplitude at 0.48 ± 0.02 . Thus, the affinity of Mss116p to bI5 is 8.1-fold lower than that of Cbp2 to bI5 and the amplitude is smaller as well.

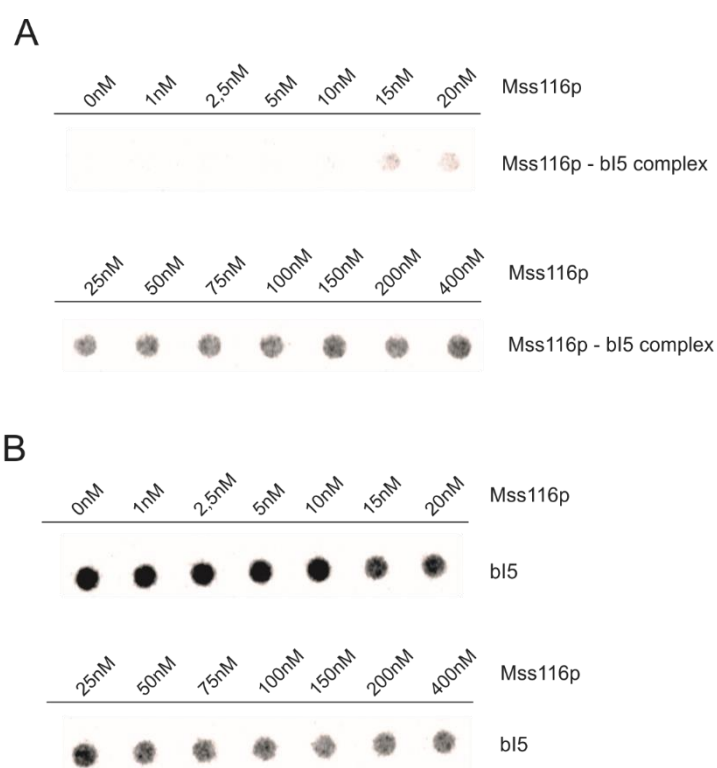


Figure 51: Determining the binding constant of Mss116p to the bI5 intron.

- A) The nitrocellulose membrane selects for bI5 bound to Mss116p.
 B) The positively charged nylon membrane selects for unbound bI5.

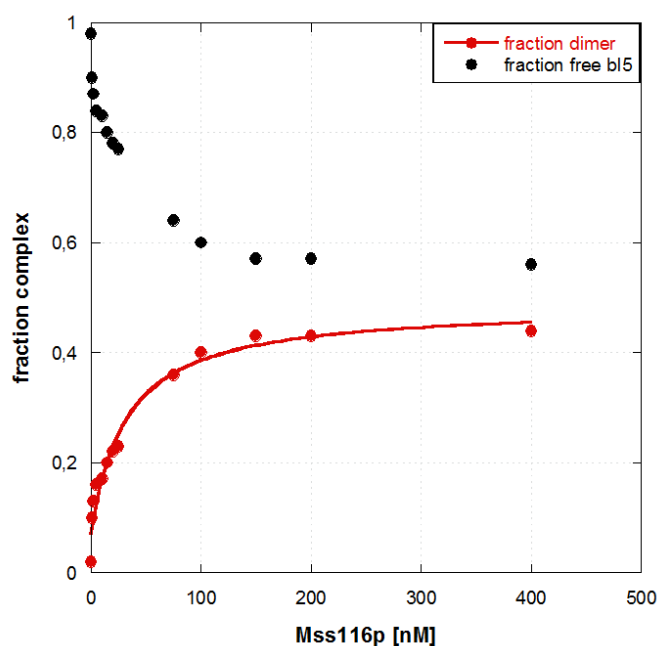


Figure 52: Binding curve of Mss116p to the bl5 intron.

The fraction of complex (red) of the fraction of unbound bl5 (black) was plotted against the protein concentrations and fit to a 1:1 binding isotherm.

3.3 Cbp2 and Mss16p do bind specifically to bl5

To ensure that binding of Cbp2 and Mss116p is specific, a filter binding assay with increasing bovine serum albumin concentrations and constant bl5 concentration was performed as well (figures 53 and 54). BSA is a protein derived from cow and is often used for unspecific binding, for example in staining experiments.

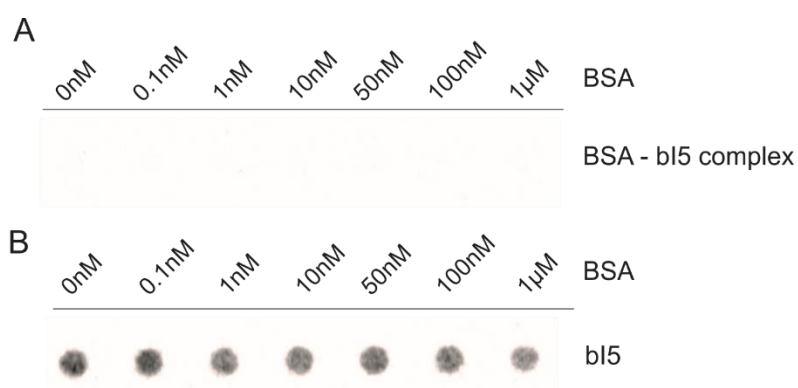


Figure 53: Determining the binding constant of BSA to the bl5 intron.

- A) The nitrocellulose membrane selects for bl5 bound to BSA.
 B) The positively charged nylon membrane selects for unbound bl5.

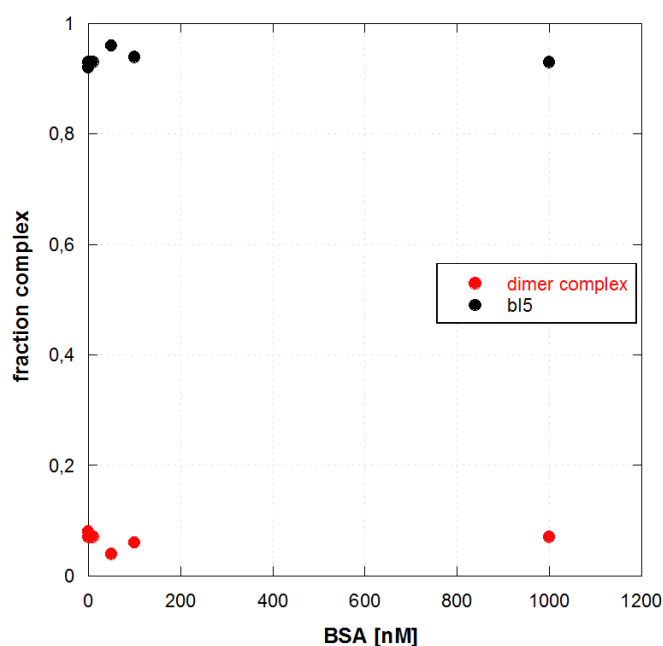


Figure 54: Binding curve of Mss116p to the bl5 intron.

The fraction of complex (red) of the fraction of unbound bl5 (black) was plotted against the protein concentrations.

Importantly, complex formation between BSA and bl5 was not observed, not even at μM concentrations of BSA (figures 52-54). This suggests that non-specific RNA-protein interactions for retention do not take place.

3.4 Influence of Cpb2 on Mss116p-bl5 affinity

We already determined the K_d of the individual proteins to bl5. Admittedly, most experiments, including splicing assays, were performed with both proteins. To see if the two proteins impact on each other's K_d , we performed additional filter binding assays. As such, we determined the dissociation constant of Mss116p to the bl5-Cbp2 complex, which was performed by incubating Cbp2 at a concentration 3-fold above the K_d with bl5.

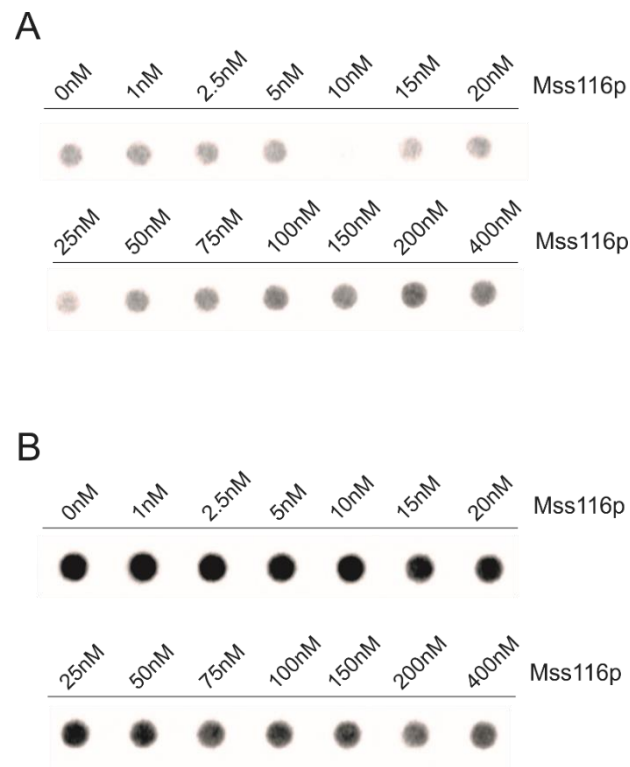


Figure 55: Determining the binding constant of Mss116p to the bl5 intron.

- A) The nitrocellulose membrane selects for bl5 bound to Mss116p/Cbp2.
 B) The positively charged nylon membrane selects for unbound bl5.

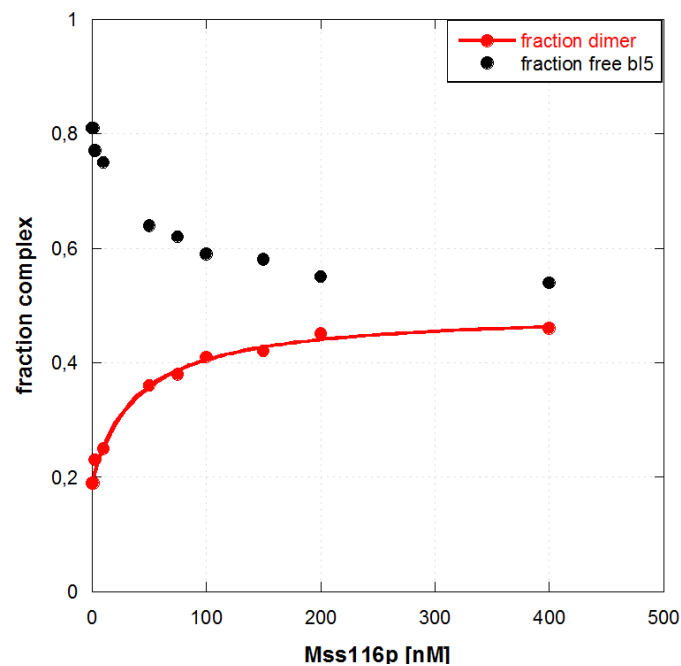


Figure 56: Binding curve of Mss116p to the bl5 intron.

The fraction of complex (red) of the fraction of unbound bl5 (black) was plotted against the protein concentrations and fit to a 1:1 binding isotherm.

The data resulted in a K_d of 40.2 ± 4.6 nM with an amplitude at 0.48 ± 0.01 . While the addition of Cbp2 did not impact on the amplitude, the K_d of Mss116p to the bl5 - Cbp2 complex (figure 56) was slightly increased compared to that to bl5 (figures 48, 51 and 52). Surprisingly, we expected to observe a similar fraction of Cbp2-bl5 complex before adding Mss116p, but instead of an amplitude of 0.6 only 0.2 was obtained repeatedly at 10nM Cbp2 (figures 50 and 56).

3.5 Influence of Mss116p on Cbp2-bl5 complex affinity

At next we examined the dissociation constant of Cbp2 to the bl5-Mss116p complex. Therefore we incubated bl5 with a Mss116p concentration, which is 3 fold above the K_d of Mss116p to bl5.

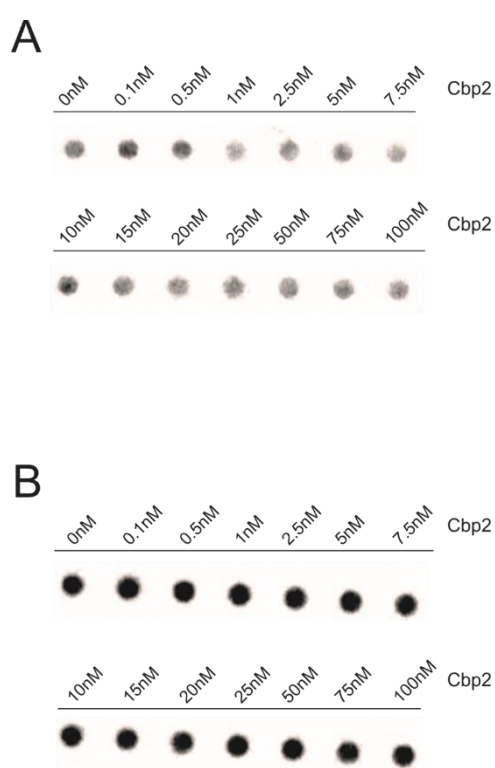


Figure 57: Determining the binding constant of Cbp2 to the bl5 intron.

- A) The nitrocellulose membrane selects for bl5 bound to Mss116p/Cbp2.
 B) The positively charged nylon membrane selects for unbound bl5

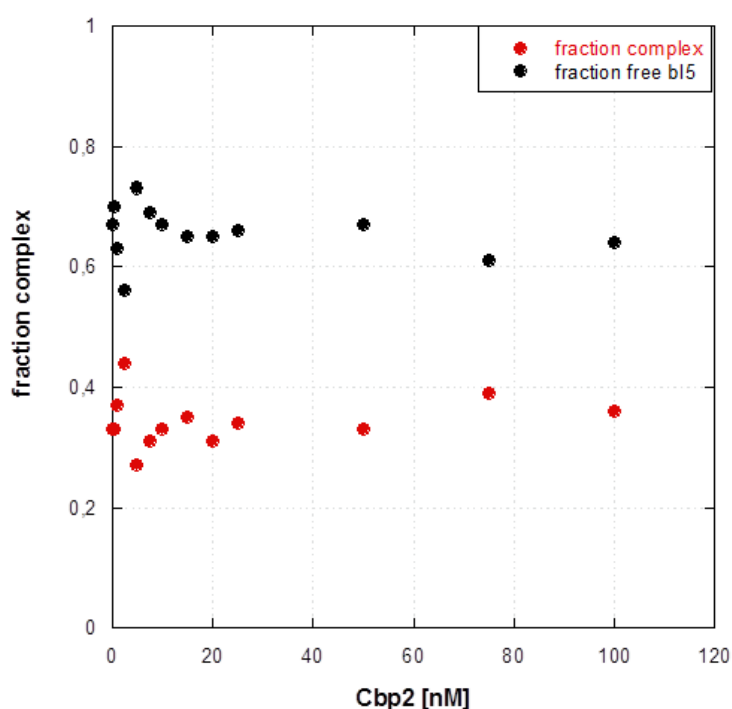


Figure 58: Binding curve of Cbp2 to the bI5 intron.

The fraction of complex (red) of the fraction of unbound bI5 (black) was plotted against the protein concentrations.

Quantification reveals that two-third of the total RNA passed the upper membrane, regardless of the added Cbp2 amount. This surprising data left room for several interpretations. For example, Cbp2 and Mss116p may in part compete for a binding site and/or Cbp2 needs to bind prior to Mss116p on bI5. Another explanation could be that Mss116p displaces Cbp2 from bI5. At last, it is also essential to consider the increased salt concentrations, which are due to protein storage buffers of either protein. These elevated salt conditions may affect binding of the proteins to bI5.

3.6 The influence of salt concentrations on the dissociation constant of Cbp2

We further investigated the influence of salt concentration on the dissociation constant of Cbp2 to bI5. Previous filter binding assays showed that binding might be influenced by salt concentrations. Mss116p and Cbp2 are stored in storage buffers, which contain high ionic concentrations 300mM KCl and 200mM NaCl, respectively. Adding both proteins to the reaction mix increases the salt concentration, compared to adding just one protein. This potentially affects the interaction of a protein with its target RNA. On the other hand, increased salt concentrations could also influence protein stability. Hence, we assayed $K_{1/2}$ of KCl to the Cbp2 - bI5 complex.

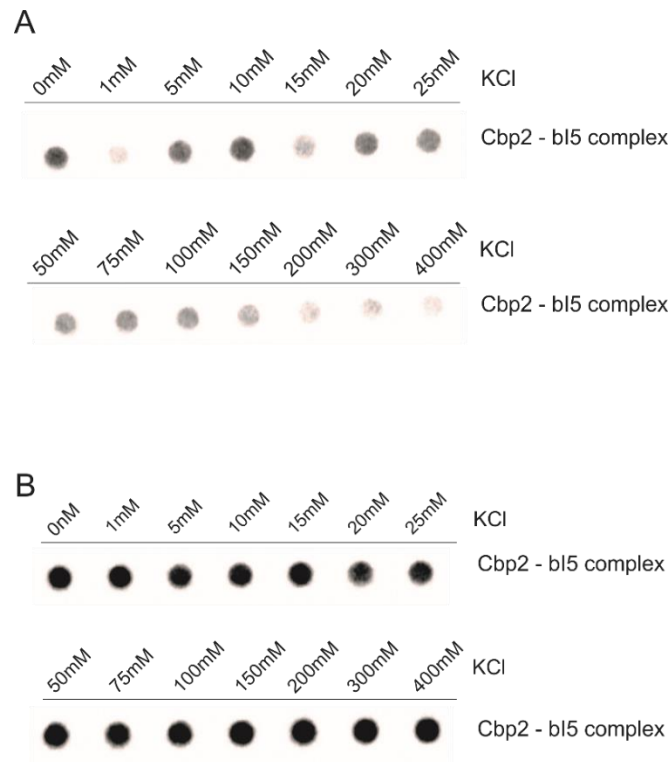


Figure 59: Determining $K_{1/2}$ of KCl to the Cbp2 – bI5 complex.

- A) The nitrocellulose membrane selects for bI5 bound to Cbp2.
 B) The positively charged nylon membrane selects for unbound bI5

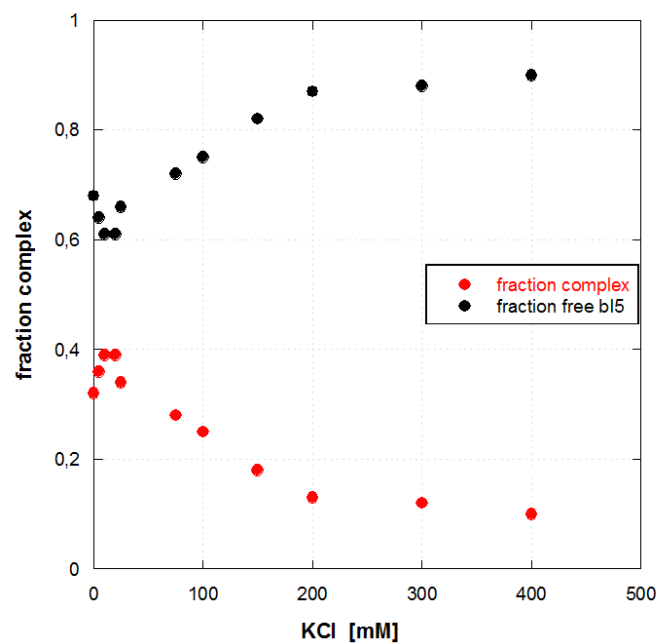


Figure 60: Binding curve of Cbp2 to the bI5 intron.

The fraction of complex (red) of the fraction of unbound bI5 (black) was plotted against the protein concentrations.

Indeed, the fraction of the Cbp2-bl5 complex decreased with increasing [KCl], whereby an addition of 400mM KCl resulted in almost no complex formation (figure 60). The lower, positively charged nylon membrane is seen figure 62. The signals on the lower membrane do not show visual changes. However, data analysis of both membranes revealed the distribution of bound and unbound bl5. The higher the salt concentration, the fewer bl5-Cbp2 complexes were formed or remain stable (figures 59-60). These results indicate that salt concentrations indeed heavily influence binding of Cbp2 to bl5. Since 200mM KCl appeared to largely interfere with complex formation of Cbp2 and bl5, we set out to determine the K_d of Cbp2 to bl5 folded in the presence of additional 200mM KCl (in addition to 7mM Mg^{2+}). However, it was not possible to derive a K_d of Cbp2 to bl5 at elevated KCl concentrations (figures 61-62). The midpoint of the curve is at ~50nM, which is ~10-fold higher than K_d of Cbp2 to bl5 at 200mM NaCl (figure 50). Also the fraction of the complex at 100nM Cbp2 is only ~0.35 compared to 0.78 determined previously (figures 50 and 64). Given that Cbp2 harbours many basic amino acids, its interaction with bl5 may be of more electrostatic nature, and thus monovalent ions can interfere with this interaction.

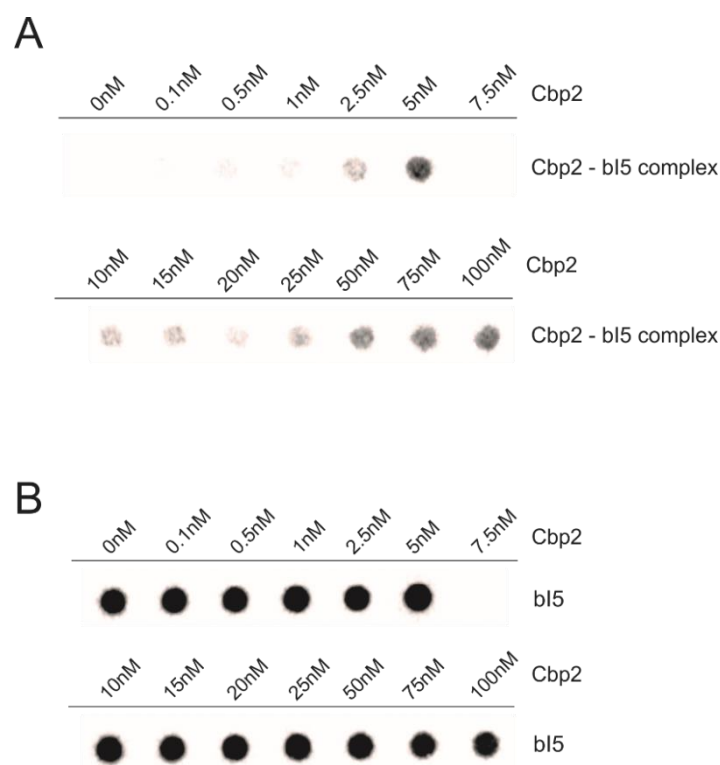


Figure 61: Determining the binding constant of Cbp2 to the bl5 intron under increasing salt concentrations

- A) The nitrocellulose membrane selects for bl5 bound to Cbp2.
 B) The positively charged nylon membrane selects for unbound bl5

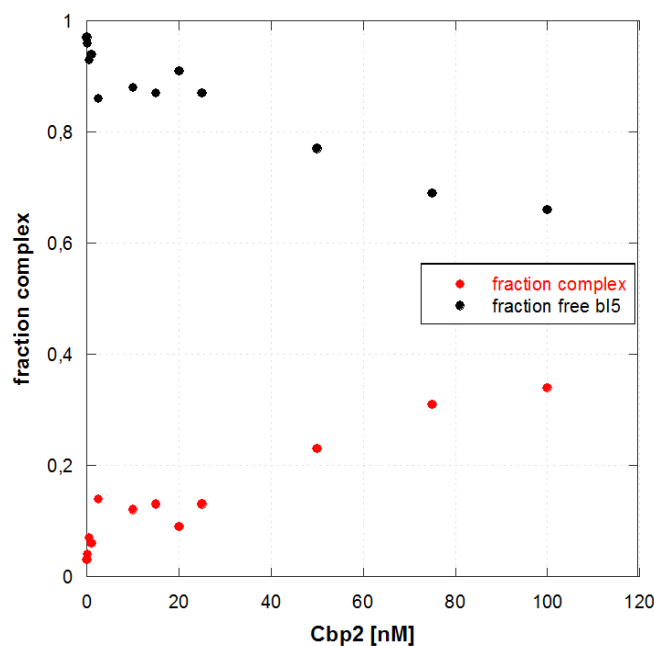


Figure 62: Binding curve of Cbp2 to the bl5 intron.

The fraction of complex (red) of the fraction of unbound bl5 (black) was plotted against the protein concentrations.

Since the Mss116p storage buffer contains 30mM KCl and thus increases the ion concentration to 50mM in the bl5 folding reaction, an attempt was made to determine the K_d of Cbp2 to bl5 in the presence of Mss116p storage buffer (figure 63-64). According to our previous results, Cbp2 is expected to not build a complex with bl5 till a certain protein concentration.

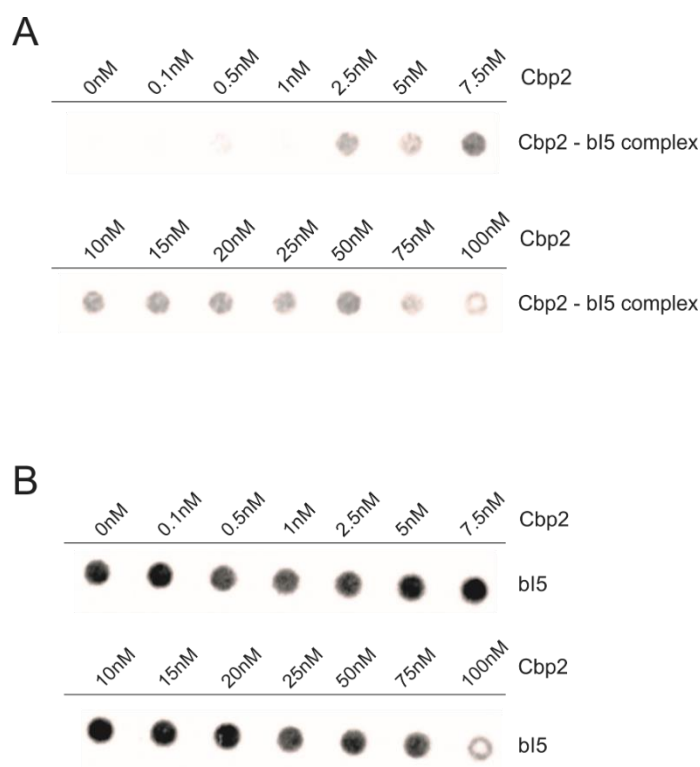


Figure 63: Determining the binding constant of Cbp2 to the bl5 intron under increased salt concentrations

A) The nitrocellulose membrane selects for bl5 bound to Cbp2.

B) The positively charged nylon membrane selects for unbound bl5.

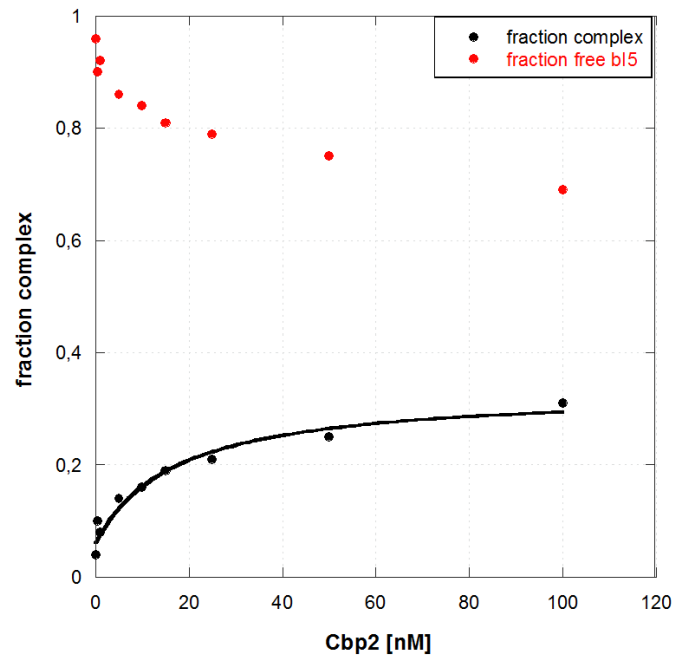


Figure 64: Binding curve of Cbp2 to the bl5 intron under high salt concentrations.

The fraction of complex (red) of the fraction of unbound bl5 (black) was plotted against the protein concentrations and fit to a 1:1 binding isotherm.

Compared to filter binding assays without Mss116p storage buffer, the dissociation constant was ~6-fold increased to a K_d of $17.25 \pm 5.7 \text{ nM}$. The amplitude was found at 0.30 ± 0.03 , which was less than half of that observed for at Cbp2 without Mss116p storage buffer (0.73 ± 0.02). This indicates that binding was much less efficient in the presence of evaluated salt amounts.

Discussion

The *Saccharomyces cerevisiae* bI5 intron belongs to the self-splicing group I introns. For efficient autocatalytic splicing, bI5 needs to reach its native conformation. *In vivo*, two proteins assist the pre-mRNA during the folding process. On the one hand, the DEAD-box helicase Mss116p is required for efficient bI5 splicing. Recently, the first insight in Mss116p's role in bI5 folding was reported (Sachsenmaier 2014). It appears that Mss116p needs to resolve a misfold bI5 folding intermediate to allow efficient bI5 splicing. On the other hand, the splicing cofactor Cbp2 is known to capture the near-native bI5 conformation and therefore facilitates efficient splicing. During this master thesis we performed several experiments for characterizing interactions of the bI5-Cbp2-Mss116p complex.

ATPase activity of Mss116p

Before studying the Mss116p-bI5 intron interaction, we tested recombinant Mss116p for its activity, using ATPase assays. Active Mss116p binds and hydrolyzes ATP (Huang et al. 2005; Séraphin et al. 1987). The amount of free phosphates can then be detected using malachite green assays. Malachite green forms a complex with ammonium molybdate and free phosphate. The absorbance of this complex gives information about the concentration of free phosphate, which further reflects activity of Mss116p. Out of 5 batches 3 Mss116p preparations were very active, while others had almost no activity. However, earlier purified proteins had higher activity (Steiner 2012). This suggest that either the protein purification was performed differently or the ATPase assay, a kit, is less effective. After trouble shooting of the protein purification procedure (i.e. fresh stock solutions, new cells, re-sequencing of the plasmid, among other strategies), the Mss116p activity remained at a low level, even for the positive control. Therefore, we considered that the kit used to determine the ATPase activity does not work properly anymore. The repeated use (i.e. freeze-thawing cycles) may have caused degradation of certain KIT compounds. In the end, we chose older Mss116p batches that were shown to have high ATPase activity for further experiments.

Mss116p stimulates efficient splicing of the bI5-Cbp2 complex

Efficient splicing is achieved by fast and correct folding of bI5 into its native structure. We performed *in vitro* splicing assays, which tested splicing of bI5 under various conditions. Similar to previously published data (Weeks & Cech 1995), we showed that splicing of bI5 *in vitro* can be achieved by high Mg^{2+} concentration around 40mM. We also tested bI5 splicing under low Mg^{2+} concentrations, with 7mM, at which bI5 collapses to the near-native state (Weeks & Cech 1995; McGraw & Tzagoloff 1983). As expected, no splicing of bI5 was observed under near-physiological conditions *in vitro*. Upon adding Cbp2 to the bI5 splicing reaction the splicing rate constant increases a 1000-fold (Weeks

& Cech 1996). In fact, Cbp2 was found to assist bI5 in folding, by capturing the collapsed near-native state of the intron and its native conformation (Weeks & Cech 1995; McGraw & Tzagoloff 1983).

In line with previously published data (Weeks & Cech 1995), we demonstrated that our recombinant Cbp2 batches promote efficient bI5 folding and in turn splicing. Previous experiments revealed a k_{obs} of $0.41 \pm 0.03 \text{ [min}^{-1}\text{]}$ for the pre-mRNA decay at 25nM Cbp2 (Debeljak 2013). This k_{obs} is 2-fold lower than in the presence of 50nM ($1.0 \pm 0.3 \text{ min}^{-1}$) respectively (Debeljak 2013; Weeks & Cech 1995). Importantly, low monovalent salt concentrations did not strongly affect bI5 splicing (k_{obs} of $0.55 \pm 0.02 \text{ min}^{-1}$ at 50mM KCl). This indicates that low salt concentrations do not compete with Cbp2 binding to the bI5 RNA.

In vivo, Mss116p is known to assist bI5 in folding (Huang et al. 2005; Séraphin et al. 1987; Sachsenmaier & Waldsich 2013). *In vitro*, however, Mss116p is not strictly required as Cbp2-assisted bI5 splicing is already very efficient (McGraw & Tzagoloff 1983; Weeks & Cech 1995). To obtain the first insights into how Mss116p and Cbp2 cooperate to facilitate bI5 folding, we tested the splicing efficiency of bI5 in the presence of Cbp2 and Mss116p *in vitro*.

Using equimolar ratios of Cbp2 and Mss116p or a 2-fold molar excess of Mss116p over Cbp2 results in a ~2-fold increase in k_{obs} , compared to Cbp2-assisted bI5 splicing (figure 65). Increasing the Mss116p to Cbp2 molar ratio to 4-fold further enhances the observed rate constant of bI5 splicing (~4-fold). Importantly, these observed effects were virtually identical whether both proteins were added concomitantly to the denatured bI5 intron or if the 2nd protein was added to either pre-formed protein-bI5 complex to (figure 65). This suggest that the order of events, in which the two proteins encounter and act on the RNA is not critical determinant for promoting efficient bI5 splicing. Also, these data imply that the two proteins do not appear to compete for a binding site. Since the increase in k_{obs} in the presence of Mss116p in addition to Cbp2, is only small, this could indicate that only a sub-population of bI5 pre-mRNAs depend on Mss116p for proper folding, while the entire bI5 population requires Cbp2 for reaching the native conformation. This is also in line with the fact that *in vivo* bI5 splicing is reduced to 50% in the *mss116* knock-out strain, while it is abolished in the *cbp2* knock-out strain (Sachsenmaier 2014).

		k_{obs} [min^{-1}]	$1/k_{\text{rel}}$
Cbp2 is added to the unfolded bI5 - RNA complex	25nM Cbp2	0.41 ± 0.03	1
	10nM Cbp2	0.64 ± 0.03	1.5
	10nM Cbp2 + 50mM KCl	0.55 ± 0.02	1.3
Cbp2 and Mss116p are added concomitantly to the unfolded bI5 - RNA	25nM Cbp2 + 25nM Mss116p	0.97 ± 0.15	2.2
	25nM Cbp2 + 50nM Mss116p	1.07 ± 0.16	2.4
	25nM Cbp2 + 100nM Mss116p	1.90 ± 0.18	4.7
Mss116p is added to the native Cbp2 - bI5 complex	25nM Cbp2 + 25nM Mss116p	0.76 ± 0.05	1.9
	25nM Cbp2 + 50nM Mss116p	0.95 ± 0.14	2.3
	25nM Cbp2 + 100nM Mss116p	1.60 ± 0.15	3.9
Cbp2 is added to the Mss116p - bI5 complex	25nM Mss116p + 25nM Cbp2	1.05 ± 0.16	2.6
	50nM Mss116p + 25nM Cbp2	1.09 ± 0.18	2.6
	100nM Mss116p + 25nM Cbp2	1.68 ± 0.25	4.1

Figure 65: Observed rate constant of bI5 splicing under various reaction conditions. k_{obs} was derived from pre-mRNA decay. The average and standard deviation were calculated for three independent experiments.

Both proteins bind with high affinity to bI5

For characterization of protein-RNA interactions, it is necessary to characterize certain thermodynamic parameters at first. For this reason, we first determined the affinity of Cbp2 and Mss116p to bI5. Cbp2 showed a dissociation constant of $3.03 \pm 0.3\text{nM}$, while that of Mss116p is $24.5 \pm 5.1\text{nM}$. As expected Cbp2 has higher affinity to bI5 than Mss116p. Additionally, the maximum binding fraction, which is represented by the amplitude, of Cbp2 was much higher (0.73 ± 0.04) than binding fraction of Mss116p (0.48 ± 0.02). While Mss116p assists in folding of all mitochondrial group I and group II intron in *Saccharomyces cerevisiae*, Cbp2 is only essential for bI5 (McGraw & Tzagoloff 1983; Weeks & Cech 1995; Gampel & Cech 1991). Hence, Cbp2 binding is very specific, which could explain this high affinity. In the low nM range Mss116p, on the other hand, needs to bind to two structurally distinct RNA classes and therefore might be less specific and have a lower affinity, but still in the moderate nM range. *In vivo*, bI5 splicing depends on both proteins. Thus, we examined the influence of either protein on the second proteins dissociation constant. Remarkably, the dissociation constant of Mss116p increased from $24.5 \pm 5.1\text{nM}$ to $40.2 \pm 4.6\text{nM}$ (1.6-fold increase). In contrast, it was not possible to determine the K_d of Cbp2 to the Mss116p-bI5 complex (figures 57-58). As the Mss116p storage buffer contains 300mM KCl, we assessed the effect of increased monovalent salt concentration on binding of Cbp2 to bI5.

However, it was not possible to derive a K_d of Cbp2 to bI5 at elevated KCl concentrations (figures 61-62). The midpoint of the curve is at $\sim 50\text{nM}$, which is ~ 10 -fold higher than K_d of Cbp2 to bI5 at 20mM

NaCl (figure 50). Also the fraction of the complex at 100nM Cbp2 is only ~0.35 compared to 0.78 determined previously (figure 50). Given that Cbp2 harbours many basic amino acids, its interaction with bI5 may be of more electrostatic nature, and thus monovalent ions can interfere with this interaction.

In line with these observations, the K_d of Cbp2 to bI5 increased 5.7-fold (from 3.03nM to 17.25nM) in the presence of the Mss116p storage buffer, which increased the final KCl concentration from 30mM to 50mM. Also the amplitude dropped from 0.78 to 0.30 (figure 50 and 64). These data decisively demonstrated Cbp2 binding to bI5 is strongly influenced by ionic conditions. Thus the fact that it was impossible to determine the binding affinity of Cbp2 to the Mss116p-bI5 complex was caused by monovalent ions interfering with the electrostatic interaction of Cbp2 with bI5 and not due to overlapping binding site of the two proteins on bI5. To shed further light on Cbp2/Mss116p-assisted bI5 folding, it was now possible to set up *in vivo* structural probing assay to monitor protein-induced conformational changes on the structured bI5 intron flanked by short exon sequences.

		K_d [nM]	$1/k_{rel}$ [min ⁻¹]
Each protein was added separately to unfolded bI5 RNA	0-100nM Cbp2	3.03nM ± 0.3	1
	0-400nM Mss116p	24.5nM ± 5.1	8.1
	0-1µM BSA	n.a.	n.a.
Mss116p is added to Cbp2 - bI5 complex	10nM Cbp2 0-400nM Mss116p	40.2nM ± 4.6	13.3
Cbp2 is added to Mss116p - bI5 complex	100nM Mss116p 0-100nM Cbp2	n.a.	n.a.
KCl is added to the Cbp2 - bI5 complex	10nM Cbp2 0-400mM KCl	n.a.	n.a.
Cbp2 is added to unfolded bI5 under high salt conditions	200mM KCl 0-100nM Cbp2	n.a.	n.a.
Cbp2 is added to unfolded bI5	0-100nM Cbp2 Mss116p PSB	17.25nM ± 5.7	5.7

Figure 66: Observed dissociation constants of proteins to bI5.

References

- Abrahams, J.P. et al, 1990. Prediction of RNA secondary structure, including pseudoknotting, by computer simulation. *Nucleic acids research*, 18(10), pp.3035–44. Available at: <http://www.pubmedcentral.nih.gov/articlerender.fcgi?artid=330835&tool=pmcentrez&rendertype=abstract> [Accessed December 2, 2014].
- Bomsztyk, K., Denisenko, O. & Ostrowski, J., 2004. hnRNP K: one protein multiple processes. *BioEssays : news and reviews in molecular, cellular and developmental biology*, 26(6), pp.629–38. Available at: <http://www.ncbi.nlm.nih.gov/pubmed/15170860> [Accessed February 15, 2015].
- Butcher, S., Hainaut, P. & Milner, J., 1994. Increased salt concentration reversibly destabilizes p53 quaternary structure and sequence-specific DNA binding. *The Biochemical journal*, 298 Pt 3, pp.513–6. Available at: <http://www.pubmedcentral.nih.gov/articlerender.fcgi?artid=1137888&tool=pmcentrez&renderertype=abstract> [Accessed December 17, 2014].
- Campbell, T.B. & Cech, T.R., 1996. Mutations in the Tetrahymena ribozyme internal guide sequence: effects on docking of the P1 helix into the catalytic core and correlation with catalytic activity. *Biochemistry*, 35(35), pp.11493–502. Available at: <http://www.ncbi.nlm.nih.gov/pubmed/8784205> [Accessed December 3, 2014].
- Del Campo, M. & Lambowitz, A.M., 2009. Structure of the Yeast DEAD box protein Mss116p reveals two wedges that crimp RNA. *Molecular cell*, 35(5), pp.598–609. Available at: <http://www.pubmedcentral.nih.gov/articlerender.fcgi?artid=2939728&tool=pmcentrez&renderertype=abstract> [Accessed February 15, 2015].
- Debeljak, F. The influence of the RNA helicase Mss116 on CBP2-assisted splicing of the bI5 group I intron in vitro. Diplomarbeit 2013, University of Vienna
- Cate, J.H. et al., 1996. Crystal structure of a group I ribozyme domain: principles of RNA packing. *Science (New York, N.Y.)*, 273(5282), pp.1678–85. Available at: <http://www.ncbi.nlm.nih.gov/pubmed/8781224> [Accessed December 17, 2014].
- Cate, J.H., Hanna, R.L. & Doudna, J.A., 1997. A magnesium ion core at the heart of a ribozyme domain. *Nature structural biology*, 4(7), pp.553–8. Available at: <http://www.ncbi.nlm.nih.gov/pubmed/9228948> [Accessed December 2, 2014].
- Cech, T.R., 1990. Self-splicing of group I introns. *Annual review of biochemistry*, 59, pp.543–68. Available at: <http://www.annualreviews.org/doi/abs/10.1146/annurev.bi.59.070190.002551?journalCode=biochem> [Accessed December 3, 2014].
- Cech, T.R., 1990. Self-splicing of group I introns. *Annual review of biochemistry*, 59, pp.543–68. Available at: <http://www.annualreviews.org/doi/abs/10.1146/annurev.bi.59.070190.002551?journalCode=biochem> [Accessed December 3, 2014].

- Cech, T.R., 2012. The RNA worlds in context. *Cold Spring Harbor perspectives in biology*, 4(7), p.a006742. Available at: http://www.pubmedcentral.nih.gov/articlerender.fcgi?artid=3385955&tool=pmcentrez&render_type=abstract [Accessed November 10, 2014].
- Cech, T.R., Damberger, S.H. & Gutell, R.R., 1994. Representation of the secondary and tertiary structure of group I introns. *Nature Structural Biology*, 1(5), pp.273–280. Available at: <https://univpn.univie.ac.at/+CSCO+00756767633A2F2F6A6A6A2E616E676865722E70627A++/nsm/journal/v1/n5/abs/nsb0594-273.html> [Accessed December 17, 2014].
- Cech, T.R., Damberger, S.H. & Gutell, R.R., 1994. Representation of the secondary and tertiary structure of group I introns. *Nature structural biology*, 1(5), pp.273–80. Available at: <http://www.ncbi.nlm.nih.gov/pubmed/7545072> [Accessed February 24, 2015].
- Chadee, A.B., Bhaskaran, H. & Russell, R., 2010. Protein roles in group I intron RNA folding: the tyrosyl-tRNA synthetase CYT-18 stabilizes the native state relative to a long-lived misfolded structure without compromising folding kinetics. *Journal of molecular biology*, 395(3), pp.656–70. Available at: http://www.pubmedcentral.nih.gov/articlerender.fcgi?artid=2813312&tool=pmcentrez&render_type=abstract [Accessed December 3, 2014].
- Chamberlin, S.I. & Weeks, K.M., 2003. Differential helix stabilities and sites pre-organized for tertiary interactions revealed by monitoring local nucleotide flexibility in the bI5 group I intron RNA. *Biochemistry*, 42(4), pp.901–9. Available at: <http://www.ncbi.nlm.nih.gov/pubmed/12549908> [Accessed December 3, 2014].
- Chen, X., Mohr, G. & Lambowitz, A.M., 2004. The *Neurospora crassa* CYT-18 protein C-terminal RNA-binding domain helps stabilize interdomain tertiary interactions in group I introns. *RNA (New York, N.Y.)*, 10(4), pp.634–44. Available at: http://www.pubmedcentral.nih.gov/articlerender.fcgi?artid=1370554&tool=pmcentrez&render_type=abstract [Accessed December 3, 2014].
- Crick, F.H., 1968. The origin of the genetic code. *Journal of molecular biology*, 38(3), pp.367–79. Available at: <http://www.ncbi.nlm.nih.gov/pubmed/4887876> [Accessed November 30, 2014].
- Debeljak, F., 2013. The influence of the RNA helicase Mss116 on CBP2-assisted splicing of the bI5 group I intron in vitro. Available at: <http://oatd.org/oatd/record?record=oai%5C:oths.univie.ac.at%5C:29931> [Accessed February 15, 2015].
- Doherty, E.A. & Doudna, J.A., 1997. The P4-P6 domain directs higher order folding of the *Tetrahymena* ribozyme core. *Biochemistry*, 36(11), pp.3159–69. Available at: <http://www.ncbi.nlm.nih.gov/pubmed/9115992> [Accessed December 17, 2014].
- Draper, D.E., 2004. A guide to ions and RNA structure. *RNA (New York, N.Y.)*, 10(3), pp.335–43. Available at: http://www.pubmedcentral.nih.gov/articlerender.fcgi?artid=1370927&tool=pmcentrez&render_type=abstract [Accessed December 2, 2014].
- Eddy, S.R. & Hughes, H., 2001. NON-CODING RNA GENES AND. , 2(December).

- Fedorova, O., Solem, A. & Pyle, A.M., 2010. Protein-facilitated folding of group II intron ribozymes. *Journal of molecular biology*, 397(3), pp.799–813. Available at: <http://www.pubmedcentral.nih.gov/articlerender.fcgi?artid=2912160&tool=pmcentrez&render type=abstract> [Accessed February 15, 2015].
- Gampel, A. & Cech, T.R., 1991. Binding of the CBP2 protein to a yeast mitochondrial group I intron requires the catalytic core of the RNA. *Genes & development*, 5(10), pp.1870–80. Available at: <http://www.ncbi.nlm.nih.gov/pubmed/1916266> [Accessed February 15, 2015].
- Gampel, A. & Tzagoloff, A., 1987. In vitro splicing of the terminal intervening sequence of *Saccharomyces cerevisiae* cytochrome b pre-mRNA. *Molecular and cellular biology*, 7(7), pp.2545–51. Available at: <http://www.pubmedcentral.nih.gov/articlerender.fcgi?artid=365389&tool=pmcentrez&rendertype=abstract> [Accessed December 3, 2014].
- Glisovic, T. et al., 2008. RNA-binding proteins and post-transcriptional gene regulation. *FEBS letters*, 582(14), pp.1977–86. Available at: <http://www.pubmedcentral.nih.gov/articlerender.fcgi?artid=2858862&tool=pmcentrez&render type=abstract> [Accessed November 17, 2014].
- Golden, B.L. et al., 1998. A preorganized active site in the crystal structure of the *Tetrahymena* ribozyme. *Science (New York, N.Y.)*, 282(5387), pp.259–64. Available at: <http://www.ncbi.nlm.nih.gov/pubmed/9841391> [Accessed December 17, 2014].
- Guenther, U.-P. et al., 2013. Hidden specificity in an apparently nonspecific RNA-binding protein. *Nature*, 502(7471), pp.385–8. Available at: <http://dx.doi.org/10.1038/nature12543> [Accessed October 18, 2014].
- Guo, F., Gooding, A.R. & Cech, T.R., 2004. Structure of the *Tetrahymena* ribozyme: base triple sandwich and metal ion at the active site. *Molecular cell*, 16(3), pp.351–62. Available at: <http://www.sciencedirect.com/science/article/pii/S1097276504005921> [Accessed December 17, 2014].
- Halls, C. et al., 2007. Involvement of DEAD-box proteins in group I and group II intron splicing. Biochemical characterization of Mss116p, ATP hydrolysis-dependent and -independent mechanisms, and general RNA chaperone activity. *Journal of molecular biology*, 365(3), pp.835–55. Available at: <http://www.pubmedcentral.nih.gov/articlerender.fcgi?artid=1832103&tool=pmcentrez&render type=abstract> [Accessed December 1, 2014].
- Henn, A. et al., 2008. The ATPase cycle mechanism of the DEAD-box rRNA helicase, DbpA. *Journal of molecular biology*, 377(1), pp.193–205. Available at: <http://www.pubmedcentral.nih.gov/articlerender.fcgi?artid=2359651&tool=pmcentrez&render type=abstract> [Accessed February 24, 2015].
- Herschlag, D. et al., 1994. An RNA chaperone activity of non-specific RNA binding proteins in hammerhead ribozyme catalysis. *The EMBO journal*, 13(12), pp.2913–24. Available at: <http://www.pubmedcentral.nih.gov/articlerender.fcgi?artid=395173&tool=pmcentrez&rendertype=abstract> [Accessed February 15, 2015].

- Herschlag, D., 1995. RNA chaperones and the RNA folding problem. *The Journal of biological chemistry*, 270(36), pp.20871–4. Available at: <http://www.ncbi.nlm.nih.gov/pubmed/7545662> [Accessed February 22, 2015].
- Huang, H.-R. et al., 2005. The splicing of yeast mitochondrial group I and group II introns requires a DEAD-box protein with RNA chaperone function. *Proceedings of the National Academy of Sciences of the United States of America*, 102(1), pp.163–8. Available at: <http://www.pubmedcentral.nih.gov/articlerender.fcgi?artid=544071&tool=pmcentrez&rendertype=abstract> [Accessed February 15, 2015].
- Jankowsky, E., 2011. RNA helicases at work: binding and rearranging. *Trends in biochemical sciences*, 36(1), pp.19–29. Available at: <http://www.pubmedcentral.nih.gov/articlerender.fcgi?artid=3017212&tool=pmcentrez&renderertype=abstract> [Accessed October 24, 2014].
- Jarmoskaite, I. & Russell, R., 2011. DEAD-box proteins as RNA helicases and chaperones. *Wiley interdisciplinary reviews. RNA*, 2(1), pp.135–52. Available at: <http://www.pubmedcentral.nih.gov/articlerender.fcgi?artid=3032546&tool=pmcentrez&renderertype=abstract> [Accessed December 3, 2014].
- Joyce, G.F., 2002. The antiquity of RNA-based evolution. *Nature*, 418(6894), pp.214–21. Available at: <http://www.ncbi.nlm.nih.gov/pubmed/12110897> [Accessed December 2, 2014].
- Koonin, E. V., 2006. The origin of introns and their role in eukaryogenesis: a compromise solution to the introns-early versus introns-late debate? *Biology direct*, 1, p.22. Available at: <http://www.pubmedcentral.nih.gov/articlerender.fcgi?artid=1570339&tool=pmcentrez&renderertype=abstract> [Accessed December 3, 2014].
- Kruger, K. et al., 1982. Self-splicing RNA: autoexcision and autocyclization of the ribosomal RNA intervening sequence of Tetrahymena. *Cell*, 31(1), pp.147–57. Available at: <http://www.ncbi.nlm.nih.gov/pubmed/6297745> [Accessed December 3, 2014].
- Laggerbauer, B., Murphy, F.L. & Cech, T.R., 1994. Two major tertiary folding transitions of the Tetrahymena catalytic RNA. *The EMBO journal*, 13(11), pp.2669–76. Available at: <http://www.pubmedcentral.nih.gov/articlerender.fcgi?artid=395141&tool=pmcentrez&rendertype=abstract> [Accessed December 17, 2014].
- Lehnert, V. et al., 1996. New loop-loop tertiary interactions in self-splicing introns of subgroup IC and ID: a complete 3D model of the Tetrahymena thermophila ribozyme. *Chemistry & biology*, 3(12), pp.993–1009. Available at: <http://www.ncbi.nlm.nih.gov/pubmed/9000010> [Accessed February 24, 2015].
- Liebeg, A., Mayer, O. & Waldsich, C., DEAD-box protein facilitated RNA folding in vivo. *RNA biology*, 7(6), pp.803–11. Available at: <http://www.pubmedcentral.nih.gov/articlerender.fcgi?artid=3073338&tool=pmcentrez&renderertype=abstract> [Accessed February 15, 2015].
- Linder, P. & Jankowsky, E., 2011a. From unwinding to clamping - the DEAD box RNA helicase family. *Nature reviews. Molecular cell biology*, 12(8), pp.505–16. Available at: <https://univpn.univie.ac.at/+CSCO+00756767633A2F2F6A6A6A2E616E676865722E70627A++/nrm/journal/v12/n8/full/nrm3154.html> [Accessed November 24, 2014].

- Linder, P. & Jankowsky, E., 2011b. From unwinding to clamping - the DEAD box RNA helicase family. *Nature reviews. Molecular cell biology*, 12(8), pp.505–16. Available at: <http://www.ncbi.nlm.nih.gov/pubmed/21779027> [Accessed February 18, 2015].
- Liu, F., Putnam, A. & Jankowsky, E., 2008. ATP hydrolysis is required for DEAD-box protein recycling but not for duplex unwinding. *Proceedings of the National Academy of Sciences of the United States of America*, 105(51), pp.20209–14. Available at: http://www.pubmedcentral.nih.gov/articlerender.fcgi?artid=2629341&tool=pmcentrez&render_type=abstract [Accessed December 1, 2014].
- Mallam, A.L. et al., 2012. Structural basis for RNA-duplex recognition and unwinding by the DEAD-box helicase Mss116p. *Nature*, 490(7418), pp.121–5. Available at: http://www.pubmedcentral.nih.gov/articlerender.fcgi?artid=3465527&tool=pmcentrez&render_type=abstract [Accessed December 3, 2014].
- Marfatia, K.A. et al., 2003. Domain analysis of the *Saccharomyces cerevisiae* heterogeneous nuclear ribonucleoprotein, Nab2p. Dissecting the requirements for Nab2p-facilitated poly(A) RNA export. *The Journal of biological chemistry*, 278(9), pp.6731–40. Available at: <http://www.ncbi.nlm.nih.gov/pubmed/12496292> [Accessed February 15, 2015].
- Mayer, O. et al., 2007. RNA chaperone activity and RNA-binding properties of the *E. coli* protein StpA. *Nucleic acids research*, 35(4), pp.1257–69. Available at: http://www.pubmedcentral.nih.gov/articlerender.fcgi?artid=1851640&tool=pmcentrez&render_type=abstract [Accessed February 15, 2015].
- McGraw, P. & Tzagoloff, A., 1983. Assembly of the mitochondrial membrane system. Characterization of a yeast nuclear gene involved in the processing of the cytochrome b pre-mRNA. *The Journal of biological chemistry*, 258(15), pp.9459–68. Available at: <http://www.ncbi.nlm.nih.gov/pubmed/6348045> [Accessed February 15, 2015].
- Michel, F., Costa, M. & Westhof, E., 2009. The ribozyme core of group II introns: a structure in want of partners. *Trends in biochemical sciences*, 34(4), pp.189–99. Available at: <http://www.ncbi.nlm.nih.gov/pubmed/19299141> [Accessed December 2, 2014].
- Michel, F. & Westhof, E., 1990. Modelling of the three-dimensional architecture of group I catalytic introns based on comparative sequence analysis. *Journal of molecular biology*, 216(3), pp.585–610. Available at: <http://www.ncbi.nlm.nih.gov/pubmed/2258934> [Accessed December 17, 2014].
- Miller, S.L., 1953. A production of amino acids under possible primitive earth conditions. *Science (New York, N.Y.)*, 117(3046), pp.528–9. Available at: <http://www.ncbi.nlm.nih.gov/pubmed/13056598> [Accessed December 2, 2014].
- Moore, P.B., 1999. Structural motifs in RNA. *Annual review of biochemistry*, 68, pp.287–300. Available at: <http://www.annualreviews.org/doi/pdf/10.1146/annurev.biochem.68.1.287> [Accessed December 1, 2014].
- O'Brien, R. et al., 1998. The effects of salt on the TATA binding protein-DNA interaction from a hyperthermophilic archaeon. *Journal of molecular biology*, 279(1), pp.117–25. Available at: <http://www.ncbi.nlm.nih.gov/pubmed/9636704> [Accessed December 17, 2014].

- Orgel, L.E., 1968. Evolution of the genetic apparatus. *Journal of molecular biology*, 38(3), pp.381–93. Available at: <http://www.ncbi.nlm.nih.gov/pubmed/5718557> [Accessed December 2, 2014].
- Pan, J., Thirumalai, D. & Woodson, S.A., 1997. Folding of RNA involves parallel pathways. *Journal of molecular biology*, 273(1), pp.7–13. Available at: <http://www.ncbi.nlm.nih.gov/pubmed/9367740> [Accessed February 22, 2015].
- Pan, J. & Woodson, S.A., 1999. The effect of long-range loop-loop interactions on folding of the Tetrahymena self-splicing RNA. *Journal of molecular biology*, 294(4), pp.955–65. Available at: <http://www.ncbi.nlm.nih.gov/pubmed/10588899> [Accessed February 14, 2015].
- Partono, S. & Lewin, A.S., 1990. Splicing of COB intron 5 requires pairing between the internal guide sequence and both flanking exons. *Proceedings of the National Academy of Sciences of the United States of America*, 87(21), pp.8192–6. Available at: <http://www.pubmedcentral.nih.gov/articlerender.fcgi?artid=54921&tool=pmcentrez&rendertype=abstract> [Accessed December 3, 2014].
- Pichler, A. & Schroeder, R., 2002. Folding problems of the 5' splice site containing the P1 stem of the group I thymidylate synthase intron: substrate binding inhibition in vitro and mis-splicing in vivo. *The Journal of biological chemistry*, 277(20), pp.17987–93. Available at: <http://www.ncbi.nlm.nih.gov/pubmed/11867626> [Accessed December 3, 2014].
- Rajkowitsch, L. et al., 2007. RNA Chaperones, RNA Annealers and RNA Helicases. *RNA Biology*, 4(3), pp.118–130. Available at: <http://www.tandfonline.com/doi/abs/10.4161/rna.4.3.5445> [Accessed December 3, 2014].
- Rana, T.M., 2007. Illuminating the silence: understanding the structure and function of small RNAs. *Nature reviews. Molecular cell biology*, 8(1), pp.23–36. Available at: <http://dx.doi.org/10.1038/nrm2085> [Accessed July 11, 2014].
- Sachsenmaier, N., 2014. *Protein-assisted folding of the b15 intron in vivo*. University of Vienna.
- Sachsenmaier, N. & Waldsich, C., 2013. Mss116p: a DEAD-box protein facilitates RNA folding. *RNA biology*, 10(1), pp.71–82. Available at: <http://www.pubmedcentral.nih.gov/articlerender.fcgi?artid=3590239&tool=pmcentrez&render type=abstract> [Accessed December 3, 2014].
- Samatanga, B. & Klostermeier, D., 2014. DEAD-box RNA helicase domains exhibit a continuum between complete functional independence and high thermodynamic coupling in nucleotide and RNA duplex recognition. *Nucleic acids research*, 42(16), pp.10644–54. Available at: <http://www.pubmedcentral.nih.gov/articlerender.fcgi?artid=4176333&tool=pmcentrez&render type=abstract> [Accessed December 3, 2014].
- Schroeder, R., Barta, A. & Semrad, K., 2004. Strategies for RNA folding and assembly. *Nature reviews. Molecular cell biology*, 5(11), pp.908–19. Available at: <http://www.ncbi.nlm.nih.gov/pubmed/15520810> [Accessed October 20, 2014].
- Sclavi, B. et al., 1998. RNA folding at millisecond intervals by synchrotron hydroxyl radical footprinting. *Science (New York, N.Y.)*, 279(5358), pp.1940–3. Available at: <http://www.ncbi.nlm.nih.gov/pubmed/9506944> [Accessed February 24, 2015].

- Semrad, K. & Schroeder, R., 1998. A ribosomal function is necessary for efficient splicing of the T4 phage thymidylate synthase intron in vivo. *Genes & development*, 12(9), pp.1327–37. Available at: <http://www.pubmedcentral.nih.gov/articlerender.fcgi?artid=316773&tool=pmcentrez&rendertype=abstract> [Accessed February 14, 2015].
- S  raphin, B. et al., 1987. Construction of a yeast strain devoid of mitochondrial introns and its use to screen nuclear genes involved in mitochondrial splicing. *Proceedings of the National Academy of Sciences of the United States of America*, 84(19), pp.6810–4. Available at: <http://www.pubmedcentral.nih.gov/articlerender.fcgi?artid=299174&tool=pmcentrez&rendertype=abstract> [Accessed February 15, 2015].
- Silverman, S.K., 2008. A forced march across an RNA folding landscape. *Chemistry & biology*, 15(3), pp.211–3. Available at: <http://www.cell.com/article/S1074552108000872/fulltext> [Accessed December 3, 2014].
- Solem, A., Chatterjee, P. & Caprara, M.G., 2002. A novel mechanism for protein-assisted group I intron splicing. *RNA (New York, N.Y.)*, 8(4), pp.412–25. Available at: <http://www.pubmedcentral.nih.gov/articlerender.fcgi?artid=1370265&tool=pmcentrez&render type=abstract> [Accessed December 3, 2014].
- Solem, A., Zingler, N. & Pyle, A.M., 2006. A DEAD protein that activates intron self-splicing without unwinding RNA. *Molecular cell*, 24(4), pp.611–7. Available at: <http://www.ncbi.nlm.nih.gov/pubmed/17188036> [Accessed February 15, 2015].
- De Souza, S.J. et al., 1998. Toward a resolution of the introns early/late debate: only phase zero introns are correlated with the structure of ancient proteins. *Proceedings of the National Academy of Sciences of the United States of America*, 95(9), pp.5094–9. Available at: <http://www.pubmedcentral.nih.gov/articlerender.fcgi?artid=20219&tool=pmcentrez&rendertype=abstract> [Accessed February 14, 2015].
- Steiner, E.M., 2012. The activity of recombinant DEAD-Box protein Mss116p. Available at: http://othes.univie.ac.at/17784/1/2012-01-10_0422531.pdf [Accessed February 15, 2015].
- Steitz, T.A. & Steitz, J.A., 1993. A general two-metal-ion mechanism for catalytic RNA. *Proceedings of the National Academy of Sciences of the United States of America*, 90(14), pp.6498–502. Available at: <http://www.pubmedcentral.nih.gov/articlerender.fcgi?artid=46959&tool=pmcentrez&rendertype=abstract> [Accessed December 17, 2014].
- Tinoco, I. & Bustamante, C., 1999. How RNA folds. *Journal of molecular biology*, 293(2), pp.271–81. Available at: <http://www.ncbi.nlm.nih.gov/pubmed/10550208> [Accessed January 22, 2015].
- Tinoco, I. & Kieft, J.S., 1997. The ion core in RNA folding. *Nature structural biology*, 4(7), pp.509–12. Available at: <http://www.ncbi.nlm.nih.gov/pubmed/9228937> [Accessed December 2, 2014].
- Tirupati, H.K., Shaw, L.C. & Lewin, A.S., 1999. An RNA Binding Motif in the Cbp2 Protein Required for Protein-stimulated RNA Catalysis. *Journal of Biological Chemistry*, 274(43), pp.30393–30401. Available at: http://www.researchgate.net/publication/12779943_An_RNA_binding_motif_in_the_Cbp2_protein_required_for_protein-stimulated_RNA_catalysis [Accessed February 22, 2015].

- Treiber, D.K. et al., 1998. Kinetic intermediates trapped by native interactions in RNA folding. *Science (New York, N.Y.)*, 279(5358), pp.1943–6. Available at: <http://www.ncbi.nlm.nih.gov/pubmed/9506945> [Accessed February 14, 2015].
- Treiber, D.K. & Williamson, J.R., 2001. Beyond kinetic traps in RNA folding. *Current opinion in structural biology*, 11(3), pp.309–14. Available at: <http://www.ncbi.nlm.nih.gov/pubmed/11406379> [Accessed December 3, 2014].
- Vicens, Q. et al., 2008. Toward predicting self-splicing and protein-facilitated splicing of group I introns. *RNA (New York, N.Y.)*, 14(10), pp.2013–29. Available at: <http://www.pubmedcentral.nih.gov/articlerender.fcgi?artid=2553746&tool=pmcentrez&render type=abstract> [Accessed December 3, 2014].
- Vicens, Q. & Cech, T.R., 2009. A natural ribozyme with 3',5' RNA ligase activity. *Nature chemical biology*, 5(2), pp.97–9. Available at: <http://www.pubmedcentral.nih.gov/articlerender.fcgi?artid=2897744&tool=pmcentrez&render type=abstract> [Accessed December 3, 2014].
- Vicens, Q. & Cech, T.R., 2006. Atomic level architecture of group I introns revealed. *Trends in biochemical sciences*, 31(1), pp.41–51. Available at: <http://www.ncbi.nlm.nih.gov/pubmed/16356725> [Accessed December 3, 2014].
- Waldsich, C., Grossberger, R. & Schroeder, R., 2002. RNA chaperone StpA loosens interactions of the tertiary structure in the td group I intron in vivo. *Genes & development*, 16(17), pp.2300–12. Available at: <http://www.pubmedcentral.nih.gov/articlerender.fcgi?artid=186668&tool=pmcentrez&render type=abstract> [Accessed February 15, 2015].
- Waldsich, C., Semrad, K. & Schroeder, R., 1998. Neomycin B inhibits splicing of the td intron indirectly by interfering with translation and enhances missplicing in vivo. *RNA (New York, N.Y.)*, 4(12), pp.1653–63. Available at: <http://www.pubmedcentral.nih.gov/articlerender.fcgi?artid=1369732&tool=pmcentrez&render type=abstract> [Accessed February 14, 2015].
- Weeks, K.M., 1997. Protein-facilitated RNA folding. *Current opinion in structural biology*, 7(3), pp.336–42. Available at: <http://www.ncbi.nlm.nih.gov/pubmed/9204274> [Accessed February 15, 2015].
- Weeks, K.M. & Cech, T.R., 1996. Assembly of a ribonucleoprotein catalyst by tertiary structure capture. *Science (New York, N.Y.)*, 271(5247), pp.345–8. Available at: <http://www.ncbi.nlm.nih.gov/pubmed/8553068> [Accessed December 2, 2014].
- Weeks, K.M. & Cech, T.R., 1995. Efficient protein-facilitated splicing of the yeast mitochondrial bI5 intron. *Biochemistry*, 34(23), pp.7728–7738.
- Winter, A.J., Groot Koerkamp, M.J. & Tabak, H.F., 1990. The mechanism of group I self-splicing: an internal guide sequence can be provided in trans. *The EMBO journal*, 9(6), pp.1923–8. Available at: <http://www.pubmedcentral.nih.gov/articlerender.fcgi?artid=551900&tool=pmcentrez&render type=abstract> [Accessed February 14, 2015].

- Woodson, S.A., 2000. Recent insights on RNA folding mechanisms from catalytic RNA. *Cellular and molecular life sciences : CMLS*, 57(5), pp.796–808. Available at: <http://www.ncbi.nlm.nih.gov/pubmed/10892344> [Accessed February 14, 2015].
- Woodson, S.A., 2005. Structure and assembly of group I introns. *Current opinion in structural biology*, 15(3), pp.324–30. Available at: <http://www.sciencedirect.com/science/article/pii/S09594440X05000916> [Accessed February 14, 2015].
- Yang, Q. & Jankowsky, E., 2006. The DEAD-box protein Ded1 unwinds RNA duplexes by a mode distinct from translocating helicases. *Nature structural & molecular biology*, 13(11), pp.981–6. Available at: <http://www.ncbi.nlm.nih.gov/pubmed/17072313> [Accessed February 24, 2015].
- Zemora, G. & Waldsich, C., 2010. RNA folding in living cells. *RNA biology*, 7(6), pp.634–41. Available at: http://www.pubmedcentral.nih.gov/articlerender.fcgi?artid=3073324&tool=pmcentrez&render_type=abstract [Accessed February 14, 2015].
- Zingler, N., Solem, A. & Pyle, A.M., 2010. Dual roles for the Mss116 cofactor during splicing of the ai5y group II intron. *Nucleic acids research*, 38(19), pp.6602–9. Available at: http://www.pubmedcentral.nih.gov/articlerender.fcgi?artid=2965245&tool=pmcentrez&render_type=abstract [Accessed February 15, 2015].

Appendix

Abstract

One of the most studied non-coding RNAs are the self-splicing group I introns. To understand their autocatalytic function, their structure and corresponding folding process need to be analysed. bI5, the fifth and terminal intron of the cytochrome b pre-mRNA of *Saccharomyces cerevisiae*, belongs to the class of group I introns. For proper folding *in vivo*, bI5 requires two assisting proteins. *In vitro*, the cofactor Cbp2 was shown to facilitate folding of bI5 by capturing the near-native conformation, reached under near-physiological Mg^{2+} conditions, and finalizes the folding process. While the DEAD-box helicase Mss116p is known to use ATP binding and hydrolysis to unwind RNA duplexes *in vitro*, the role of Mss116p is not fully understood. To understand the *in vivo* interplay of proteins and pre-mRNA, it is necessary to define the roles of both proteins during the splicing and folding process. Therefore, we determined the observed rate constant (k_{obs}), derived from the pre-mRNA decay, by performing splicing assays under various *in vitro* conditions. Using equimolar ratios of Cbp2 and Mss116p in the splicing process of bI5 or a 2-fold molar excess of Mss116p over Cbp2 results in a ~1.5-fold increase in k_{obs} , compared to Cbp2-assisted bI5 splicing. Increasing the Mss116p to Cbp2 molar ratio to 4-fold further enhances the observed rate constant of bI5 splicing (~2.5 - 3-fold). Importantly, these observed effects were virtually identical whether both proteins were added concomitantly to the denatured bI5 intron or if the 2nd protein was added to either pre-formed protein-bI5 complex. This suggests that the order of events, in which the two proteins encounter and act on the RNA, is not a critical determinant for promoting efficient bI5 splicing. Also, our data implies that the two proteins do not appear to compete for a binding site. Since the increase in k_{obs} in the presence of Mss116p in addition to Cbp2 is only small, this could indicate that only a sub-population of bI5 pre-mRNAs depends on Mss116p for proper folding, while the entire bI5 population requires Cbp2 for reaching the native conformation. This is also in line with the fact that *in vivo* bI5 splicing is reduced to 50% in the *mss116* knock-out strain, while it is abolished in the *cbp2* knock-out strain. For characterization of protein-RNA interactions we determined the affinity of Cbp2 and Mss116p to bI5. Cbp2 showed a dissociation constant of 3.03 ± 0.3 nM, while that of Mss116p is 24.5 ± 5.1 nM. Cbp2 binding is very specific, which could explain the higher affinity compared to Mss116p. Mss116p, on the other hand, needs to bind to two structurally distinct RNA classes, group I and group II introns respectively, and therefore might be less specific and have a lower affinity.

Zusammenfassung

Zu den meist analysierten und studierten nicht codierenden RNAs gehört die Gruppe der selbst spleißenden Gruppe I Introns. Um deren autokatalytische Funktion zu verstehen, müssen deren Struktur und der dazugehörige Faltungsprozess analysiert werden. bI5, das fünfte und terminale Intron der Cytochrom b pre-mRNA von *Saccharomyces cerevisiae*, gehört zu den Gruppe I Introns. *In vivo* benötigt bI5 zwei Hilfsproteine um seine native Konformation zu erreichen. Der Kofaktor Cbp2 unterstützt die Faltung von bI5, indem es mit Intermediat-Konformationen interagiert und den Faltungsprozess finalisiert. Die DEAD-box Helikase Mss116p bindet und hydrolysiert ATP um stabile, aber kinetisch gefangene Konformationen aufzulösen. Der genaue Interaktionsmechanismus von Mss116p ist noch unklar. *In vitro* kann die native Konformation von bI5 ohne Mss116p, aber mit Cbp2 und einer Mg^{2+} Konzentration von $\sim 7\text{mM}$ erreicht werden. Um das Zusammenspiel von bI5, Cbp2 und Mss116p *in vivo* verstehen zu können, muss die Rollenverteilung der beiden Proteine während des Faltungs- und Splicing Prozesses evaluiert werden. Hierfür haben wir die Transformationsrate der pre-mRNA zu dessen Splicing-Produkten, anhand von Splicing Experimenten *in vitro* ermittelt. Bei einem äquimolaren Verhältnis Cbp2/Mss116p und bei einem 2 fachen Überschuss an Mss116p, stieg die Transformationsrate, verglichen mit Cbp2 ohne Mss116p Unterstützung, lediglich 1.5-fach an. Bei einem 4 fachen Überschuss an Mss116p stieg die Transformationsrate auf das 2.5-3 fache. Diese Ergebnisse waren sowohl bei gleichzeitiger Zugabe der Proteine zu denaturiertem bI5, bei Zugabe von Mss116p zu vorgeformten Cbp2 – bI5 Komplex und bei der Zugabe von Cbp2 zu vorgeformtem Mss116p-bI5 Komplex zu beobachten. Das lässt vermuten, dass es keine hierarchische Ordnung der beiden Proteine gibt. Außerdem scheint es kein Konkurrieren der beiden Proteine um Bindungsstellen zu geben. Da der Anstieg der Transformationsrate in Anwesenheit von Mss116p nur gering ist, scheint nur eine Sub-Population Mss116p für den Faltungsprozess zu benötigen. Im Gegensatz dazu benötigt die gesamte Population von bI5 den Kofaktor Cbp2. Diese Beobachtung geht konform mit dem Fakt, dass Splicing von bI5 *in vivo* um 50% reduziert ist, wenn Mss116p abgeschaltet ist. Im Gegensatz dazu findet bei einem Cbp2 knock-out kein Splicing von bI5 mehr statt (Sachsenmaier 2014). Für weitere Charakterisierung der Protein-RNA Interaktionen haben wir die Bindungsaffinitäten von Cbp2 und Mss116p ermittelt. Cbp2 weist eine Dissoziationskonstante von $3.03 \pm 0.3\text{nM}$, Mss116p eine von $24.5 \pm 5.1\text{nM}$ auf. Hohe Affinität von Cbp2 zu bI5 ist mit der sehr spezifischen Bindung zu erklären. Mss116p assistiert beim Splicing-Prozess von Gruppe I und Gruppe II Introns und muss daher weniger Spezifität in der Bindung vorweisen. Dies erklärt die verhältnismäßig niedrige Bindungsaffinität von Mss116p zu bI5.

Danksagungen:

In erster Linie bedanke ich mich bei meiner Betreuerin Christina Waldsich für die tolle Unterstützung bei diesem Projekt. Unabhängig mit welchen Problemen man konfrontiert war, Christina hatte immer ein offenes Ohr und Ratschläge parat.

Außerdem möchte ich mich bei allen Labormitarbeitern bedanken. Sie haben das Labor zu mehr gemacht, als einem einfachen Arbeitsplatz. Unzählige Stunden Lachen, Diskutieren und Philosophieren haben dazu geführt, dass aus Arbeitskollegen Freunde geworden sind. Danke an Andreas, Ela, Franka, Geta, Michael, Nora und Stefan.

Bedanken möchte ich mich außerdem bei all meinen Freunden, im speziellen Alex, Betzi, Martin und Jim. Freundschaften wie diese sind einzigartig und machen das Leben erst komplett. Ihr seid die Besten!

Ganz besonderer Dank geht an meine gesamte Familie, ins besondere an meine Eltern und an meine Schwester Sigrid. Ohne deren Unterstützung wäre ein Studium nicht möglich gewesen. Zu wissen, dass man selbst in den schwierigsten Zeiten auf deren Rückhalt zählen kann, ist ein unbeschreibliches Gefühl. Danke!

Außergewöhnlicher Dank geht an Verena: Ich danke dir, dass du immer für mich da bist und dein Leben mit mir teilst. Hättest du eine „Superkraft“, dann wäre es ein unaufhörliches Glücksgefühl in mir hervorzurufen. Mehr Glück als ein Mensch sich erträumen kann.

Curriculum vitae

Mühlhölzl Lukas, BSc

Persönliche Angaben

GEBURTSDATUM, ORT:	11.03.1986, Wien (Österreich)
ANSCHRIFT:	Kirchstetterngasse 46/6, 1160 Wien
TELEFON:	+43 (0)664 485 06 03
EMAILADRESSE:	lukas_muehlhoelzl@gmx.at
FAMILIENSTAND:	Ledig, keine Kinder
STAATSANGEHÖRIGKEIT:	Österreichischer Staatsbürger

Berufserfahrung

AB 08/2008	Mitarbeiter der Risikoberatungsfirma Risk Experts und Risk Consult GmbH
03/2013-06/2014	Praktisches Arbeiten im Rahmen der Masterarbeit „Kinetic and thermodynamic analysis of the bI5 intron bound to its protein cofactors“ (Labor: Dr. Christina Waldsich, Universität Wien)
02/2012-03/2012	Projekt Biochemie (Universität Wien): Herstellung von Proteinmutanten (Modellorganismus: Bäckerhefe)
09/2005-07/2008	Mitarbeiter der Kinderordination Dr. Susanne Bernhardt, Gesundheitszentrum Hetzendorf
09/2004-05/2005	Grundwehrdienst – Ausbildung zum Rettungssanitäter

Schulbildung

09/1996-06/2004	BG und BRG Fichtnergasse, Wien (Österreich)
09/1992-06/1996	Private Volksschule Waldkloster, Wien (Österreich)

Weitere Qualifikationen

SPRACHKENNTNISSE:	Deutsch (Muttersprache)
	Englisch (fließend)
	Französisch (Grundkenntnisse)
EDV KENNTNISSE:	Microsoft Office, Corel draw, Corel PHOTO-PAINT, Image quant
PERSÖNLICHE INTERESSEN:	Lesen, Brettspiele, Fussball